

BLAST LOAD SIMULATION USING SHOCK TUBE SYSTEMS

BLAST LOAD SIMULATION USING SHOCK TUBE SYSTEMS

By

AHMED ANWAR MOHAMED ISMAIL

B.Sc., M.A.Sc.

A Thesis Submitted to the School of Graduate Studies in Partial Fulfillment of the
Requirements for the Degree of Master of Applied Science

McMaster University

© Copyright by Ahmed Ismail

June 2017

Master of Applied Science (2017)

(Civil Engineering)

McMaster University

Hamilton, Ontario

TITLE: Blast Load Simulation using Shock Tube Systems

AUTHOR: **Ahmed A. M. Ismail**

B.Sc., M.Sc. (Cairo University)

SUPERVISORS: **Dr. Wael W. El-Dakhakhni (Co-Supervisor)**

Dr. Michael Tait (Co-Supervisor)

NUMBER OF PAGES: xx, 99

ABSTRACT

With the increased frequency of accidental and deliberate explosions, the response of civil infrastructure systems to blast loading has become a research topic of great interest. However, with the high cost and complex safety and logistical issues associated with live explosives testing, North American blast resistant construction standards (e.g. ASCE 59-11 & CSA S850-12) recommend the use of shock tubes to simulate blast loads and evaluate relevant structural response.

This study aims first at developing a 2D axisymmetric shock tube model, implemented in ANSYS Fluent, a computational fluid dynamics (CFD) software, and then validating the model using the classical Sod's shock tube problem solution, as well as available shock tube experimental test results. Subsequently, the developed model is compared to a more complex 3D model in terms of the pressure, velocity and gas density. The analysis results show that there is negligible difference between the two models for axisymmetric shock tube performance simulation. However, the 3D model is necessary to simulate non-axisymmetric shock tubes.

The design of a shock tube depends on the intended application. As such, extensive analyses are performed in this study, using the developed 2D axisymmetric model, to evaluate the relationships between the blast wave characteristics and the shock tube design parameters. More specifically, the blast wave characteristics (e.g. peak reflected pressure, positive phase duration and the reflected impulse), were compared to the shock tube design parameters (e.g. the driver section pressure and length, the driven

section length, and perforation diameter and their locations). The results show that the peak reflected pressure increases as the driver pressure increases, while a decrease of the driven length increases the peak reflected pressure. In addition, the positive phase duration increases as both the driver length and driven length are increased. Finally, although shock tubes generally generate long positive phase durations, perforations located along the expansion section showed promising results in this study to generate short positive durations.

Finally, the developed 2D axisymmetric model is used to optimize the dimensions of a proposed large-scale conical shock tube system developed for civil infrastructure blast response evaluation applications. The capabilities of this proposed shock tube system are further investigated by correlating its design parameters to a range of explosion threats identified by different hemispherical TNT charge weight and distance scenarios.

KEYWORDS: 2D axisymmetric flow simulation model, 3D flow simulation model, ANSYS Fluent, blast loads, blast shock tube, blast wave parameters, shock tube control parameters, TNT equivalent charge weights.

*To my father's soul,
my mother and my lovely wife*

ACKNOWLEDGEMENTS

All praise and thanks to Almighty Allah for providing me with the power and support to finish this work. I would like to express my sincere gratitude to my father, may Allah bless and have mercy on his soul, and to my mother, may Allah grant her a long and healthy life. I would also like to thank my lovely wife, Maria Vanessa, for her encouragement and support during hard times.

I would like to thank my co-supervisors Drs. Wael El-Dakhakhni and Michael Tait for their support and encouragement throughout this study. They gave me the opportunity to learn new things and understand how research should be conducted.

Finally, special thanks to Dr. Mohamed Ezzeldin and Dr. Manuel Campidelli for their valuable advices and suggestions during my study.

TABLE OF CONTENT

ABSTRACT	IV
ACKNOWLEDGEMENTS	VII
LIST OF TABLES	XI
LIST OF FIGURES	XII
CHAPTER 1 : INTRODUCTION	1
1.1. Research motivation	1
1.2. Objective	2
1.3. Scope	2
1.4. Blast shock tube review	3
1.4.1. The DRDC Suffield shock tube	4
1.4.2. The CEG Large Blast Simulator (LBS)	5
1.4.3. The USA Large Blast Thermal Simulator (LB/TS)	6
1.4.4. The Ernst Mach Institute (EMI) shock tube	7
1.4.5. The Central Laboratory, France shock tube	7
1.4.6. The ERDC Blast Load Simulator (BLS)	8
1.4.7. The University of Ottawa shock tube	8
1.4.8. The University of Rhode Island shock tube	9
1.4.9. The Laboratory of Politecnico Di Milano shock tube	9
1.5. Shock tube simulation approaches	10

1.6.	Computational fluid dynamics schemes-----	13
1.7.	Influence of perforation on shock tube performance-----	15
1.8.	Summary of review-----	17
1.9.	Layout of Thesis-----	18
CHAPTER 2 : NUMERICAL SIMULATIONS -----		22
2.1.	Introduction-----	22
2.2.	Two-dimensional axisymmetric model -----	22
2.2.1.	Validation using classical problems -----	24
2.2.2.	Validation using experimental tests in literature -----	25
2.2.3.	Mesh sensitivity analysis -----	27
2.2.4.	Planarity of the pressure profile -----	29
2.3.	Three-dimensional model -----	30
CHAPTER 3 : PARAMETRIC ANALYSIS -----		45
3.1.	Introduction-----	45
3.2.	Driver pressure variation -----	45
3.3.	Driver length variation -----	46
3.4.	Driven length variation -----	47
3.5.	Circular perforation diameter and location -----	48
CHAPTER 4 : PROPOSED CONICAL SHOCK TUBE -----		57

4.1. Introduction	57
4.2. Dimensions	57
4.3. Performance	58
CHAPTER 5: CONCLUSIONS AND FUTURE RECOMMENDATIONS	65
5.1. Conclusions	65
5.2. Future recommendations	67
APPENDIX A	68
REFERENCES	92

LIST OF TABLES

Table 1.1: The available blast shock tubes, their capabilities, and applications -----	19
Table 2.1: Comparison between measured (Awad, 2014) and predicted wavefront parameters at different distances from the exit of the ADL shock tube (207 kPa driver pressure)-----	32
Table 2.2: Shockwave metrics at various distances from the center of the ADL shock tube exit (262 kPa driver pressure) -----	33

LIST OF FIGURES

Figure 1.1: Typical Friedlander waveform -----	20
Figure 1.2: Typical shock tube schematic -----	20
Figure 1.3: Typical test setup, (Lloyd, 2010)-----	21
Figure 1.4: A conical shock tube with a perforation-----	21
Figure 2.1: Schematic diagram of a conical shock tube; (a) 3D computational flow domain, (b) the reduced 2D axisymmetric flow domain -----	34
Figure 2.2: Sod’s analytical and 2D model numerical results -----	35
Figure 2.3: Quadrilateral mesh used for 2D axisymmetric domain of ADL shock tube--	36
Figure 2.4: Residuals versus iterations of 2D axisymmetric simulation of ADL shock tube -----	36
Figure 2.5: Flow propagation through the ADL shock tube at various times: (a) $t = 0$ ms, (b) $t = 2.20$ ms, (c) $t = 4.40$ ms, and (d) $t = 4.50$ ms-----	37
Figure 2.6: Numerical predictions at four different distances from the exit section of the ADL shock tube (driver pressure = 205 kPa; driver length = 0.25 m): (a) incident pressures, (b) impulses -----	39
Figure 2.7: Quadrilateral mesh used for 2D axisymmetric domain of Ottawa shock tube	40
Figure 2.8: Pressure contours at different times ($t = 0, 1.90, 6.10$ and 15.20 ms) -----	40
Figure 2.9: 2D axisymmetric numerical simulation of Ottawa shock tube test compared with experimental results (driver pressure = 207 kPa; driver length = 2.74 m)	41
Figure 2.10: Mesh sensitivity of the Fluent model compared to the experimental results by (Awad, 2014) -----	41

Figure 2.11: Schematic diagram of Ottawa shock tube	42
Figure 2.12: 3D flow domain meshing of Ottawa shock tube.....	42
Figure 2.13: 3D numerical simulation of Ottawa shock tube test compared with experimental results (driver pressure = 207 kPa; driver length = 2.74 m).....	43
Figure 2.14: Comparison between 2D axisymmetric and 3D simulation results at the tube exit	43
Figure 2.15: Flow properties through conical shock tube after 8.40 ms for 3D simulation (upper half plane) and 2D axisymmetric simulation (lower half plane): (a) Pressure, (b) Density and (c) Axial velocity.....	44
Figure 3.1: Peak reflected pressure versus driver pressure when the driven section length is 4.0 m and the driver section length is changed from 2.0 to 4.0 m	51
Figure 3.2: Reflected impulse versus driver pressure when the driven section length is 4.0 m and the driver section length is changed from 2.0 to 4.0 m.....	51
Figure 3.3: Positive phase duration versus driver pressure when the driven section length is 4.0 m and the driver section length is changed from 2.0 to 4.0 m	52
Figure 3.4: Peak reflected pressure versus driver section length when the driver pressure is 1379 kPa and the driven section length is changed from 4.0 to 6.0 m	52
Figure 3.5: Reflected impulse versus driver section length when the driver pressure is 1379 kPa and the driven section length is changed from 4.0 to 6.0 m	53
Figure 3.6: Positive phase duration versus driver section length when the driver pressure is 1379 kPa and the driven section length is changed from 4.0 to 6.0 m	53

Figure 3.7: Peak reflected pressure versus driven section length when the driver pressure is 4137 kPa and the driver section length is changed from 1.0 to 4.0 m ----- 54

Figure 3.8: Reflected impulse versus driven section length when the driver pressure is 4137 kPa and the driver section length is changed from 1.0 to 4.0 m----- 54

Figure 3.9: Positive phase duration versus driven section length when the driver pressure is 4137 kPa and the driver section length is changed from 1.0 to 4.0 m ----- 55

Figure 3.10: Peak reflected pressure contour as function of perforation size and location when the driver pressure is 4137 kPa, driver length is 3.0 m, driven length is 4.0 m ----- 55

Figure 3.11: Reflected impulse contour as function of perforation size and location when the driver pressure is 4137 kPa, driver length is 3.0 m, driven length is 4.0 m 56

Figure 3.12: Positive phase duration contour as function of perforation size and location when the driver pressure is 4137 kPa, driver length is 3.0 m, driven length is 4.0 m ----- 56

Figure 4.1: The designed shock tube ----- 61

Figure 4.2: The pressure-impulse relation: (a) the performance of the proposed shock tube as function of driver pressure and length (over 1.0 m x 1.0 m specimen), (b) the simulated equivalent hemispherical TNT charges scenarios ----- 62

Figure 4.3: Mapping of the pressure-impulse performance of the proposed shock tube (dashed lines) in terms of equivalent hemispherical TNT charges scenarios (charge weight and standoff distance combinations, solid lines) ----- 63

Figure 4.4: Pressure-impulse performance: (a) The proposed shock tube (dashed lines) if the specimen is 2.0 m x 2.0 m in terms of equivalent blast loads scenarios (charge weight and standoff distance combinations, solid lines), (b) the University of Ottawa shock tube performance (Lloyd, 2010)----- 64

Figure A.1: Peak reflected pressure versus driver pressure when the driven section length is 3.0 m and the driver section length is changed from 2.0 to 3.0 m ----- 68

Figure A.2: Reflected impulse versus driver pressure when the driven section length is 3.0 m and the driver section length is changed from 2.0 to 3.0 m----- 68

Figure A.3: Positive phase duration versus driver pressure when the driven section length is 3.0 m and the driver section length is changed from 2.0 to 3.0 m ----- 69

Figure A.4: Peak reflected pressure versus driver pressure when the driven section length is 5.0 m and the driver section length is changed from 2.0 to 4.0 m ----- 69

Figure A.5: Reflected impulse versus driver pressure when the driven section length is 5.0 m and the driver section length is changed from 2.0 to 4.0 m----- 70

Figure A.6: Positive phase duration versus driver pressure when the driven section length is 5.0 m and the driver section length is changed from 2.0 to 4.0 m ----- 70

Figure A.7: Peak reflected pressure versus driver pressure when the driven section length is 6.0 m and the driver section length is changed from 2.0 to 4.0 m ----- 71

Figure A.8: Reflected impulse versus driver pressure when the driven section length is 6.0 m and the driver section length is changed from 2.0 to 4.0 m----- 71

Figure A.9: Positive phase duration versus driver pressure when the driven section length is 6.0 m and the driver section length is changed from 2.0 to 4.0 m ----- 72

Figure A.10: Peak reflected pressure versus driver pressure when the driver section length is 2.0 m and the driven section length is changed from 3.0 to 6.0 m----- 72

Figure A.11: Reflected impulse versus driver pressure when the driver section length is 2.0 m and the driven section length is changed from 3.0 to 6.0 m----- 73

Figure A.12: Positive phase duration versus driver pressure when the driver section length is 2.0 m and the driven section length is changed from 3.0 to 6.0 m----- 73

Figure A.13: Peak reflected pressure versus driver pressure when the driver section length is 3.0 m and the driven section length is changed from 3.0 to 6.0 m----- 74

Figure A.14: Reflected impulse versus driver pressure when the driven section length is 3.0 m and the driver section length is changed from 3.0 to 6.0 m----- 74

Figure A.15: Positive phase duration versus driver pressure when the driver section length is 3.0 m and the driven section length is changed from 3.0 to 6.0 m----- 75

Figure A.16: Peak reflected pressure versus driver pressure when the driver section length is 4.0 m and the driven section length is changed from 4.0 to 6.0 m----- 75

Figure A.17: Reflected impulse versus driver pressure when the driver section length is 4.0 m and the driven section length is changed from 4.0 to 6.0 m----- 76

Figure A.18: Positive phase duration versus driver pressure when the driver section length is 4.0 m and the driven section length is changed from 4.0 to 6.0 m----- 76

Figure A.19: Peak reflected pressure versus driver section length when the driver pressure is 103 kPa and the driven section length is changed from 4.0 to 6.0 m----- 77

Figure A.20: Reflected impulse versus driver section length when the driver pressure is 103 kPa and the driven section length is changed from 4.0 to 6.0 m----- 77

Figure A.21: Positive phase duration versus driver section length when the driver pressure is 103 kPa and the driven section length is changed from 4.0 to 6.0 m ----- 78

Figure A.22: Peak reflected pressure versus driver section length when the driver pressure is 4137 kPa and the driven section length is changed from 4.0 to 6.0 m ----- 78

Figure A.23: Reflected impulse versus driver section length when the driver pressure is 4137 kPa and the driven section length is changed from 4.0 to 6.0 m ----- 79

Figure A.24: Positive phase duration versus driver section length when the driver pressure is 4137 kPa and the driven section length is changed from 4.0 to 6.0 m ----- 79

Figure A.25: Peak reflected pressure versus driver section length when the driver pressure is 6895 kPa and the driven section length is changed from 4.0 to 6.0 m ----- 80

Figure A.26: Reflected impulse versus driver section length when the driver pressure is 6895 kPa and the driven section length is changed from 4.0 to 6.0 m ----- 80

Figure A.27: Positive phase duration versus driver section length when the driver pressure is 6895 kPa and the driven section length is changed from 4.0 to 6.0 m ----- 81

Figure A.28: Peak reflected pressure versus driven section length when the driver pressure is 103 kPa and the driver section length is changed from 1.0 to 4.0 m ----- 81

Figure A.29: Reflected impulse versus driven section length when the driver pressure is 103 kPa and the driver section length is changed from 1.0 to 4.0 m ----- 82

Figure A.30: Positive phase duration versus driven section length when the driver pressure is 103 kPa and the driver section length is changed from 1.0 to 4.0 m ----- 82

Figure A.31: Peak reflected pressure versus driven section length when the driver pressure is 1379 kPa and the driver section length is changed from 1.0 to 4.0 m
----- 83

Figure A.32: Reflected impulse versus driven section length when the driver pressure is 1379 kPa and the driver section length is changed from 1.0 to 4.0 m----- 83

Figure A.33: Positive phase duration versus driven section length when the driver pressure is 1379 kPa and the driver section length is changed from 1.0 to 4.0 m
----- 84

Figure A.34: Peak reflected pressure versus driven section length when the driver pressure is 6895 kPa and the driver section length is changed from 1.0 to 4.0 m
----- 84

Figure A.35: Reflected impulse versus driven section length when the driver pressure is 6895 kPa and the driver section length is changed from 1.0 to 4.0 m----- 85

Figure A.36: Positive phase duration versus driven section length when the driver pressure is 6895 kPa and the driver section length is changed from 1.0 to 4.0 m
----- 85

Figure A.37: Peak reflected pressure versus perforation size when the driver pressure is 103 kPa, driver length is 3.0 m, driven length is 4.0 m and the perforation is located at 20.0, 50.0 and 70.0 % of the driven length ----- 86

Figure A.38: Reflected impulse versus perforation size when the driver pressure is 103 kPa, driver length is 3.0 m, driven length is 4.0 m and the perforation is located at 20.0, 50.0 and 70.0 % of the driven length ----- 86

Figure A.39: Positive phase duration versus perforation size when the driver pressure is 103 kPa, driver length is 3.0 m, driven length is 4.0 m and the perforation is located at 20.0, 50.0 and 70.0 % of the driven length ----- 87

Figure A.40: Peak reflected pressure versus perforation size when the driver pressure is 6895 kPa, driver length is 3.0 m, driven length is 4.0 m and the perforation is located at 20.0, 50.0 and 70.0 % of the driven length ----- 87

Figure A.41: Reflected impulse versus perforation size when the driver pressure is 6895 kPa, driver length is 3.0 m, driven length is 4.0 m and the perforation is located at 20.0, 50.0 and 70.0 % of the driven length ----- 88

Figure A.42: Positive phase duration versus perforation size when the driver pressure is 6895 kPa, driver length is 3.0 m, driven length is 4.0 m and the perforation is located at 20.0, 50.0 and 70.0 % of the driven length ----- 88

Figure A.43: Peak reflected pressure versus perforation location when the driver pressure is 103 kPa, driver length is 3.0 m, driven length is 4.0 m and the perforation size is increased from 20.0 to 60.0 % of the driver diameter----- 89

Figure A.44: Reflected impulse versus perforation location when the driver pressure is 103 kPa, driver length is 3.0 m, driven length is 4.0 m and the perforation size is increased from 20.0 to 60.0 % of the driver diameter ----- 89

Figure A.45: Positive phase duration versus perforation location when the driver pressure is 103 kPa, driver length is 3.0 m, driven length is 4.0 m and the perforation size is increased from 20.0 to 60.0 % of the driver diameter----- 90

Figure A.46: Peak reflected pressure versus perforation location when the driver pressure is 4137 kPa, driver length is 3.0 m, driven length is 4.0 m and the perforation size is increased from 20.0 to 60.0 % of the driver diameter----- 90

Figure A.47: Reflected impulse versus perforation location when the driver pressure is 4137 kPa, driver length is 3.0 m, driven length is 4.0 m and the perforation size is increased from 20.0 to 60.0 % of the driver diameter ----- 91

Figure A.48: Positive phase duration versus perforation location when the driver pressure is 4137 kPa, driver length is 3.0 m, driven length is 4.0 m and the perforation size is increased from 20.0 to 60.0 % of the driver diameter----- 91

CHAPTER 1 : INTRODUCTION

1.1. RESEARCH MOTIVATION

In the last three decades, the response of critical infrastructure systems to blast loading has become a topic of great interest to a number of researchers due to the increased frequency of blasts (accidental or deliberate). Government organizations and military agencies have studied the vulnerability of structural components to blast loads and their findings have been codified in several blast resistant design guidelines and retrofit procedures [e.g. Unified Facilities Criteria (UFC) (UFC 3-340-02, 2008; UFC 4-010-01, 2013) and UK Glazing Hazard Guide (United Kingdom Glazing Hazard Guide, 1997)]. However, relatively limited research has been carried out by the civil engineering community due to the constraints and safety concerns associated with the use of live explosives (Carriere, et al., 2009; Abou-Zeid, et al., 2011; Wu, et al., 2011). However, due to the safety and logistical issues as well as the multiple sources of uncertainty associated with the blast wavefront parameters generated by live explosions, shock tubes have been considered as an alternative testing approach to simulate blast loadings, as specified by the Canadian (CSA S850-12) and American (ASCE 59-11) standards.

Due to the scarcity of relevant information in open literature, the motivation of this study is to develop a numerical model that can be used to simulate axisymmetrical and non-axisymmetrical shock tube systems. The aim of this model is to facilitate a better understanding of the influences of shock tube design parameters on blast wave characteristics that can be used subsequently to propose a large-scale shock tube design

that can generate shock waves similar to those experienced by civil structural components under blast.

1.2. OBJECTIVE

The current study aims at numerically evaluating the performance of a versatile shock tube that can be used to test different structural components at full- or reduced scale. In this respect, a 2D axisymmetric shock tube model is developed and compared to a more complex 3D model using ANSYS Fluent, a computational fluid dynamics (CFD) software. In addition, an extensive parametric study is performed to investigate the capability of a conical shock tube to simulate hemispherical TNT charge weights at different stand-off distances. Finally, a conical expansion section is used in this study to create a relatively stronger shock wave than its counterpart of a squared-pyramid expansion section, as recommended by (Armstrong, 2015).

1.3. SCOPE

The scope of the current study is to:

- Present a comprehensive literature review describing the available blast shock tubes and their applications.
- Validate a shock tube model using 2D axisymmetrical and 3D non-axisymmetrical FLUENT models.
- Investigate the effect of the shock tube design parameters on the generated blast wave characteristics.

- Propose a large-scale shock tube design that is capable of simulating the effects of large explosions.

1.4. BLAST SHOCK TUBE REVIEW

To the best of the author's knowledge, the first shock tube was originally constructed in 1899 by Vieille, as reported by (Fomin, 2010) to study the speed of sound. Afterwards, shock tubes were mainly considered as laboratory-scale devices that could reproduce shock waves, including those generated by live explosives. As such, shock tubes have become standard scientific laboratory instruments in several fields (e.g. medicine, physics, chemistry, aerodynamics, and, more recently, civil engineering). Literature shows that shock tubes can reproduce a Friedlander waveform (Chandra, et al., 2012) simulating the pressure history of a typical blast scenario, as shown in Figure 1.1.

A typical shock tube is composed of a high-pressure driver, a low-pressure driven test section, and a diaphragm to separate these two sections, as shown in Figure 1.2. The sudden rupture of the diaphragm leads to the generation of a shock wave traveling through the low-pressure section. The energy needed to produce the desired driven shock can be generated in a number of ways, including the detonation of a small amount of low or high explosive material or the use of compressed air in the driver section. The next sections summarize some aspects of large-scale shock tubes systems used to simulate blast load in Canada and internationally.

1.4.1. THE DRDC SUFFIELD SHOCK TUBE

The Defense Research and Development Canada (DRDC) has one of the highest performance shock tubes in North America (Ritzel, 2007). The DRDC blast shock tube was not only designed to simulate nuclear-scale blast, but also can be upgraded to simulate new blast threats on military and civil infrastructures (e.g. close-in blast damage and injury) that can be caused by terrorist attacks. A computational structural dynamics (CSD) approach was used to design the tube and the mounting frame, while computational fluid dynamics (CFD) modeling approach was used to validate the shock tube performance (Ritzel, 2007).

The DRDC blast shock tube consists of a thick-walled steel conical driver section and straight tubular driven section. Later on, a square cross-section (pyramidal horn) and venting system were attached to the driven section. The conical driver section is of 2,600 mm length and 460 mm diameter with a truncated apex opening, where a breech plug can be mounted. The driver system was initially incapable of properly simulating near-field blast scenarios (i.e. high intensity and short duration). Therefore, the breech was upgraded by installing a breech plug to facilitate using low-explosive charges (e.g. black-powder, propellants, and thermobaric explosives). The expansion (driven) section is a straight tubular section of 44.6 m length and 1,800 mm diameter. Because of its size, the expansion section houses a relocatable target-mounting station, allowing the position of a target to be varied within the tube. In addition, an extension section of 2.50 m square cross-section, is attached to the 1,800 mm diameter circular tube end-section to facilitate testing of full-scale structural panels. The pyramidal horn can produce planar blast

profiles over the cross section at the horn end. As the filling, firing and purging operations of this explosive-driven shock tube require at least two highly-skilled personnel in explosive handling, such systems are less than ideal for use at academic institutions.

1.4.2. THE CEG LARGE BLAST SIMULATOR (LBS)

The large blast simulator (LBS) is a multi-driver shock tube facility designed and constructed for the Ballistic Research Laboratory (BRL), located at Centre d'Etude Gramat (CEG) in France, to minimize the use of expensive tests to simulate large-scale nuclear explosions. This simulator is composed of multiple driver tubes, conical nozzles and a semi-cylindrical driven test section. Parametric studies were performed to identify the dimensions of this simulator and to predict the system performance and simulate the required range of blast waves (Opalka, 1987). The multi-driver section has an array of seven tubes, the length of this array can be changed to four different lengths (19.0, 26.0, 35.0 and 44.0 m). The main tubes are made up of 760 mm and 1,060 mm long sections with thicknesses chosen to contain driver pressures up to 24.0 MPa. The test section is a U-shape cross-section of 105.0 m length and 12.0 m wide on the floor. The multi-driver section is not preferable, because the diaphragms of the tubes may not be ruptured simultaneously. As mentioned in (Amman, 1977), a three-driver tube generally produce a shock front with severe distortions as a consequence of the delayed diaphragm openings.

1.4.3. THE USA LARGE BLAST THERMAL SIMULATOR (LB/TS)

A Large Blast Thermal Simulator (LB/TS) facility has been constructed by the Defence Nuclear Agency (DNA) for the US Army to simulate the blast and thermal environment resulting from nuclear explosions. This simulator is used to evaluate the survivability as well as the vulnerability of military equipment (e.g. trucks, tanks, and helicopters). This simulator is unique due to its large cross-section associated with a compressed gas driver section with a thermal radiation source system for heating the gas driver. The expansion tunnel consists of a semicircular cross-section 190.0 m in length and 20.0 m wide at the floor. As can be seen in Table 1.1, the LB/TS facility has the capabilities of producing a long positive phase duration which can simulate a nuclear-scale blast.

The LB/TS shock tube was designed based on the LBS facility at the CEG in France to include additional test conditions which could not be simulated at the CEG facility. This simulator consists of multiple driver sections, convergent nozzles and a large semicircular cross-section expansion tunnel. The driver section is composed of nine tubes for releasing the compressed gas in a large expansion tunnel. The diameter of each tube is 1,830 mm and its length is 80.0 m, divided into 10 sections connected by flanges to facilitate changes in length. Liquid nitrogen has been used as the driver gas, which is stored in tanks then evaporates and gets superheated in the driver section. The use of nitrogen allows an inherent flattop blast wave to be generated and subsequently, the wave profile maintains its peak overpressure value for a certain period of time before decay starts (Sundaramurthy & Chandra, 2014). Convergent nozzles have been used to retard

the driver gas, thus obtaining long flow durations through the flow area at the exit of the driver. This can also be achieved by using longer drivers.

1.4.4. THE ERNST MACH INSTITUTE (EMI) SHOCK TUBE

In 1964, Ernst Mach Institute (EMI) designed and installed an air-driven shock tube 17.0 m in length with a 1,000 mm diameter pressure chamber. This chamber was connected to a conical expansion section 37.0 m long with a diameter of 2,400 mm. Although this shock tube was designed to have a relatively large cross-section, it is reported that it can produce up to 150 kPa maximum reflected pressure at the end of the tube. This pressure is associated with a load duration varying from 15.0 to 38.0 ms that can be used to conduct blast research (Reichenbach, 1992).

1.4.5. THE CENTRAL LABORATORY, FRANCE SHOCK TUBE

In 1990, the Central Laboratory for Roads and Bridges in France developed a compressed-air shock tube, to better understand the behavior of concrete structures under blast loadings. This shock tube consists of a 3.0 to 19.0 m long driver section and can contain up to 6.0 MPa pressure to generate a quasi-plane shock wave in a 35.0 m long and 666 mm diameter expansion section. The reflected pressure at the end of the tube can reach 1,700 kPa, while the duration of the blast wave plateau ranges from 10 to 100 ms, depending on the pressure and the length of the driver section (Toutlemonde, et al., 1993). This shock tube can produce high-intensity signatures, but the diameter of the tube is relevant only for a portion of the concrete specimen.

1.4.6. THE ERDC BLAST LOAD SIMULATOR (BLS)

The Blast Load Simulator (BLS), located at the U.S. Army Corps of Engineers (USACE) Engineer Research and Development Center (ERDC), is used to study the impact resistance of composite structures for Navy ships (Zipf, et al., 2009). The driver section of BLS shock tube was designed to contain air or helium gases pressurized up to 10,340 kPa. This shock tube is 15.20 m in length with a 1,300 mm diameter at the test section. This BLS shock tube can produce planar waveforms of peak reflected pressures and impulses of 552 kPa and 11,000 kPa-ms, respectively.

1.4.7. THE UNIVERSITY OF OTTAWA SHOCK TUBE

The University of Ottawa shock tube is driven by compressed air to simulate blast loads on structural components (i.e. columns, walls and etc.). Testing relatively thin components can be achieved by installing a load-transferring device (curtains) to collect and transfer the shock wave pressure and impulse to the test specimen (e.g. column), as illustrated in Figure 1.3. The University of Ottawa shock tube can produce ranges of reflected pressure (78 – 104) kPa and impulse (217 – 2690) kPa-ms, that are approximately equivalent to TNT 8 – 10,000 kg charge mass and 12 – 106 m standoff distance combinations.

The University of Ottawa shock tube driver section can withstand 520 kPa maximum internal pressure and its length varies from 310 to 5,180 mm, which can be adjusted based on the required pressure profile. The shock tube also has a spool section which consists of a double diaphragm system that is responsible for the control of the

shock tube firing. The spool section is approximately pressurized to half of the driver section pressure. The expansion section is 6.1 m long and the diameter of the spool section increases from 597 mm to 2,032 mm square opening at the other end. This square opening was intended to ensure the uniformity of the generated shock wave across the entire surface of the structural element being tested. However, it was reported that the use of a square expansion caused a pressure drop in the driven section (Lloyd, 2010).

1.4.8. THE UNIVERSITY OF RHODE ISLAND SHOCK TUBE

The shock tube of the University of Rhode Island was designed to study the effect of blast loading on composite materials (Leblanc, et al., 2007). Helium is used as a driver gas, while two diaphragms are used to contain internal pressure up to 17,230 kPa. The total length of the shock tube is 7.0 m; consisting of a 1,800 mm long driver section with a diameter of 150 mm and 5,200 mm long driven section with a diameter 70 mm. Although this facility could produce a shock wave with high intensity, the diameter of the test specimen is limited to 70 mm.

1.4.9. THE LABORATORY OF POLITECNICO DI MILANO SHOCK TUBE

Laboratory of Politecnico di Milano developed a double-diaphragm shock tube to investigate the underground tunnel lining under blast loads (Colombo, et al., 2011). This shock tube has a total length of 14.90 m and consists of a driver, buffer and driven sections having an internal diameter of 481 mm with lengths of 2.35, 0.26 and 10.50 m. All sections have been designed with a 13.50 mm wall thickness to withstand an internal pressure of up to 6.0 MPa, but the incident pressure inside the driven section is

approximately half this pressure. Helium is used as a driver gas with only a single driver section length. The buffer section is filled with a pressure approximately half of the driver pressure to reduce the pressure loads on each diaphragm. However, the use of a thinner diaphragm complicates the system compared to its counterpart with a single diaphragm.

1.5. SHOCK TUBE SIMULATION APPROACHES

Several studies have been conducted to simulate the behavior of shock tubes with different configurations. These studies can be divided into two approaches of simulation: (1) One-dimensional (1D) simulation approach, where 1D flow assumption is a valid approximation to solve the flow properties across the shock wave (Lamnaouer, 2010), and (2) Two-dimensional (2D) simulation approach, where the investigations of complex phenomena associated with the shock tube are inherently two-dimensional. This section presents brief description of different applications that used either modelling approaches to simulate the experimental and/or analytical performance of shock tubes.

One-dimensional (1D) Euler equations were used in (Cocchi, et al., 1996) to capture the shock and contact discontinuities in the flow. In this respect, Monotonic Upstream-Centered Schemes for Conservation Laws (MUSCL) scheme (discussed in Section 1.6) was employed and the results were compared to the analytical solution of a two-phase (i.e. gas-gas, gas-liquid) shock tube. In addition, (Argow, 1996)'s study employed Total Variation Diminishing (TVD)-MacCormack predictor-corrector schemes for discretizing the 1D Euler equations and solving the flow in a conventional shock tube. These schemes showed an acceptable agreement with experimental results in terms of

predicting the evolution of the shock tube flow field. An updated Riemann solver for unsteady 1D inviscid flows developed by (Gottlieb & Groth, 1988), was employed in order to locate the contact surface in a shock tube by (Sheng, et al., 1998).

(Mark, 1981)'s study reported that the 1D Beam and Warming scheme can be used to simulate large blast simulators (i.e. CEG Large Blast Simulator). However, some calibration factors had to be introduced to achieve good agreement with the experimental results. For example, the initial driver pressure was increased by 20% and the driven length was decreased by 30% from the corresponding values of the CEG Large Blast Simulator (Mark, 1981). A 1/37 scale model of the LBS shock tube was investigated using a numerical model, as reported in (Hisley, et al., 1985). This numerical model used the same scheme (i.e. 1D Beam and Warming) to discretize the quasi-one-dimensional unsteady Euler equations. The Ballistic Research Laboratory (BRL) Quasi one-dimensional (Q1D) code was also used to validate the performance of the LBS simulator (Hisley, et al., 1985). This code was created by BRL to simulate the shock tube performance. This code was also used as an adiabatic, inviscid and unsteady Eulerian flow using a 1D finite differences formulation. The code has been validated using a wide range of flow problems and the results demonstrated that the 1D analysis approach can produce reasonable results, albeit with introducing some calibration factors.

The LB/TS facility was modeled using BRL-Q1D code (Opalka, 1989), similar to that used in the CEG LBS facility, and was designed using BRL BLAST2D code at a 1/57 scale (Hisley & Molvik, 1988). This code used Total Variation Diminishing (TVD) scheme to discretize steady, inviscid and compressible 2D Euler equations. The results

were in good agreement with the experimental data at low shock overpressures with greater variation observed at higher shock overpressures.

A parametric study and the ideal performance of Laboratory of Politecnico di Milano shock tube (Colombo, et al., 2011) have been investigated using the 1D code KASIMIR (KASIMIR, 1996). This program employs a Riemann solver and neglects the losses produced by the diaphragm's rupture and the influence of the boundary layer. The program is also able calculate the wave diagram of the shock tube flow with given dimensions and initial conditions for several driver gases (i.e. air, helium, nitrogen and hydrogen). However, it can only evaluate the performance of shock tubes with straight driven sections.

Although 1D simulation approach is not computationally intensive, there are still some aspects (e.g. non-axisymmetrical shock tube flow), that cannot be adequately represented using this simulation approach. The 2D axisymmetrical and non-axisymmetrical simulation approaches have been widely used by several researchers to capture these aspects. For example, unsteady 2D inviscid flow in a constant cross-section shock tube was studied by (Vasil'ev & Danil'chuck, 1994). The same authors used Godunov scheme to capture shock tube non-idealities such as the opening of the diaphragm. The solution of Euler equations in non-conservative formulation discretized by Godunov scheme showed a significant improvement of the accuracy (Cocchi, et al., 1998). A finite volume code was employed for solving Euler equations by (Petrie-Repar & Jacobs, 1998) and MUSCL scheme was used for discretization. The results showed that

the 2D axisymmetrical model had better estimation of the experimental flow characteristics compared to 1D models (Petrie-Repar & Jacobs, 1998).

Inviscid flow solution in shock tube was carried out using Fluent (Lamnaouer, 2010), where the simulations were compared with the full geometry of the high-pressure shock tube at Texas A&M University. According to (White, 1958; Ikui, et al., 1969), the simulated and experimental shock wave characteristics were in a good agreement when the pressure ratios across the diaphragm were below 1000. The accuracy and stability of the solution were investigated by discretizing the space with different schemes, upwind and MUSCL schemes (Lamnaouer, 2010). In addition, Advection Upstream Splitting Method (AUSM) method was used to compute the flux vectors. However, the Roe-Flux Difference Splitting (FDS) method has an advantage over AUSM method in that it can produce an oscillatory solution near flow discontinuities (Arisman, et al., 2015).

1.6. COMPUTATIONAL FLUID DYNAMICS SCHEMES

Two main schemes, classical and modern, have widely used in CFD to capture the shock wave and contact discontinuities in shock tube systems. The classical schemes include Lax-Friedrichs (Lax, 1954), Godunov (Godunov, 1959), Lax-Wendroff (Lax & Wendroff, 1960), MacCormack (MacCormack, 1969), and Beam-Warming (Beam & Warming, 1976) schemes for discretization, as well as others. Classical schemes can only offer accurate results in the case of weak-shock solutions (Lamnaouer, 2010). These schemes do not consider any information about the wave propagation in the discretization which can lead to nonlinear instabilities and oscillations across discontinuities. For example,

Lax-Friedrichs (Lax, 1954) is a first-order scheme and is typically used to capture weak-shock solutions due to its simplicity. Like the Lax-Friedrichs scheme, Godunov is a first-order scheme that was introduced to solve the Riemann (shock tube) problem by discretizing procedure at cell interfaces. The Lax-Wendroff scheme (Lax & Wendroff, 1960) is not only a second-order dissipative scheme for hyperbolic equations, but it also yields accurate results in terms of both space and time. The MacCormack scheme (MacCormack, 1969) is a two-step Lax-Wendroff, which uses backward differencing in the predictor and forward differencing in the corrector. Unlike the first-order schemes, MacCormack scheme does not produce diffusive errors in the solution. Finally, the Beam-Warming scheme (Beam & Warming, 1976) is a second-order accurate implicit scheme, which has improved stability over explicit schemes.

Modern higher order schemes are able to deal with a diverse range of problems, including MUSCL (Van Leer, 1979), Roe scheme (Roe, 1981), and TVD (Harten, 1983) schemes. The MUSCL is a finite volume scheme that yield accurate numerical solutions for strong-shocks discontinuities. This scheme replaces the piecewise constant approximation of the Godunov scheme and derives the flux states from cell-averaged states obtained from the previous time-step (Van Leer, 1979). Roe-Flux Difference Splitting (FDS) scheme (Roe, 1981) is an approximate Riemann (shock tube) solver based on the Godunov scheme, which may be used to reduce the number of iterations needed to obtain exact solutions. The TVD scheme is an explicit second-order accurate finite difference scheme in which high order spatial discretization was developed and obtained non-oscillatory solutions at flow discontinuities (Harten, 1983). However, there

is no guarantee that schemes with high order spatial discretization and higher order time discretization are strongly stable (Gottlieb, et al., 2009). Finally, the Advection Upstream Splitting Method (AUSM) (Liou & Steffen, 1993) is a robust scheme and converges as fast as the Roe-FDS scheme. However, unlike the Roe-FDS scheme, AUSM has no operation matrix, is much simpler to construct and subsequently is not subject to the difficulty arising from the differentiation.

1.7. INFLUENCE OF PERFORATION ON SHOCK TUBE PERFORMANCE

Compressed-gas shock tubes simulate typically blast pressure profiles that are characterized by long positive phase durations (explosions at long stand-off distances). However, explosions at short stand-off distances can be simulated by such shock tubes by creating a suddenly increase in the volume (as perforations along the expansion section) driving the flow to expand behind the shockwave (Figure 1.4). Positive phase duration, and thus impulse, reduction can be obtained by using the venting (perforation) system similar to that obtained by decreasing the driver length, as found in (Thomas, et al., 2004). It was also observed that venting the shock tube leads to increase both the duration and amplitude of negative phase, although venting configuration was not described in this study (Thomas, et al., 2004).

The influences of venting shock tubes were studied in (Ritzel, 2007). The DRDC shock tube was designed to include controllable side-venting through a pattern of vents (perforations) along its length to reduce the wave duration, simulating close-in explosions. The results showed that the venting system at the end of the shock tube (near

to the target specimen) reduces the positive phase duration, while maintaining reasonably high peak pressures. This allows reduction in the net impulse and positive phase duration while minimizing the reduction of the blast front. However, the effects of venting system locations on the blast wave were not investigated in this study.

More recently, (Armstrong, 2015)'s study investigated the influences of annular vents on the negative phase duration of the blast profile using CFD with an adaptive mesh refinement. In this respect, several pressure profiles were produced using shock tube with different vent configurations. The same author reported that the distance between the vent and the tube end is inversely proportional to the pressure amplitude in the negative phase. The amplitude of the negative phase pressure was also sensitive to the vent size, where the amplitude of the negative phase reduced as the vent size reduced. However, the effect of the vents on the peak pressure and positive phase duration was not discussed in the same study. In addition, it was reported that in case the vent size beyond a certain value, the reflected shock, at the end of the vent, returns to the main flow resulting large pressure fluctuations in the pressure profile (Armstrong, 2015).

Simulations with four different mesh sizes were conducted to capture the shock wave interaction with perforated plate in (Britan, et al., 2004). It was obvious that as the mesh size decreases, the resolution of the simulated flow in neighborhood to the reflected shock wave is more apparent. The turbulent nature in vicinity area to the perforation depend on the mesh size. (Wan & Eliasson, 2015)'s study used an adaptive mesh refinement to capture the physical gradients near complex regions, when a shock wave is attenuated by an obstacle in a 2D duct. Furthermore, several studies used a fixed mesh

size to capture the shock wave interactions with barriers (Berger, et al., 2015; Berger, et al., 2016) or obstacles (Chaudhuri, et al., 2013; Sha, et al., 2014).

1.8. SUMMARY OF REVIEW

Considering the shock tubes described in the literature, the intended application of a shock tube plays an important role in its design. It was reported in (Ritzel, 2007) that standard or conventional shock tubes, particularly those driven by compressed gas, cannot be used to simulate real blasts. However, driven compressed gas shock tubes are suitable for producing simulated blast loads with well-controlled amplitude and long durations for educational purposes. These types of shock tubes avoid the hazards of using low or high explosives and follow high safety procedures in each test. Table 1.1 shows and summarizes the available blast shock tubes, their capabilities, and applications. In addition, 1D & 2D simulation approaches using several CFD schemes and the influence of perforation on shock tube performance are reviewed.

The following points have been observed from other facilities as follows:

- The explosive-driven section may generate blast profiles with high intensity, but its risk is much higher than the compressed-air section.
- Helium and air gases are the most appropriate driver gases to generate a proper typical blast profile.
- Multi-driver section may generate distorted blast wave and the system becomes more sophisticated.

- Conical expansion section is a must to simulate blast wave over different scaled structural components.

1.9. LAYOUT OF THESIS

This thesis is divided into 5 chapters as follow:

- Chapter 1 presents a literature review on the available blast shock tubes and their applications, findings, and constraints. In addition, a literature review on shock tube simulation approaches and the influence of perforation on shock tube performance is presented.
- Chapter 2 develops 2D axisymmetric & 3D numerical models to simulate the shock tube performance. These models are investigated and validated using FLUENT program.
- Chapter 3 discusses an extensive parametric study to investigate the influences of the shock tube design parameters on its blast wave parameters.
- Chapter 4 presents a proposed conical shock tube and its capabilities to simulate hemispherical TNT charge weights versus two key control parameters (driver pressure and driver length).
- Chapter 5 includes the conclusions based on the findings of this research and the recommended future work.

Table 1.1: The available blast shock tubes, their capabilities, and applications

Designation	Dimensions at Exit	Capability			Application
		Pressure (kPa)	Impulse (kPa-ms)	Duration (ms)	
DRDC SUFFIELD	Square with 2,500 mm a side.	10 – 1,000	-	5 – 100	Military and civilian infrastructure components
CEG LBS	U-shape with 12.0 m wide.	14 – 240	-	-	Military equipment
LB/TS	Semicircular with 20.0 m wide.	13.80 - 241.30	80 – 43,110	150 – 4,300	Military equipment such as trucks, tanks, and helicopters
EMI	Circular with 2,400 mm diameter.	150	-	15 – 38	Several full-scale structural panels
CENTRAL LAB IN FRANCE	Circular with 666 mm diameter.	1,700	-	10 - 100	A portion of the concrete specimen
ERDC BLS	Circular with 1,300 mm diameter.	552	11,000	-	Composite structures for Navy ships
UNIVERSITY OF OTTAWA	Squared with 2,032 mm a side	78 – 104	217 – 2,690	-	Structural components such as columns
UNIVERSITY OF RHODE ISLAND	Circular with 70.0 mm diameter	2,200 – 12,400	-	-	Composite materials under high blast loads
LAB OF POLITECNICO DI MILANO	Circular with 481 mm diameter	350 – 1,070	3,850 – 9,610	-	A portion of an underground tunnel under blast loads

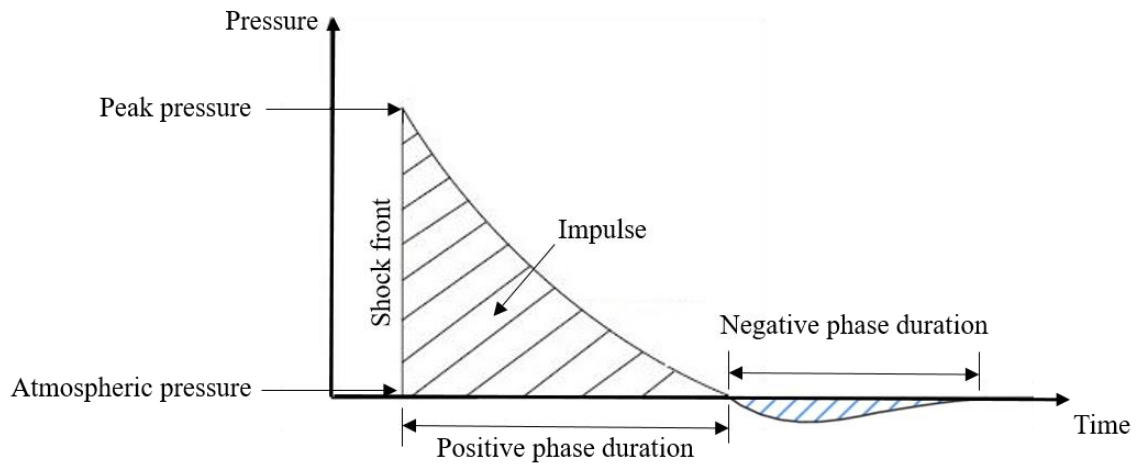


Figure 1.1: Typical Friedlander waveform

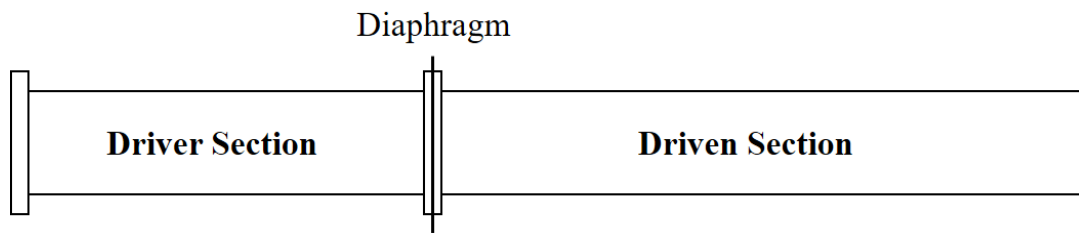


Figure 1.2: Typical shock tube schematic



Figure 1.3: Typical test setup, (Lloyd, 2010)

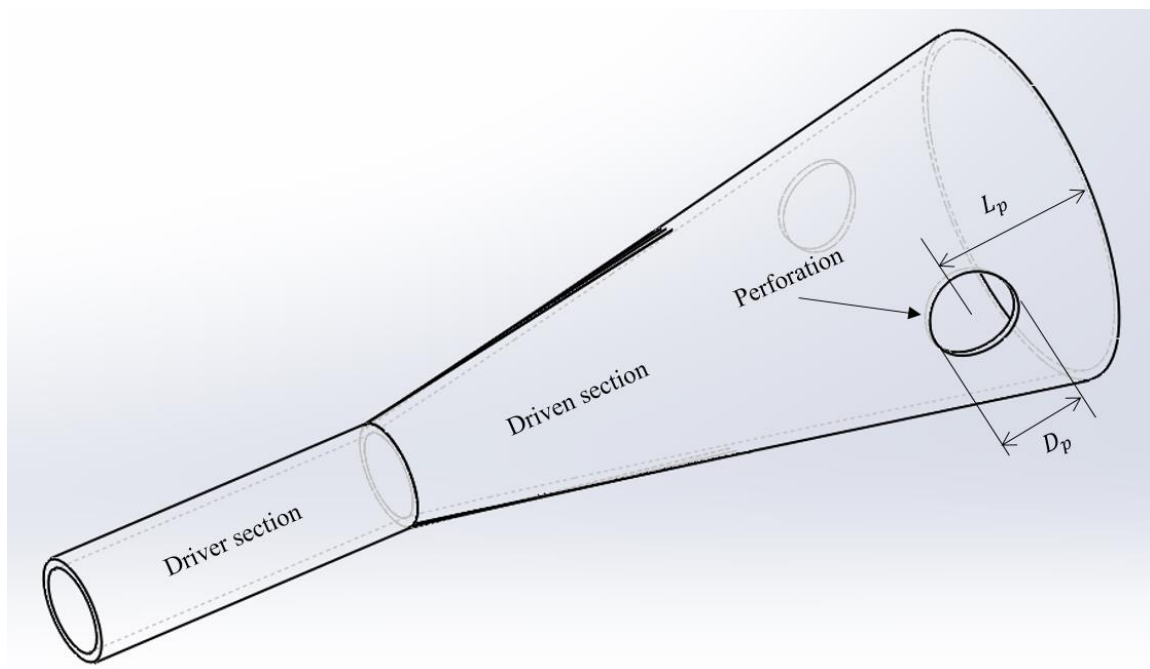


Figure 1.4: A conical shock tube with a perforation

CHAPTER 2 : NUMERICAL SIMULATIONS

2.1. INTRODUCTION

A simple one-dimensional (1D) model cannot simulate, with reasonable accuracy, the complex three-dimensional (3D) nature of the flow process in a large blast shock tube (Mark, 1981). As such, 2D axisymmetrical as well as and 3D non-axisymmetrical models are studied in this chapter to investigate the degree of their flow prediction within large shock tube systems.

2.2. TWO-DIMENSIONAL AXISYMMETRIC MODEL

The 3D domain requires significant computational resources, as can be seen in Figure 2.1a. However, it is possible to reduce the computational resources, if the domain, the initial conditions, and the boundary conditions can be simplified considering symmetry with respect to a straight axis (Holst, 1975). As shown in Figure 2.1, the flow properties of a shock tube with a conical expansion section can be reduced from 3D flow to 2D axisymmetrical flow. Thus, the reduction of such a 2D domain dramatically reduces the computational cost and the memory required to simulate the flow.

For 2D axisymmetrical, unsteady, inviscid and compressible flow, the equations of continuity, conservation of momentum and energy, and the equation of state (perfect gas) in cylindrical coordinates (r , θ , and z) are (Holst, 1975) are:

Continuity equation:

$$\frac{\partial \rho}{\partial t} + \frac{1}{r} \frac{\partial (\rho u_r r)}{\partial r} + \frac{1}{r} \frac{\partial (\rho u_z r)}{\partial z} = 0 \quad (2.1)$$

Axial momentum equation:

$$\frac{\partial(\rho u_r)}{\partial t} + \frac{1}{r} \frac{\partial(\rho u_r^2 r + Pr)}{\partial r} + \frac{1}{r} \frac{\partial(\rho u_r u_z r)}{\partial z} - \frac{P}{r} = 0 \quad (2.2)$$

Radial momentum equation:

$$\frac{\partial(\rho u_z)}{\partial t} + \frac{1}{r} \frac{\partial(\rho u_r u_z r)}{\partial r} + \frac{1}{r} \frac{\partial(\rho u_z^2 r + Pr)}{\partial z} = 0 \quad (2.3)$$

Energy equation:

$$\frac{\partial \rho \left(e + \frac{u_r^2 + u_z^2}{2} \right)}{\partial t} + \frac{1}{r} \frac{\partial(\rho e + \frac{1}{2} \rho u_r^2 + P) u_r}{\partial r} + \frac{1}{r} \frac{\partial(\rho e + \frac{1}{2} \rho u_z^2 + P) u_z}{\partial z} = 0 \quad (2.4)$$

where P , ρ , u_r , u_z , t and e are the pressure, density, radial velocity, axial velocity, time and internal energy, respectively. It should be noted that the axisymmetrical flow is independent of θ ($\frac{\partial}{\partial \theta} = 0$) and the circumferential velocity $u_\theta = 0$. In addition, the ideal-gas equation of state can be written in the following form,

$$P = (\gamma - 1) \left[e - \rho \frac{u_r^2 + u_z^2}{2} \right] \quad (2.5)$$

where γ denotes the specific heat ratio.

The above axisymmetrical flow equations are coupled differential equations to be solved analytically. ANSYS Fluent 17.0 (ANSYS, 2013), which has the above axisymmetrical flow model, is used in this study to solve such equations. The Fluent model is set as an inviscid, axisymmetrical, second-order, explicit, and density-based solver in (ANSYS, 2013) in order to carry out computational fluid dynamics simulations. The flow is modeled using an explicit, second-order Roe-FDS method where the gradient

is estimated using Green-Gauss Node Based technique (ANSYS, 2013). The ANSYS Fluent has two solver schemes, AUSM and Roe-FDS, however the Roe-FDS scheme is chosen to compute the flux vectors without oscillatory solution at the flow discontinuities according to (Arisman, et al., 2015).

2.2.1. VALIDATION USING CLASSICAL PROBLEMS

To validate the developed 2D axisymmetrical model, the analytical solution of the Sod (Sod, 1978) 1D shock tube problem is used in this study as a benchmark. In the Sod problem, an ideal diaphragm separates the fluids in the shock tube driver and driven sections. This classical problem is used to simulate the flow properties in a dimensionless form. The two fluids in both sections are initially at rest. The pressure and density in the driver section are set equal to one, while the pressure and density in the driven section are 0.10 and 0.125, respectively. In the current study, a 2D axisymmetric ANSYS Fluent model is used to simulate a shock tube of 1.0 m long (in the longitudinal x-direction) and with a 20 mm diameter (in the transverse y-direction). The domain is partitioned by adopting a uniform mesh with 100 quadrilateral cells. The diaphragm is placed at the middle of the tube. Both driver and driven sections are filled with air at rest and feature different pressures and densities.

Comparison between the analytical solution and the numerical results of the adopted 2D model is shown in Figure 2.2. The predicted pressure, density, and velocity profiles along the entire tube are compared at 100 ms following the rupture of the diaphragm. As can be seen in Figure 2.2, both solutions are in good agreement and

demonstrated that the adopted 2D axisymmetric model can adequately capture the shock and expansion waves inside a shock tube.

2.2.2. VALIDATION USING EXPERIMENTAL TESTS IN LITERATURE

Experimental data are used to verify the effectiveness of the Fluent model to predict the incident pressure at the exit of a bench top shock tube (Awad, 2014). Figure 2.3 shows the quadrilateral meshed 2D axisymmetric flow domain used for the validation. The shock tube has a tubular driver and expansion sections with symmetry around the center axis. Therefore, it is acceptable to simulate the flow using the axisymmetrical flow governing equations. The residuals of continuity, x-velocity, y-velocity and energy equations versus iterations are shown in Figure 2.4, while the generation and propagation of shock wave through Awad's (Awad, 2014) shock tube are shown at various times in Figure 2.5. The predicted incident pressure and impulse at four different distances from the exit section are also illustrated in Figure 2.6. In Awad's study (Awad, 2014), the performance of the tube was simulated using LS-DYNA software (Hallquist, 2006), an explicit finite element code used to model large deformations under short duration dynamic loads. Table 2.1 compares between the experimental, LS-DYNA and 2D axisymmetric model results in terms of the incident pressure, the positive phase duration and impulse at four distances from the exit section, given a 207 kPa driver pressure. As shown in Table 2.1, the results show that the maximum error between the experimental measurements and the Fluent outputs is 36.0% in the incident pressure and the positive phase duration. In addition, the errors between LS-DYNA and Fluent outputs are up 9.0% in the incident pressure and 18.0% in the positive phase duration.

An additional test is also performed to validate the Fluent model in terms of the reflected pressure at the exit of the University of Ottawa shock tube (Lloyd, 2010). The test setup involved 2.74 m driver length and 207 kPa driver pressure. The quadrilateral meshed 2D axisymmetric flow domain used for Ottawa shock tube is shown in Figure 2.7. Figure 2.8 shows the pressure contour at different times, while the experimental and numerical reflected pressure and reflected impulse histories are shown in Figure 2.9. The variations between the numerical and experimental peak reflected pressure, positive phase duration and reflected impulse results are 17.0%, 26.0%, and 1.50% (or 2.20% if assumed as triangular-shaped), respectively. It should be noted that the error in the reflected impulse is deceptive because the reflected impulse is calculated from the peak reflected pressure and positive phase duration and thus, the error in the reflected impulse is cumulative. Discrepancies between the numerical blast wave parameters and the experimental results are expected for many reasons. First, the numerical model does not account for the losses caused by the rupture of the diaphragm, especially that the University of Ottawa's shock tube has a double diaphragm section (spool). This might cause higher losses than what expected from a single membrane. In other words, the pressure expansion time history inside the driver section is needed to properly model a doubled diaphragm shock tube. Secondly, it is worth noting that the expansion section of this shock tube is square-pyramid cross-section. More specifically, the geometry has no rotational symmetry and therefore the flow inside this section is not axisymmetric. Based on these results, the Fluent outputs are considered acceptable in this study given the simplicity of the developed model. However, when the computational domain cannot be

reduced to 2D axisymmetrical, a 3D model is still needed to simulate the shock tube with a square expansion cross-section.

2.2.3. MESH SENSITIVITY ANALYSIS

An investigation is performed to evaluate the sensitivity of the Fluent model to the mesh size. The shock instability appears to depend on the geometry, mesh size and Mach number based on an extensive testing and analysis (Xu, 2014). As reported in (Armstrong, 2015), the grid convergence was characterized by the number of grid cells within the tube radius. (Armstrong, 2015) showed that the refinement level affects not only the pressure value, but also the shape of the profile at the tube exit. For very low resolutions the pressure value was significantly underestimated. As the resolution increased, the pressure values began to converge until results showed no significant change. Thus, the results showed that the optimal refinement level is 96 grid cells per tube radius.

Similarly, the resolution was characterized by the length of the domain divided by the number of cells (cell size) in (Bokil, 2010). The mesh sensitivity study was carried out at several cell sizes, 10.0, 5.0, 2.50, 1.25 and 0.625 mm, evaluating the pressure profile. The results showed that pressure profiles with cell size of 1.25 mm and 0.625 mm are nearly equivalent. As such, the cell size of 1.25 mm was chosen for further study.

Adaptive mesh refinement is typically used to study the shock tube non-idealities such as non-ideal rupture of the diaphragm, contact surface instabilities, boundary layer effects and reflected shock/boundary layer interactions. (Lamnaouer, 2010)'s study

performed mesh refinement studies at four mesh levels; 100,000, 150,000, 200,000 and 250,000 nodes. The pressure profile was shown to be independent of the mesh size for grid resolution over 150,000 nodes. The results showed that all adaptive mesh refinement cases had no effect on the pressure profile at the tube end (Lamnaouer, 2010). As such, within its objective, the current thesis does not consider the adaptive mesh refinement approach with the models presented herein, as the main objective of the thesis is to simulate the pressure profile at the shock tube exit sections.

Often times, the shock thickness and contact discontinuity can be physically much smaller than the mesh size, however it can be numerically enlarged and treated on the order of mesh size (Xu, 2014). Therefore, mesh refinement studies of any shock capturing problem should be in order of the shock thickness. Six cases with different cell size were tested for 1D shock-capturing problem in (Xu, 2001), $\Delta x = 1/100, 1/200, 1/400, 1/800, 1/1,600$ and $1/3,200$, where dimensionless shock thickness equals approximately $1/300$. The results showed that the shock revealed to converge to the exact solution as the mesh was refined, however the use of the coarse mesh facilitated capturing the shockwave with good agreement. The cell size was chosen to be less than shock thickness to investigate the dependency of mesh refinement for shock-capturing and contact surface discontinuity (Kawai & Lele, 2008). In case of the cell size is smaller than the numerical shock thickness, the results showed that the shock thickness is relatively insensitive to the grid resolution which is in agreement with the conclusion of (Cook, 2004)'s work.

The pertinent simulation is based on the geometry of the shock tube used by (Awad, 2014). The pressure in the driver section is set to 262 kPa and the sensor is placed

at 50 mm from the exit. A second-order discretization scheme is employed assuming unsteady, laminar, and compressible flow of an ideal gas with variable density. The convergence criterion in Fluent is set to 0.001 for each iteration for the continuity, momentum and energy equations. Four mesh sizes are considered in this study, with size of the quadrilateral elements equals to, considering that the shock wave thickness in air (τ) is 3.0×10^{-3} mm constant (Puckett & Stewart, 1950), 15000τ , 6500τ , 3000τ and 1500τ . Air flow and the incident pressure at the tube exit are simulated for these four meshes, where the experimental results; incident pressure is 91 kPa and positive phase duration is 5.30 ms (Awad, 2014), as shown in Figure 2.10. As can be seen, there are significant differences between the results obtained from the large mesh sizes (15000τ and 6500τ) and their counterparts of small sizes (3000τ and 1500τ), where the incident pressure is 86 kPa and the positive phase duration is 5.60 ms. The mesh sizes of 3000τ and 1500τ are coarse meshes (much larger than the shock thickness) even though they are similar to each other and yield a good agreement with the experimental results. Thus, the 1500τ mesh size is suggested to be used to minimize the computational time of the model.

2.2.4. PLANARITY OF THE PRESSURE PROFILE

The planarity of the shock wave can be evaluated by comparing pressure profiles at different points over the same cross-section. Therefore, additional analyses are performed using the ADL shock tube with a pressure of 262 kPa in the driver section and three different diameters at the exit section. The pressure profiles at the center axis with four points at the exit sections are obtained from the model. The incident pressures, impulses, and positive phase durations at all the points are compared in Table 2.2. To illustrate the

results of the comparison, the ratios between the blast wave parameters at each point and their correspondings at the center axis are listed in the same table. As expected, due to the no-slip condition, the blast wave parameters decrease as the point moves closer to the tube wall. The minimum ratios associated with incident pressure, impulse and positive phase duration are 0.94, 0.87 and 0.94, respectively. Based on these values, it is concluded that the shock wave can be considered reasonably plane. Consequently, the values at the shock tube axis can be considered adequately representative.

2.3. THREE-DIMENSIONAL MODEL

The 3D modeling approach is essential to properly simulate the experimental data of complicated large shock tube with no rotational symmetry. Therefore, Fluent 17.0, an inviscid, explicit, and density-based solver in ANSYS, is used to carry out computational fluid dynamics simulations in the 3D domain.

To validate the 3D model, an experimental test of the shock tube at the University of Ottawa (Figure 2.11) is used (Lloyd, 2010). The Hex Dominant method (ANSYS, 2013) is used for meshing the 3D flow domain of the University of Ottawa shock tube, as shown in Figure 2.12. The test setup involved 2.74 m driver length and 207 kPa driver pressure. As shown in Figure 2.13, the numerical and experimental results are in agreement. The differences between the peak reflected pressure, positive phase duration and reflected impulse results are 4.80%, 14.90%, and 7.70% (or 9.80% if assumed as triangular-shaped), respectively. According to these results, the 3D simulation is more suitable to model the University of Ottawa shock tube compared to the 2D axisymmetric simulation.

A comparison between the flow properties through a conical shock tube using 2D axisymmetric model and 3D model is executed, as shown in Figure 2.14. The conical shock tube is used for this comparison with the same dimensions of the University of Ottawa shock tube. However, the expansion section is considered as a conical-shaped, as shown in Figure 2.1 to facilitate direct comparison as previously discussed. The results in Figure 2.14 show differences between the peak reflected pressure, positive phase duration and reflected impulse of 5.80%, 0.10%, and 0.90%, respectively. In addition, Figure 2.15 shows flow property contours inside the conical shock tube at 8.40 ms using the 3D (upper half plane) and the 2D axisymmetric (lower half plane) simulations. The flow properties in terms of pressure, density, and velocity calculated by the 2D axisymmetric model differs from the 3D model by 2.60%, 1.50%, and 2.50%, respectively. As can be seen in the Figure 2.15, these two contours show that there is negligible difference between the two models for axisymmetric shock tube performance simulation. Consequently, a computational expensive 3D unsteady flow simulation can be replaced by a relatively simple 2D axisymmetric flow simulation, when the shock tube is axisymmetrical.

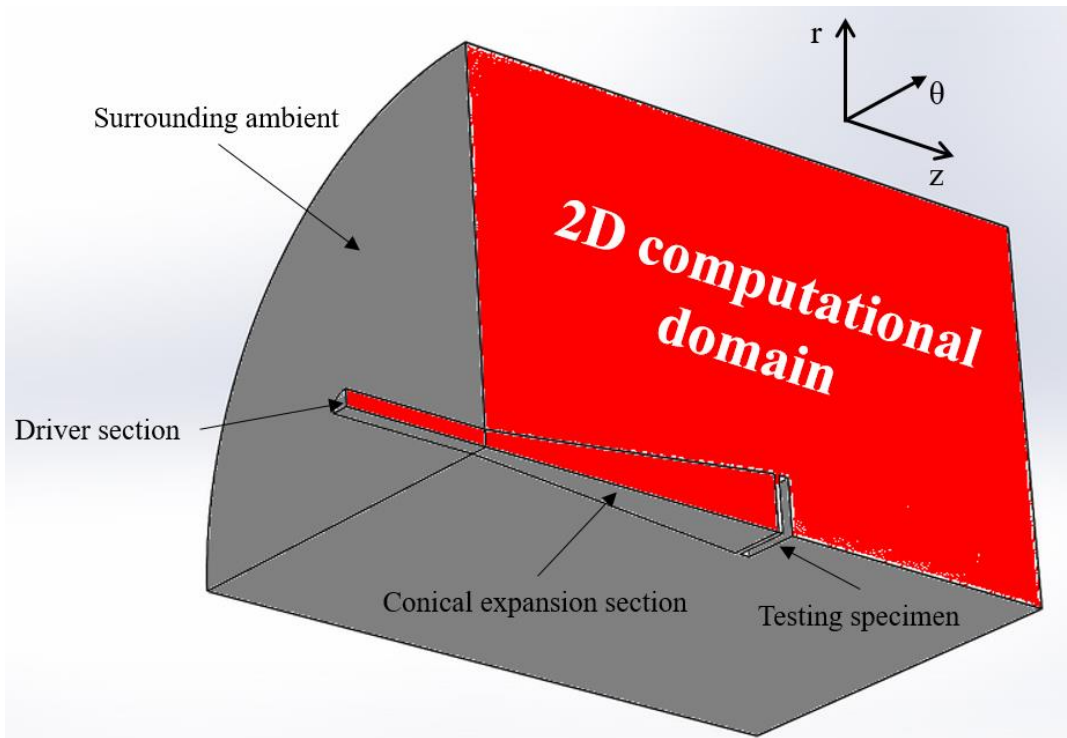
Table 2.1: Comparison between measured (*Awad, 2014*) and predicted wavefront parameters at different distances from the exit of the ADL shock tube (207 kPa driver pressure)

Blastwave parameter	Distance from the tube exit (mm)	LS – DYNA	Experimental results			Fluent	Err. (%) (Fluent & Exper.)	Discrepancy (%) (Fluent & LS-DYNA)
			Test (1)	Test (2)	Test (3)			
Peak incident pressure (kPa)	50	70	92	90	94	73	20	4
	100	66	60	80	83	71	4	7
	150	60	59	59	57	66	13	9
	450	37	22	20	20	34	36	8
Positive phase duration (ms)	50	0.97	0.73	0.57	0.68	1.03	35	5
	100	1.06	0.71	0.75	0.74	1.18	36	10
	150	1.17	1.08	1.11	1.12	1.37	18	14
	450	1.33	1.23	1.07	0.93	1.63	24	18

Table 2.2: Shockwave metrics at various distances from the center of the ADL shock tube exit (262 kPa driver pressure)

Diameter (mm)	Location from center axis (mm)	Incident pressure (kPa)	Incident impulse (kPa.ms)	Positive phase duration (ms)	Incident pressure ratio	Incident impulse ratio	Positive phase duration ratio
300	0	85	62	1.27	1.00	1.00	1.00
	30	85	61	1.23	1.00	0.98	0.97
	80	82	55	1.22	0.96	0.89	0.96
	120	80	53	1.19	0.94	0.87	0.94
400	0	85	75	1.47	1.00	1.00	1.00
	50	85	73	1.46	1.00	0.98	0.99
	100	85	71	1.43	1.00	0.95	0.97
	150	82	69	1.41	0.96	0.92	0.96
600	0	85	96	1.80	1.00	1.00	1.00
	70	85	94	1.79	1.00	0.98	0.99
	130	85	90	1.77	1.00	0.94	0.98
	200	84	85	1.75	0.99	0.89	0.97

(a)



(b)

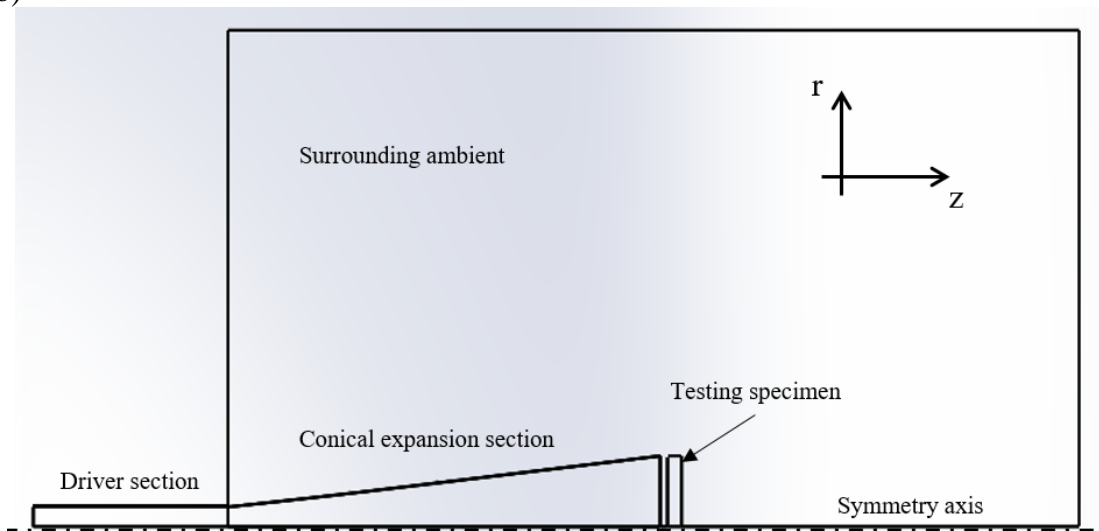


Figure 2.1: Schematic diagram of a conical shock tube; (a) 3D computational flow domain, (b) the reduced 2D axisymmetric flow domain

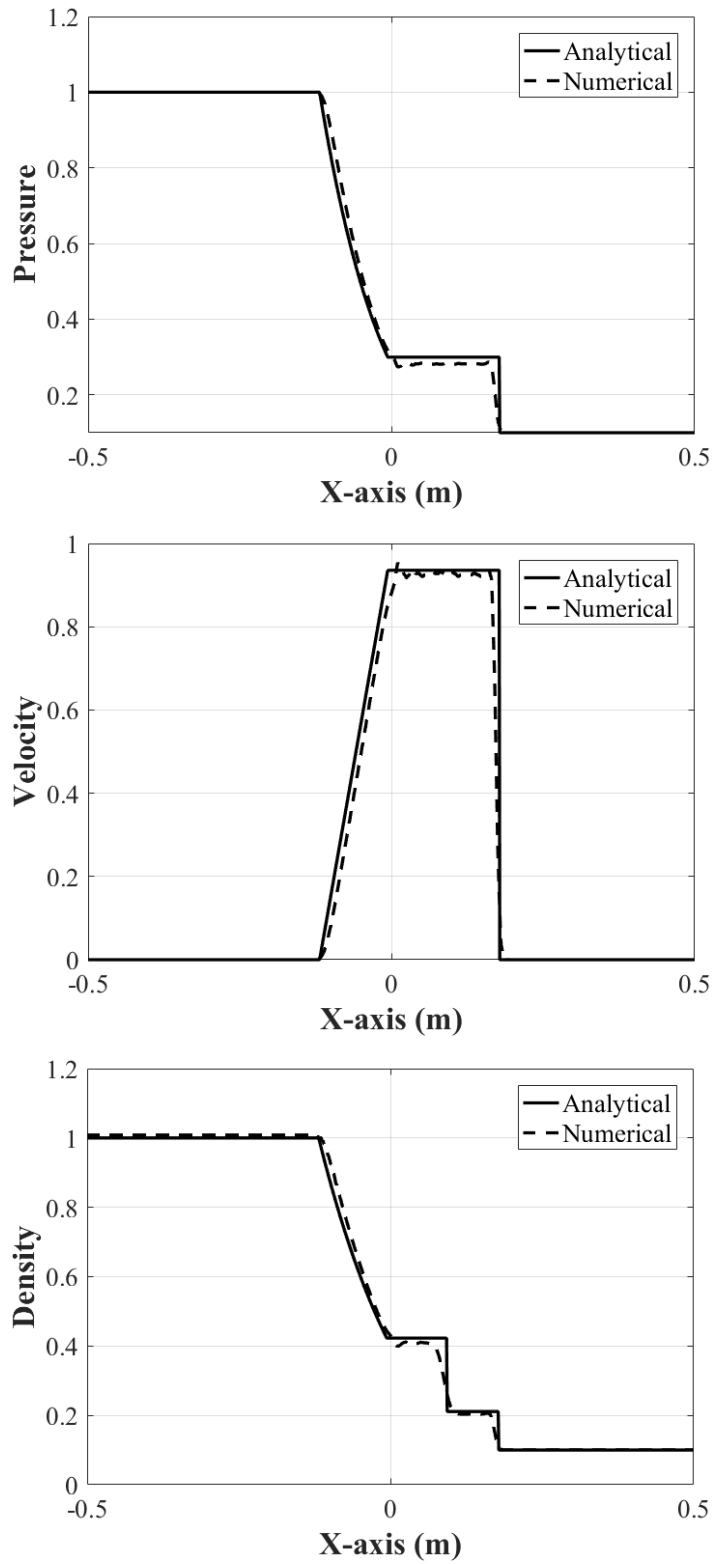


Figure 2.2: Sod's analytical and 2D model numerical results

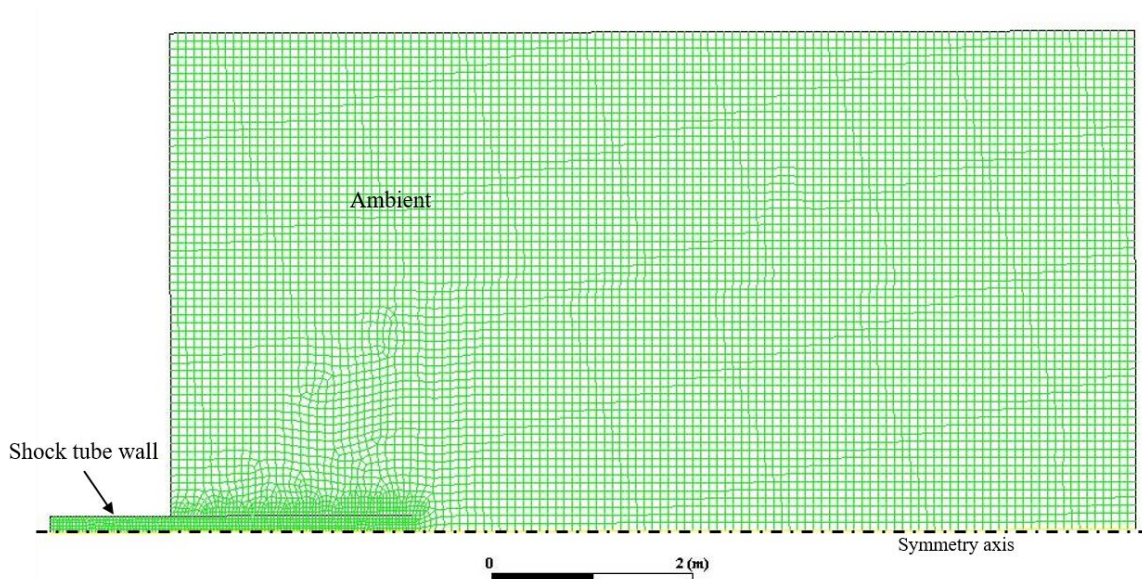


Figure 2.3: Quadrilateral mesh used for 2D axisymmetric domain of ADL shock tube

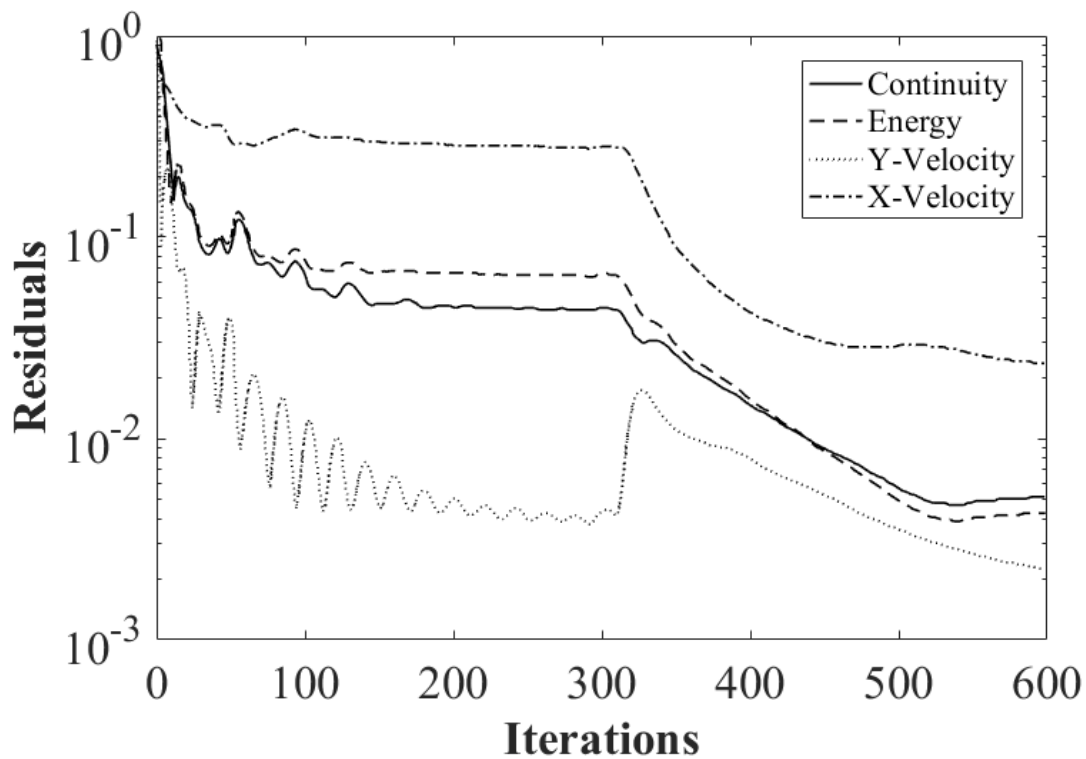


Figure 2.4: Residuals versus iterations of 2D axisymmetric simulation of ADL shock tube

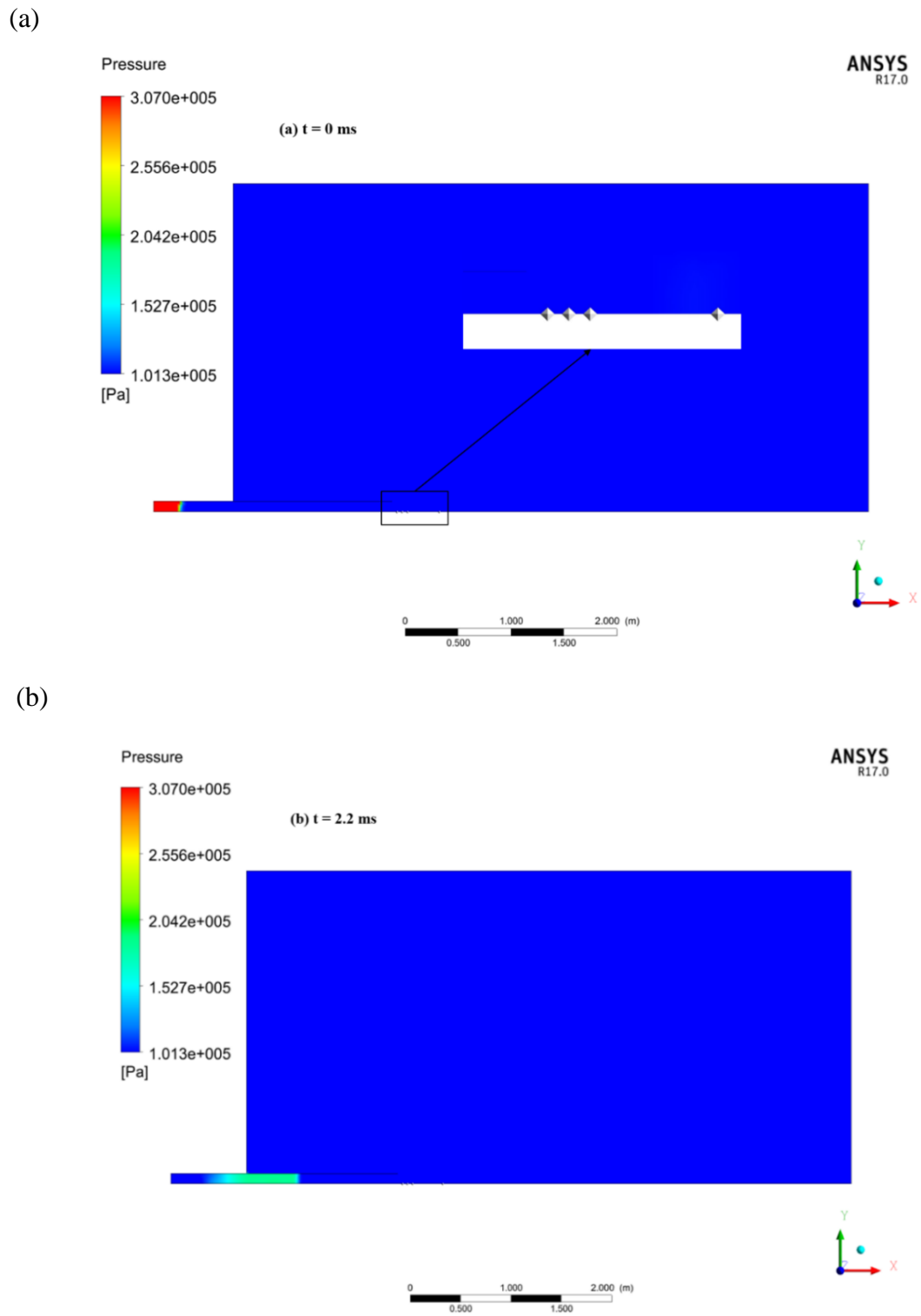
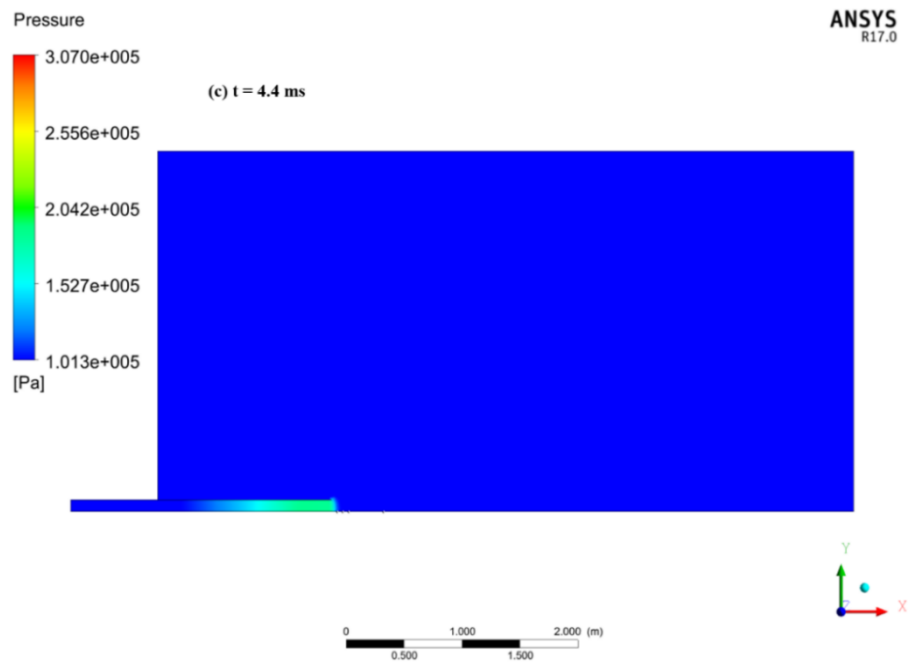


Figure 2.5: Flow propagation through the ADL shock tube at various times: (a) $t = 0$ ms, (b) $t = 2.20$ ms, (c) $t = 4.40$ ms, and (d) $t = 4.50$ ms

(c)



(d)

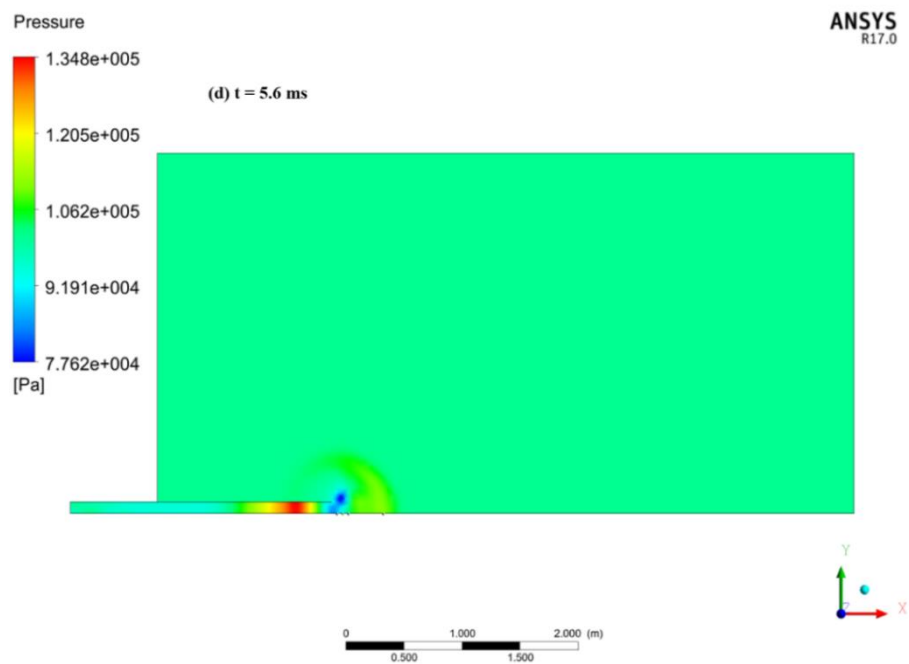


Figure 2.5: Flow propagation through the ADL shock tube at various times: (a) $t = 0 \text{ ms}$, (b) $t = 2.20 \text{ ms}$, (c) $t = 4.40 \text{ ms}$, and (d) $t = 4.50 \text{ ms}$ (Continued)

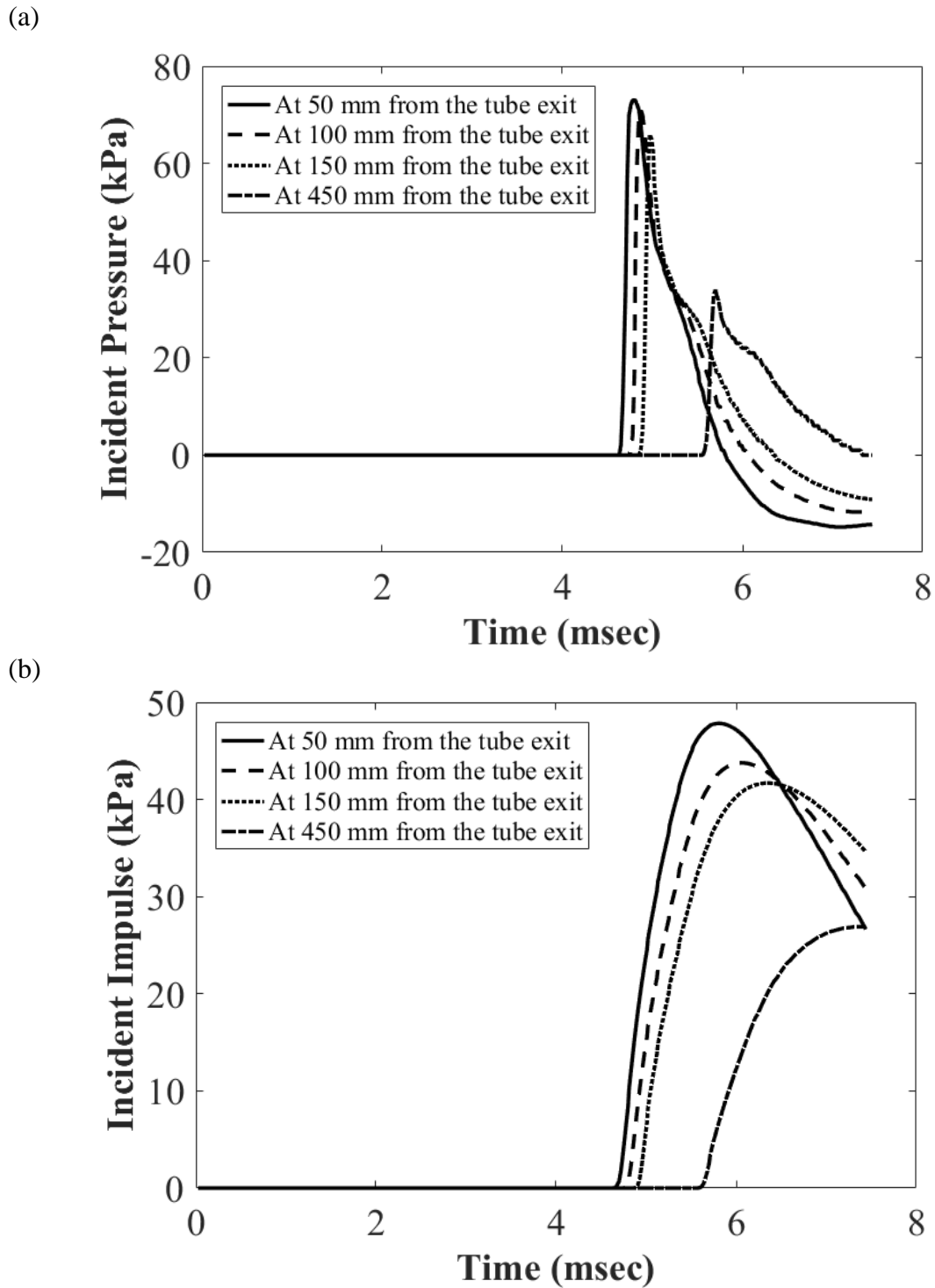


Figure 2.6: Numerical predictions at four different distances from the exit section of the ADL shock tube (driver pressure = 205 kPa; driver length = 0.25 m): (a) incident pressures, (b) impulses

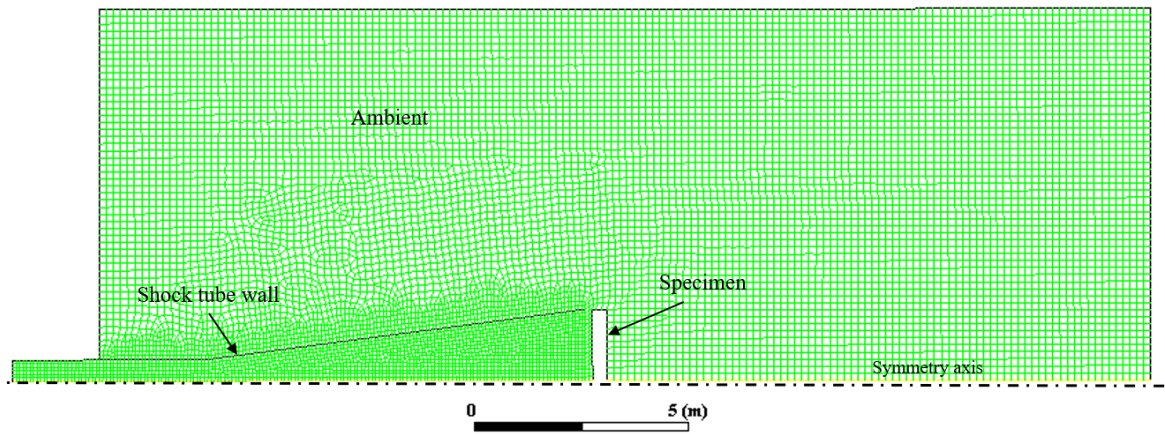


Figure 2.7: Quadrilateral mesh used for 2D axisymmetric domain of Ottawa shock tube

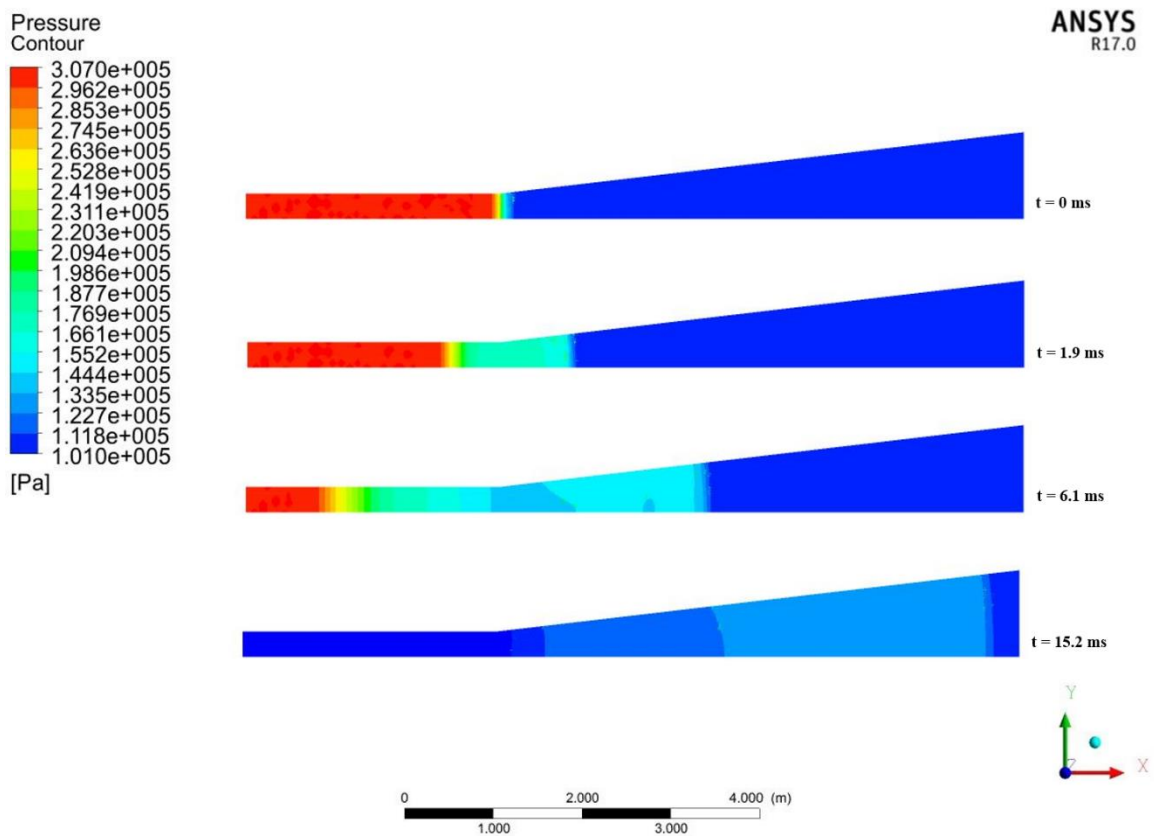


Figure 2.8: Pressure contours at different times (t = 0, 1.90, 6.10 and 15.20 ms)

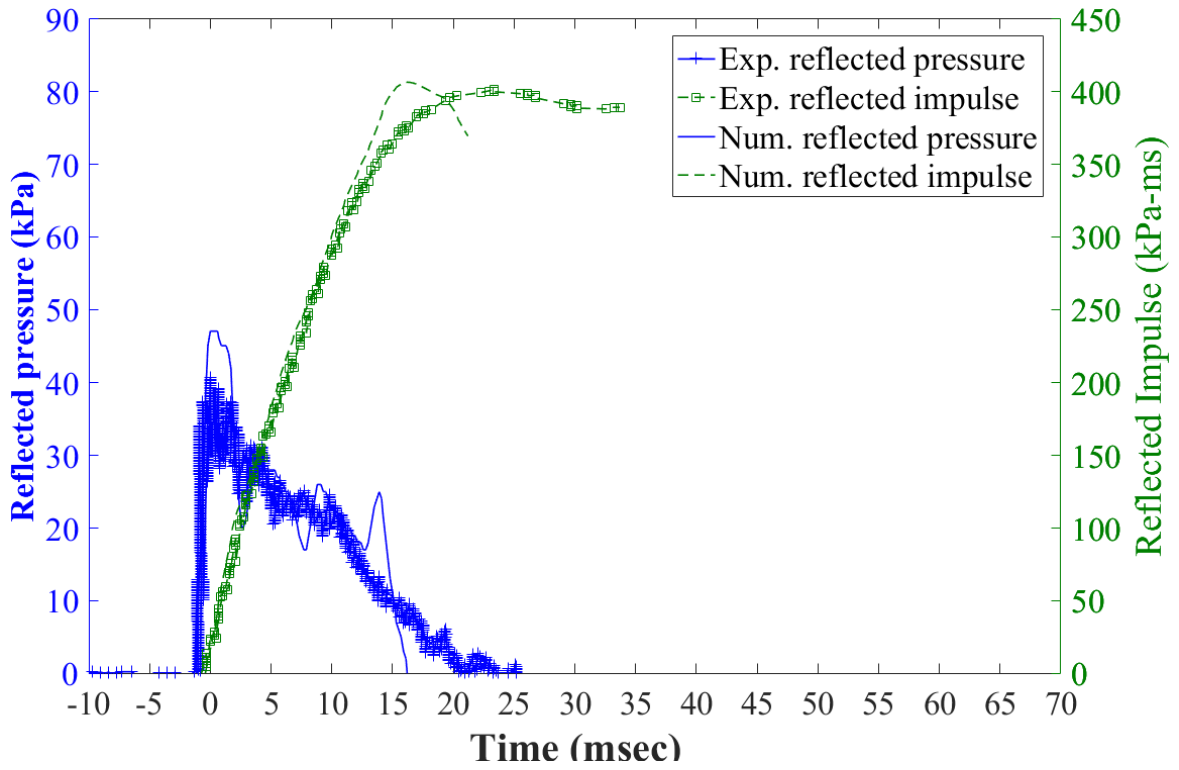


Figure 2.9: 2D axisymmetric numerical simulation of Ottawa shock tube test compared with experimental results (driver pressure = 207 kPa; driver length = 2.74 m)

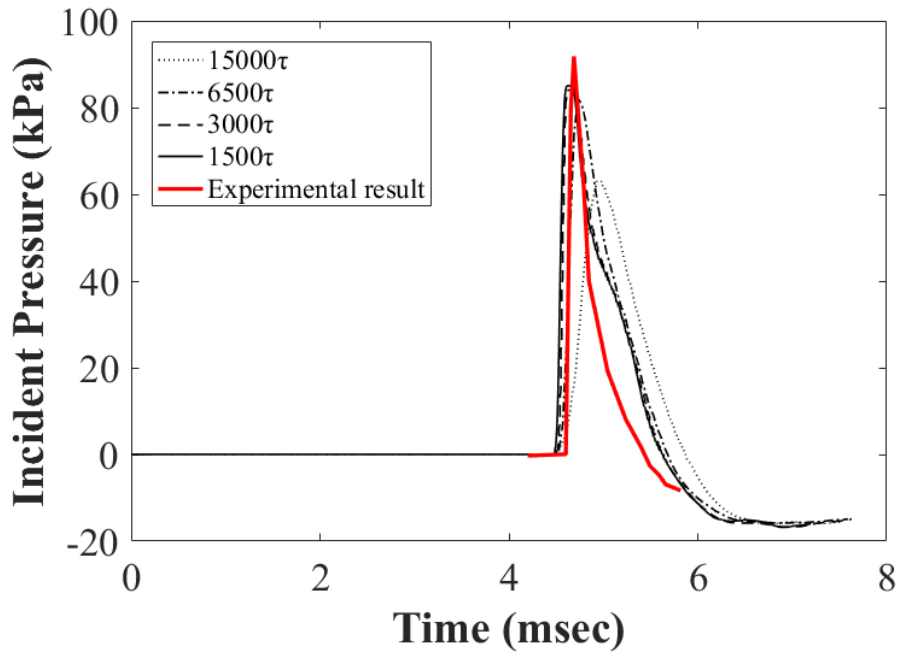


Figure 2.10: Mesh sensitivity of the Fluent model compared to the experimental results by (Awad, 2014)

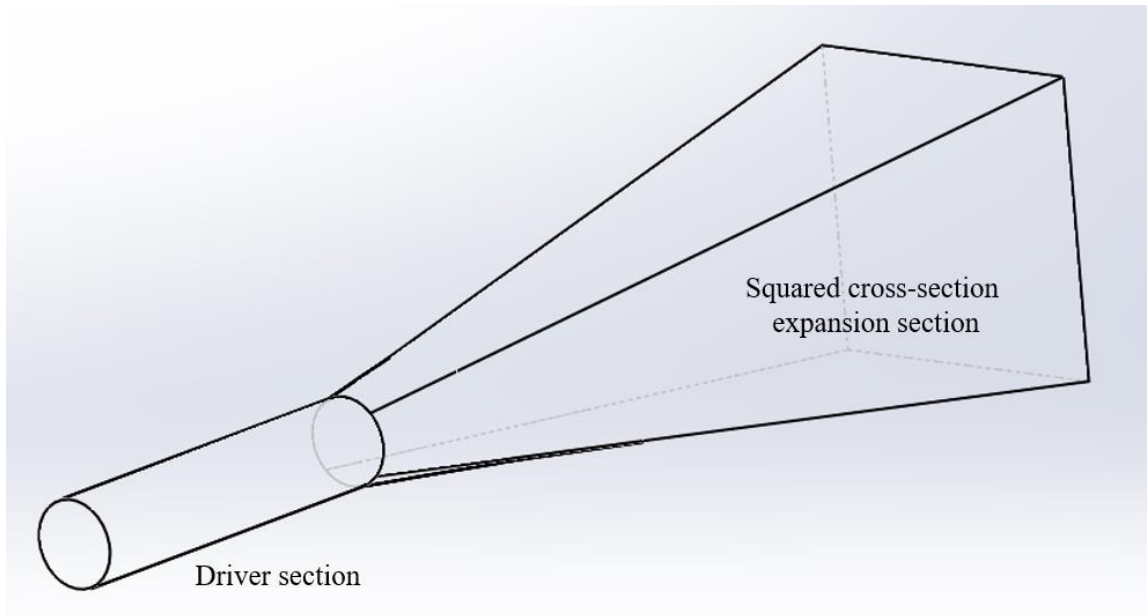


Figure 2.11: Schematic diagram of Ottawa shock tube

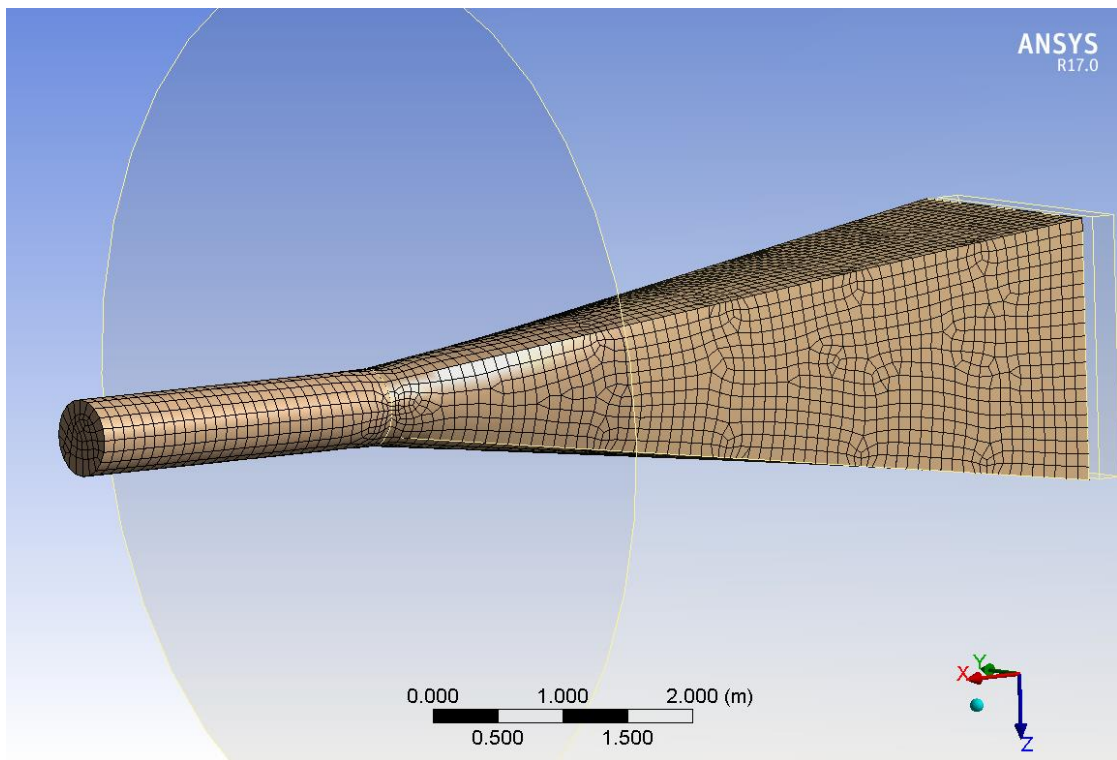


Figure 2.12: 3D flow domain meshing of Ottawa shock tube

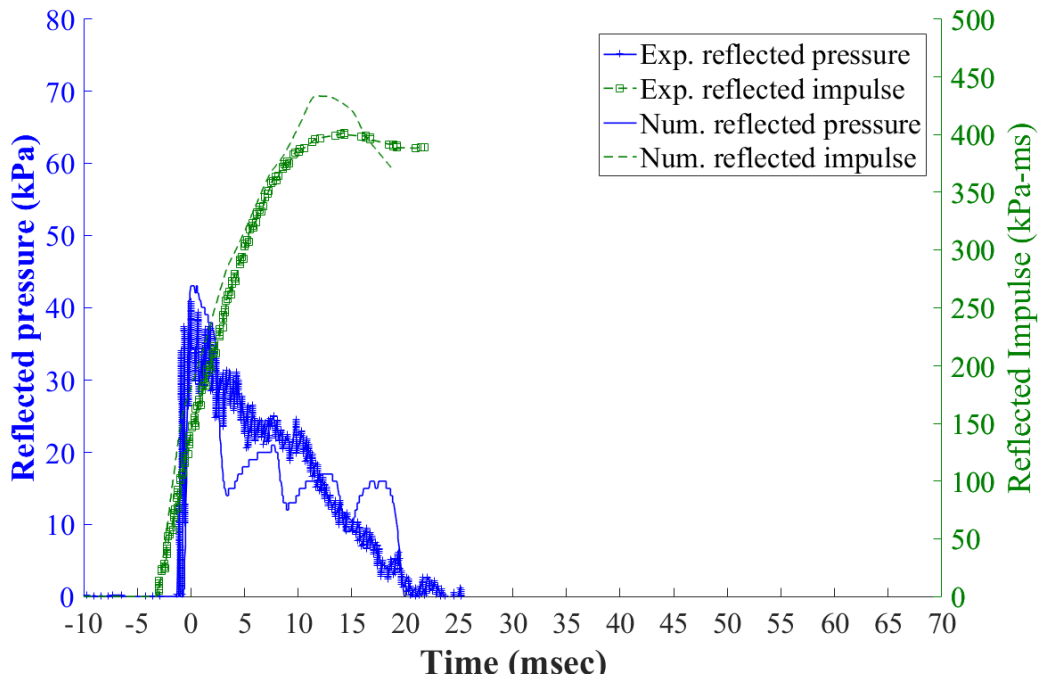


Figure 2.13: 3D numerical simulation of Ottawa shock tube test compared with experimental results (driver pressure = 207 kPa; driver length = 2.74 m)

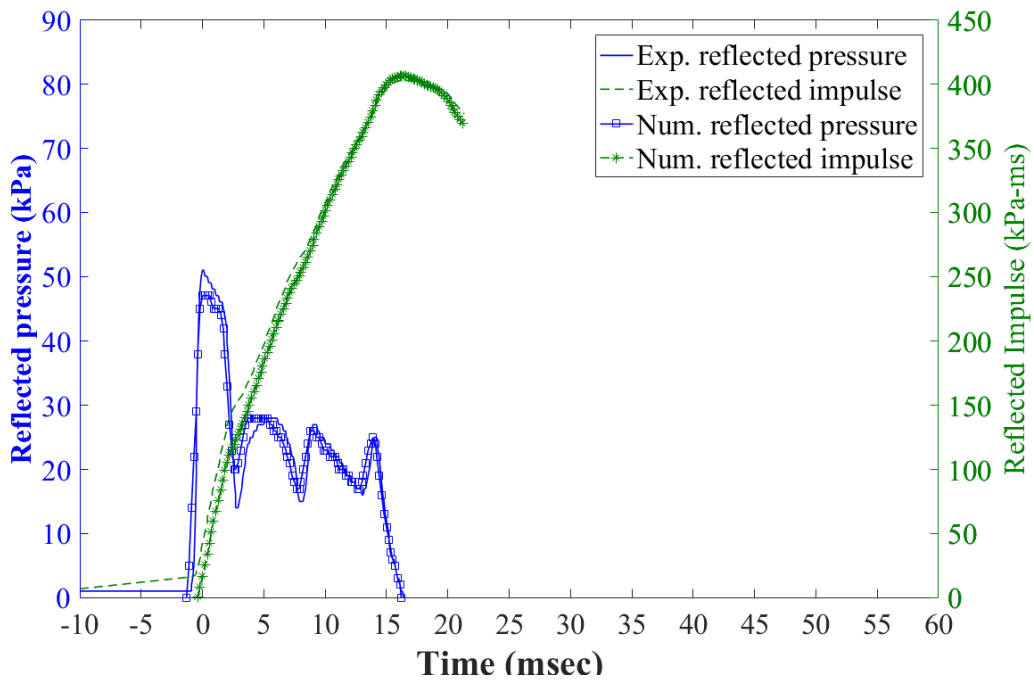


Figure 2.14: Comparison between 2D axisymmetric and 3D simulation results at the tube exit

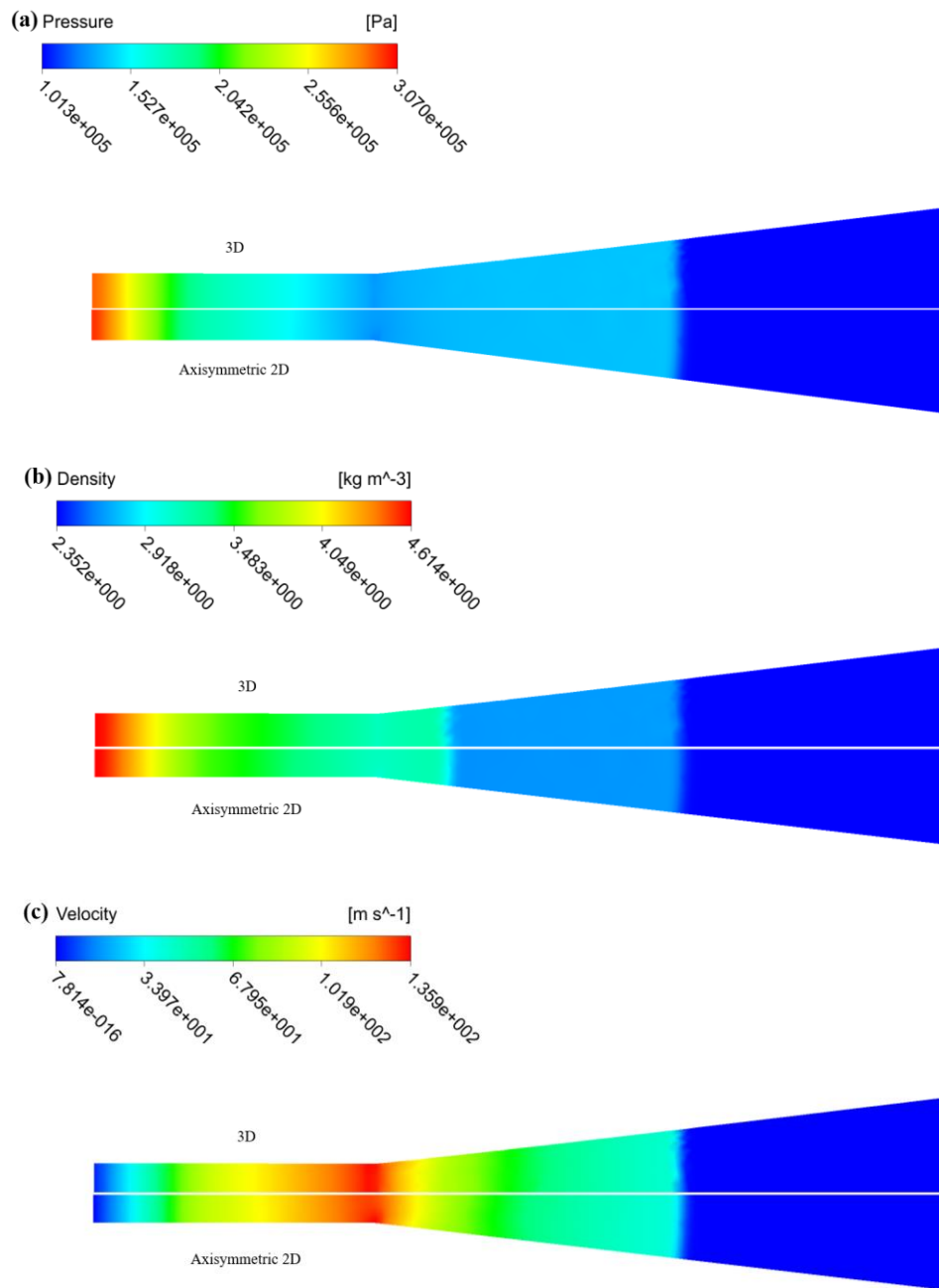


Figure 2.15: Flow properties through conical shock tube after 8.40 ms for 3D simulation (upper half plane) and 2D axisymmetric simulation (lower half plane): (a) Pressure, (b) Density and (c) Axial velocity

CHAPTER 3 : PARAMETRIC ANALYSIS

3.1. INTRODUCTION

The pressure profile on a structural specimen at the exit of a shock tube can be characterized as a function of several shock tube control variables, and thus the resulting blast wave characteristics. The control (independent) variables of a shock tube are the driver section pressure p_{dr} , the driver section length L_{dr} , the driven section length L_{dn} , the circular perforation diameter D_p and the location of perforation L_p . The subsequent (dependent) reflected blast wave characteristics are the peak reflected pressure, the reflected impulse and the positive phase duration. A parametric analysis on each individual variable of the shock tube is performed in this chapter. To investigate the effect of each shock tube control parameter on the blast wave characteristics, this parameter is considered as a variable, while all other shock tube variables are held constant to facilitate direct comparison.

3.2. DRIVER PRESSURE VARIATION

The influence of the driver pressure variation is studied by performing a number of simulations with different driver air pressures ranging from 103 to 6,895 kPa. This range is selected because relatively thick diaphragms are needed to withstand very high pressures in the driver section which would lead to a more complex membrane behavior when the diaphragm is approaching failure (Amman, 1977). The developed 2D axisymmetrical model is used to simulate a conical shock tube with a driver section of 600 mm in diameter. The driver length of this shock tube varies from 2.0 to 4.0 m and the

conical expansion section diameter ranges from 600 mm to 1,414 mm (1/3 scaled structural specimen) over a length of 4.0 m.

Figures 3.1, 3.2 and 3.3 show the influence between the driver section pressure and the different blast wave characteristics; peak reflected pressure, reflected impulse and positive phase duration, respectively. Additional figures, for different conical expansion section lengths (3.0, 5.0 and 6.0 m), are available in Appendix A. As shown in Figure 3.1, the peak reflected pressure increases in a near linearly manner as the driver pressure increases. However, there is no discernible difference in the peak reflected pressure with respect to the driver length, especially when the driver pressure is relatively low. In other words, the peak reflected pressure at the cone end depends only on the pressure inside the driver section and the expansion of the generating shock-wave. The other two blast parameters (i.e. reflected impulse and positive phase duration) are also found to increase as the driver pressure is increased, as shown in Figures 3.2 and 3.3. However, the driver length increase leads to different values of reflected impulse and positive phase duration at the same driver pressure.

3.3. DRIVER LENGTH VARIATION

The influence of driver length on the blast wave parameters is investigated by performing number of simulations with different driver lengths ranging from 1.0 to 4.0 m with an increment of 1.0 m. A conical shock tube with driver section of 600 mm diameter and a driver pressure of 1,379 kPa is used. The conical expansion section diameter of this shock

tube ranges from 600 to 1,414 mm over three different driven lengths of 4.0, 5.0 and 6.0 m.

The relation between the driver section length and blast wave parameters; peak reflected pressure, reflected impulse and positive phase duration are shown in Figure 3.4, 3.5 and 3.6, respectively. Additional figures are provided in Appendix A for different driver pressures (103, 4137 and 6895 kPa). As can be seen in Figure 3.4, the peak reflected pressure increases as the driver length increases until it reaches saturated value and then remains constant. In other words, the reflected rarefaction waves, at the closed end of the driver section, prematurely catch the shock front when the driver length is relatively short (Sundaramurthy & Chandra, 2014). Consequently, a nonlinear decay occurs in the shock front and subsequently the time taken by the reflected rarefaction waves to reach the shock front can be increased as the driver section length is increased. Moreover, the peak reflected pressure shows a variation of 3.0% as the driven section length increases from 4.0 to 6.0 m. This is due to the increase of the expansion cone volume that allows the shock-wave to be minimized at the cone end for the particular shock tube dimensions. As can be seen from Figure 3.5 and 3.6, the reflected impulse and positive phase duration increase as the driver length increases due to the decrease of the decaying time of the overpressure.

3.4. DRIVEN LENGTH VARIATION

The influence of driven length on the blast wave parameters is investigated by performing a number of simulations with conical expansion section diameter ranging from 600 mm

1,414 mm and driven length values varying from 4.0 to 6.0 m with an increment of 1.0 m. A conical shock tube with driver section of 600 mm diameter with 4,137 kPa of pressurized air assumed in the driver section and different driver lengths that vary from 1.0 to 4.0 m.

The relation between the driven section length and blast wave parameters; peak reflected pressure, reflected impulse and positive phase duration are shown in Figure 3.7, 3.8 and 3.9, respectively. Additional figures, for different driver pressures (103, 1379 and 6895 kPa), are shown in Appendix A. Figure 3.7 shows that the peak reflected pressure decrease as the driven length increases with no obvious difference (4.50% maximum difference) when the driver length is varied above 2.0 m. However, the peak reflected pressure shows a large variation (about 21.0%) when the driver length is 1.0 m. As previously mentioned, this variation is due to the short length of the driver and subsequently, the reflected rarefaction waves reach the shock front leading to a high decrease in the peak reflected pressure value. The reflected impulse and positive phase duration both depend on the driver length and the driven lengths, as shown in Figures 3.8 and 3.9, respectively. This is expected as the increase of the driven section decreases the decay time behind the overpressure for the particular shock tube dimensions.

3.5. CIRCULAR PERFORATION DIAMETER AND LOCATION

The influences of the diameter of a circular perforation D_p and perforation location L_p on the blast wave profile are studied using a conical shock tube of 3.0 m length with a driver section of 600 mm diameter and a maximum driver pressure up to 4,137 kPa. The conical

expansion section diameter increases from 600 mm to 1,414 mm over a length of 4.0 m. The perforation diameter varies between 20.0% to 60.0% of the driver diameter, and is located at three different positions along the driven section length (i.e. 20.0, 50.0 and 70.0%). It is worth to mention that the effect of mesh refinement around the perforation is not considered in this study, where the mesh size is kept constant in the whole study to be consistent in the results. The mesh at perforation is very coarse (typically only 2-3 control volumes) across the opening. As such, the detailed behavior of the shock interaction with the opening is not expected to be modeled well.

The relation between perforation diameter, perforation location and blast wave parameters; peak reflected pressure, reflected impulse and positive phase duration are shown in Figure 3.10, 3.11 and 3.12, respectively. Additional figures, for different driver pressures (103 and 6895 kPa), are provided in Appendix A. As can be seen from Figures 3.10 and 3.12, the peak reflected pressure and positive phase duration decrease as the perforation diameter increases. It should be also noted that the blast wave parameters depend on the perforation location. As the perforations are placed away from the diaphragm, the peak reflected pressure is reduced (the value without perforation is 948 kPa); dropped by about 8% when the largest perforation is located at 70% of the driven length, and 22% when it is located at 20% of the driven length. However, the positive phase duration is found to decrease as the perforation is moved away from the driven section end. It is decreased by about 15.0 – 55.0%, from the corresponding value with no perforation (the value without perforation is 63 ms), when the perforation is located close enough (20.0% of the driven section length) from the driven section end. These results

have the same trend as the results obtained by (Thomas, et al., 2004; Ritzel, 2007). According to these results, the disadvantage of compressed-gas shock tubes that simulate explosions at short stand-off distances can be avoided; where the corresponding simulated pressure profiles are characterized by long positive phase durations. Placing a perforation furthest away from the driven section end can lead to a pressure profile with high peak pressure and short positive phase duration.

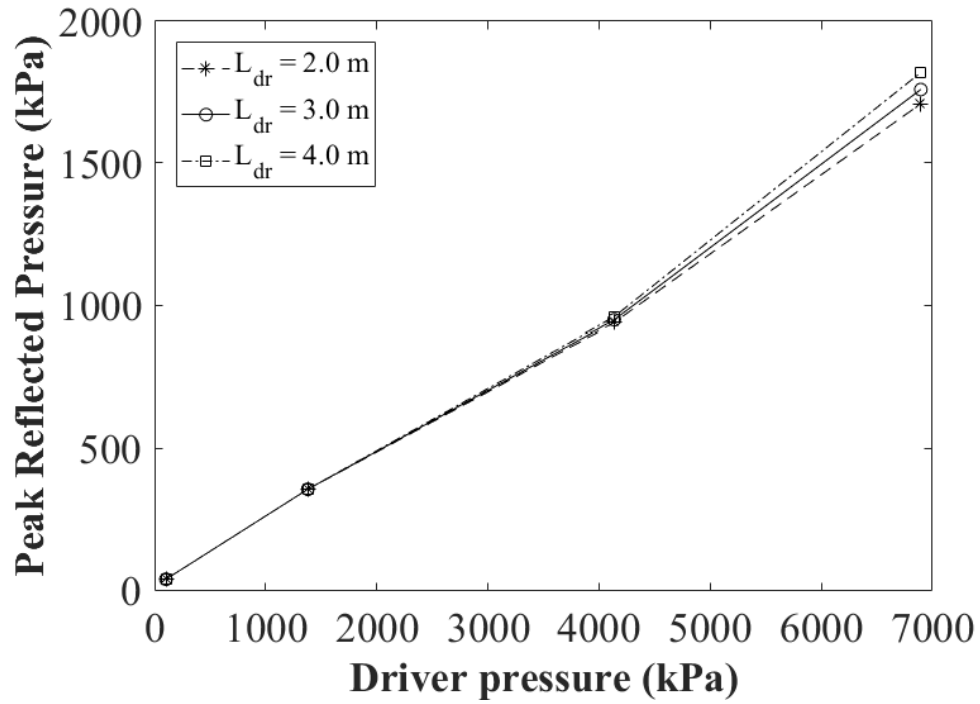


Figure 3.1: Peak reflected pressure versus driver pressure when the driven section length is 4.0 m and the driver section length is changed from 2.0 to 4.0 m

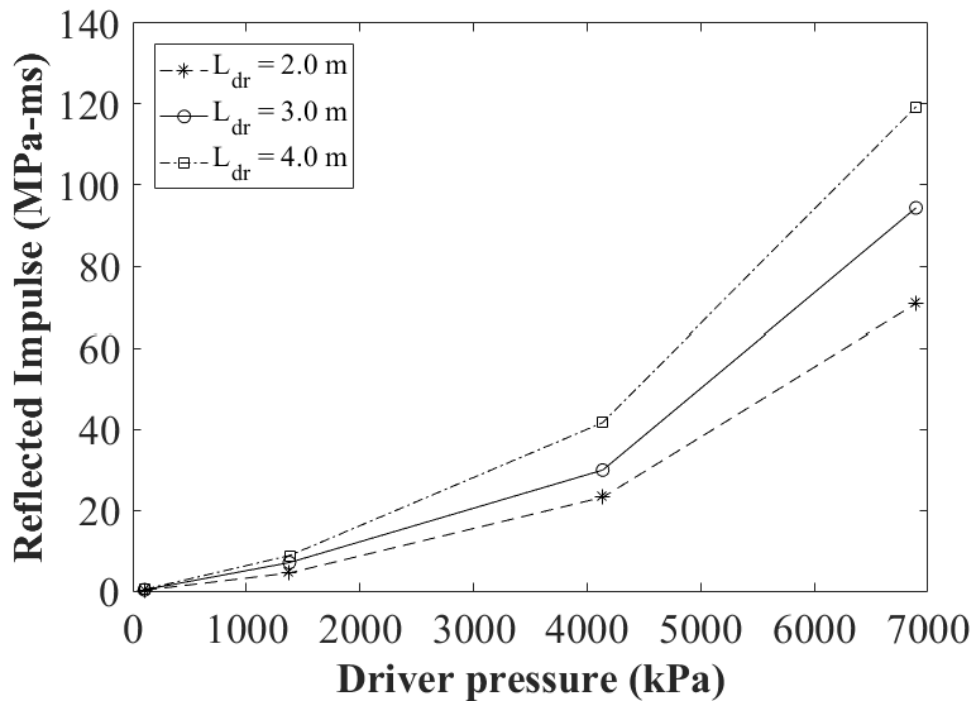


Figure 3.2: Reflected impulse versus driver pressure when the driven section length is 4.0 m and the driver section length is changed from 2.0 to 4.0 m

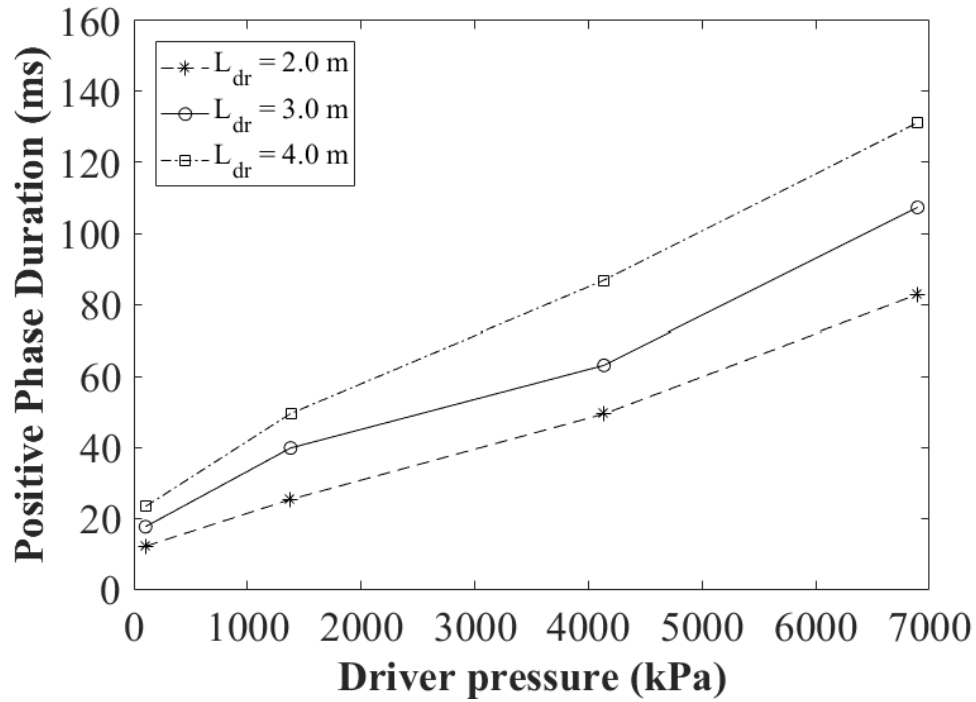


Figure 3.3: Positive phase duration versus driver pressure when the driven section length is 4.0 m and the driver section length is changed from 2.0 to 4.0 m

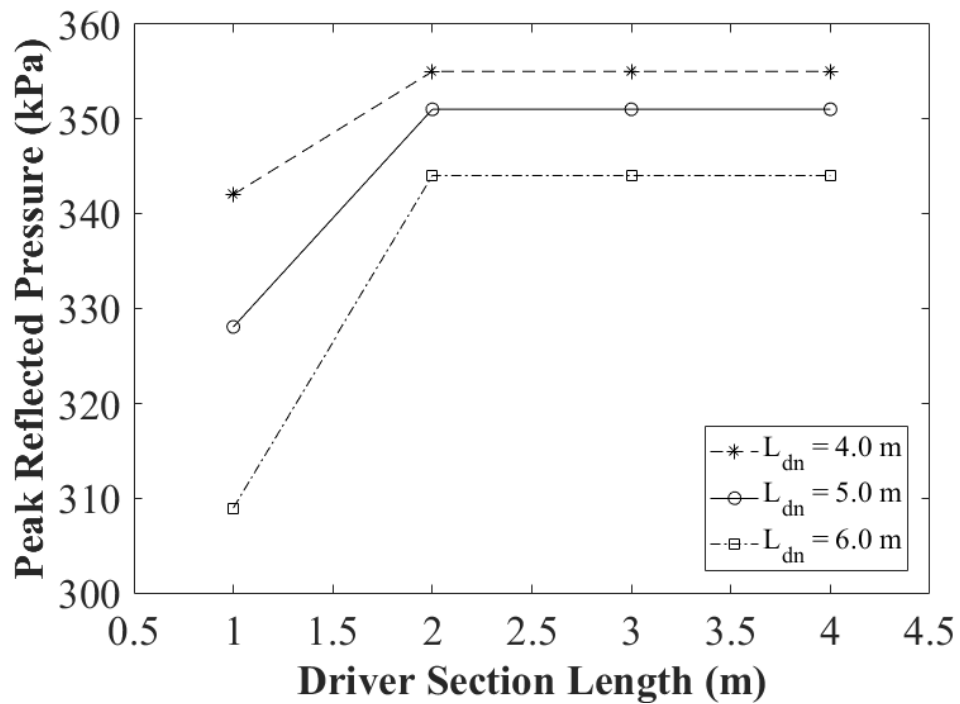


Figure 3.4: Peak reflected pressure versus driver section length when the driver pressure is 1379 kPa and the driven section length is changed from 4.0 to 6.0 m

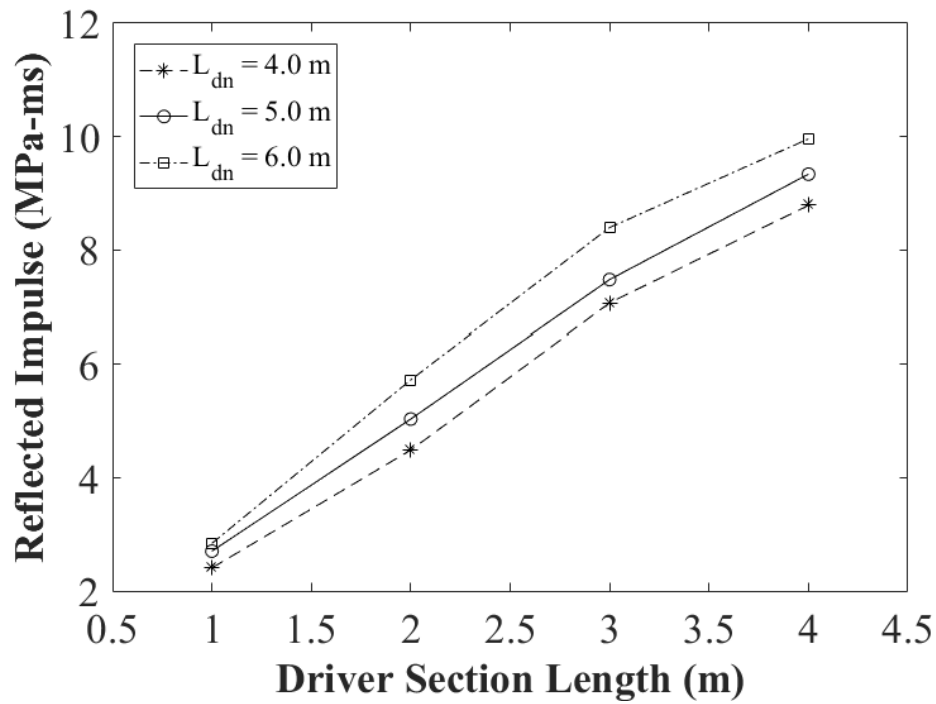


Figure 3.5: Reflected impulse versus driver section length when the driver pressure is 1379 kPa and the driven section length is changed from 4.0 to 6.0 m

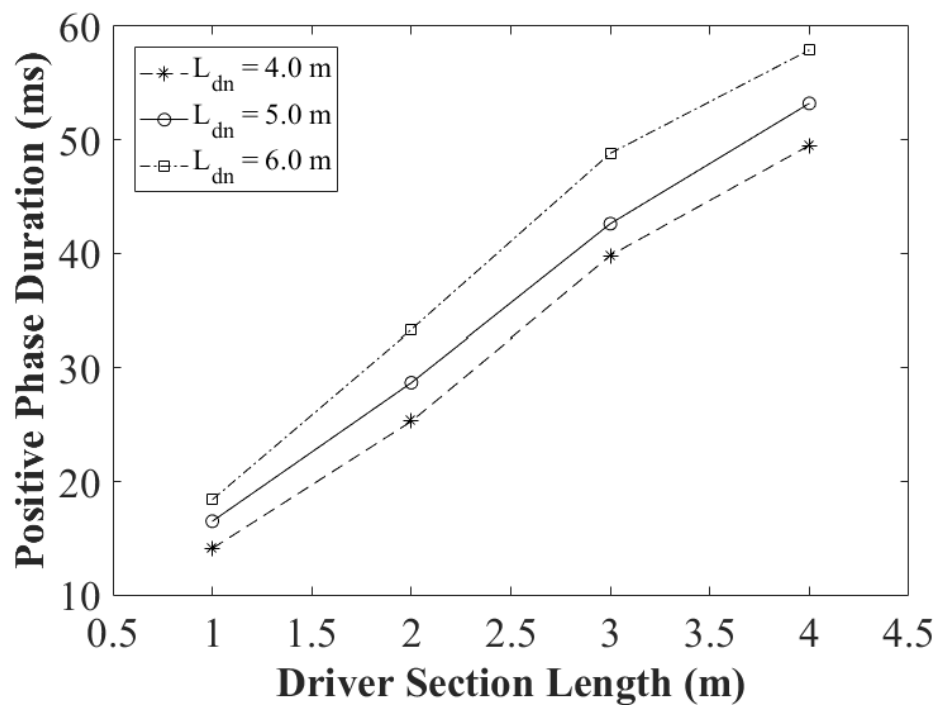


Figure 3.6: Positive phase duration versus driver section length when the driver pressure is 1379 kPa and the driven section length is changed from 4.0 to 6.0 m

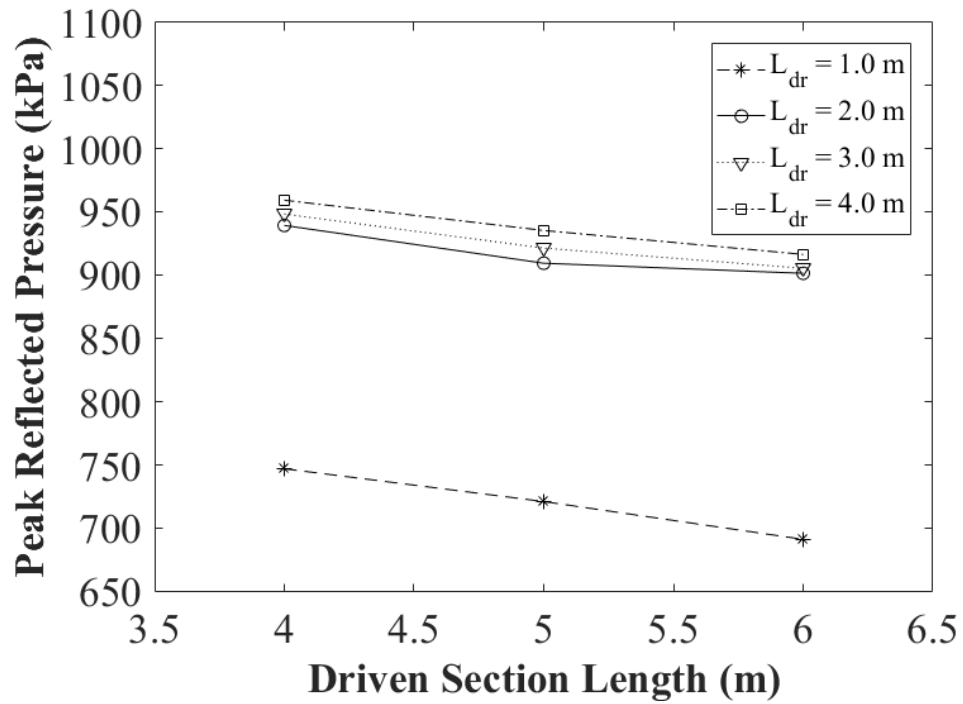


Figure 3.7: Peak reflected pressure versus driven section length when the driver pressure is 4137 kPa and the driver section length is changed from 1.0 to 4.0 m

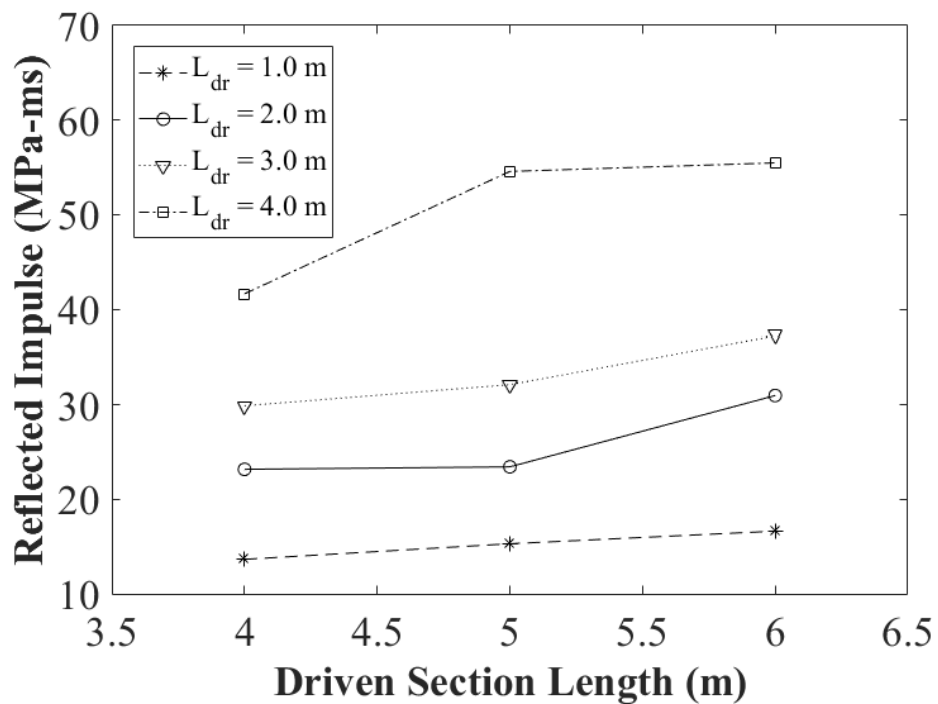


Figure 3.8: Reflected impulse versus driven section length when the driver pressure is 4137 kPa and the driver section length is changed from 1.0 to 4.0 m

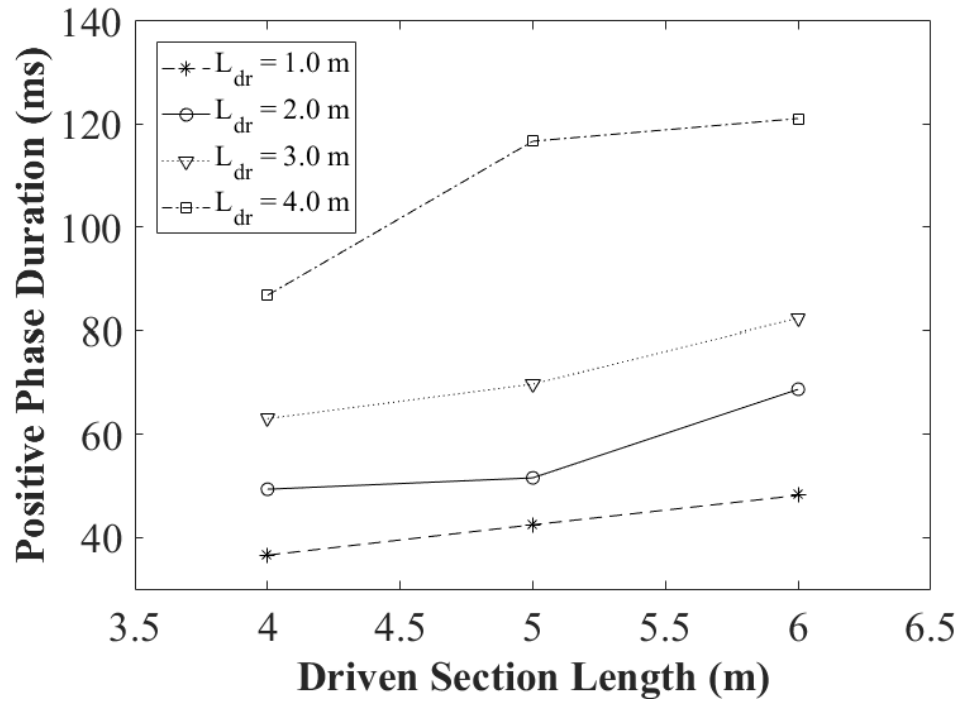


Figure 3.9: Positive phase duration versus driven section length when the driver pressure is 4137 kPa and the driver section length is changed from 1.0 to 4.0 m

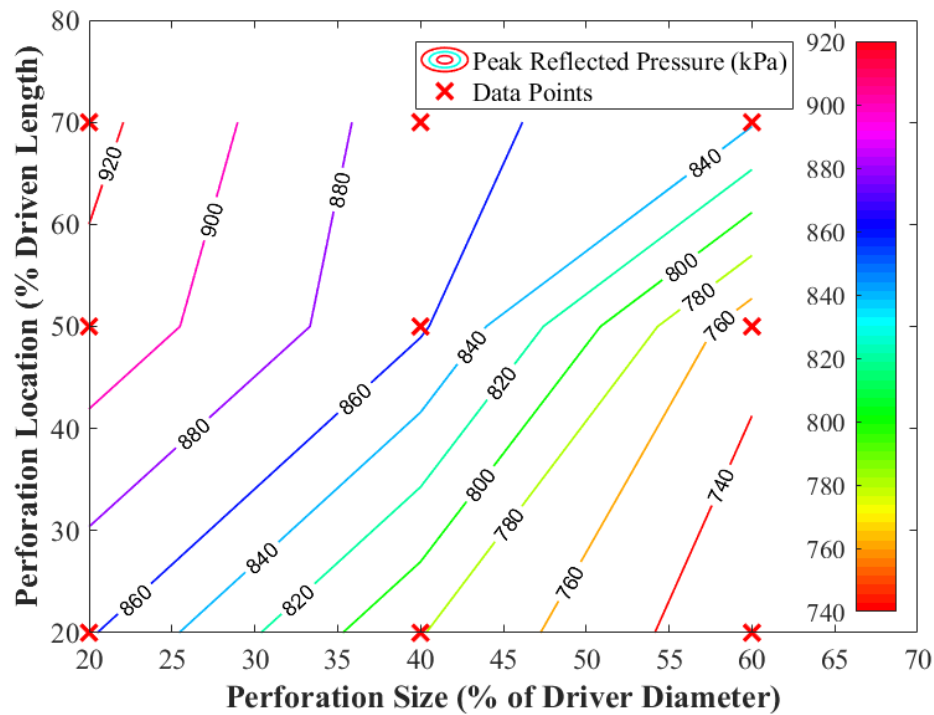


Figure 3.10: Peak reflected pressure contour as function of perforation size and location when the driver pressure is 4137 kPa, driver length is 3.0 m, driven length is 4.0 m

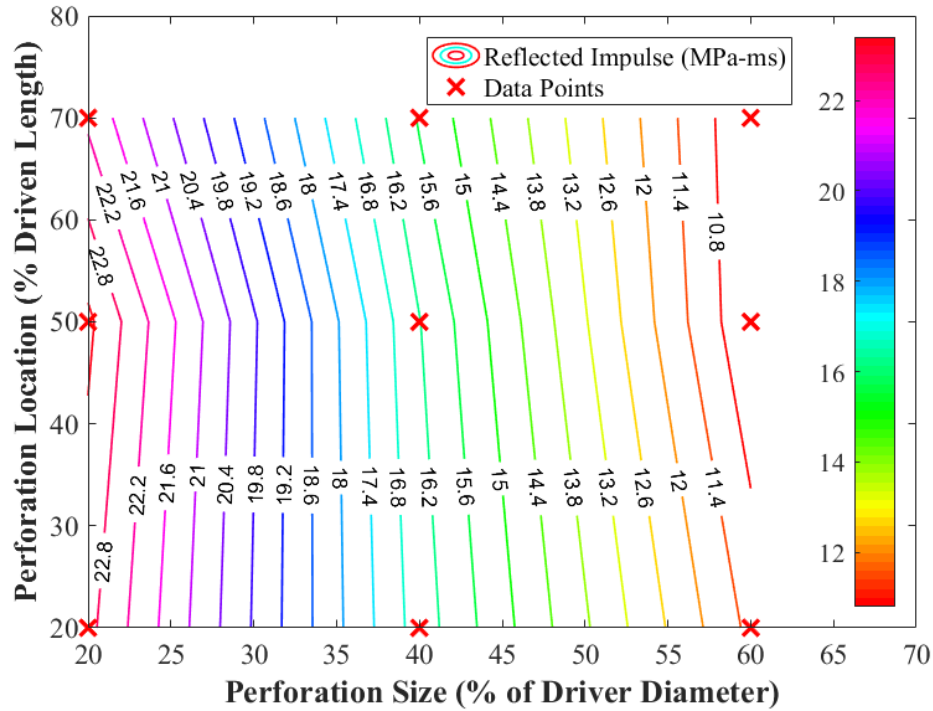


Figure 3.11: Reflected impulse contour as function of perforation size and location when the driver pressure is 4137 kPa, driver length is 3.0 m, driven length is 4.0 m

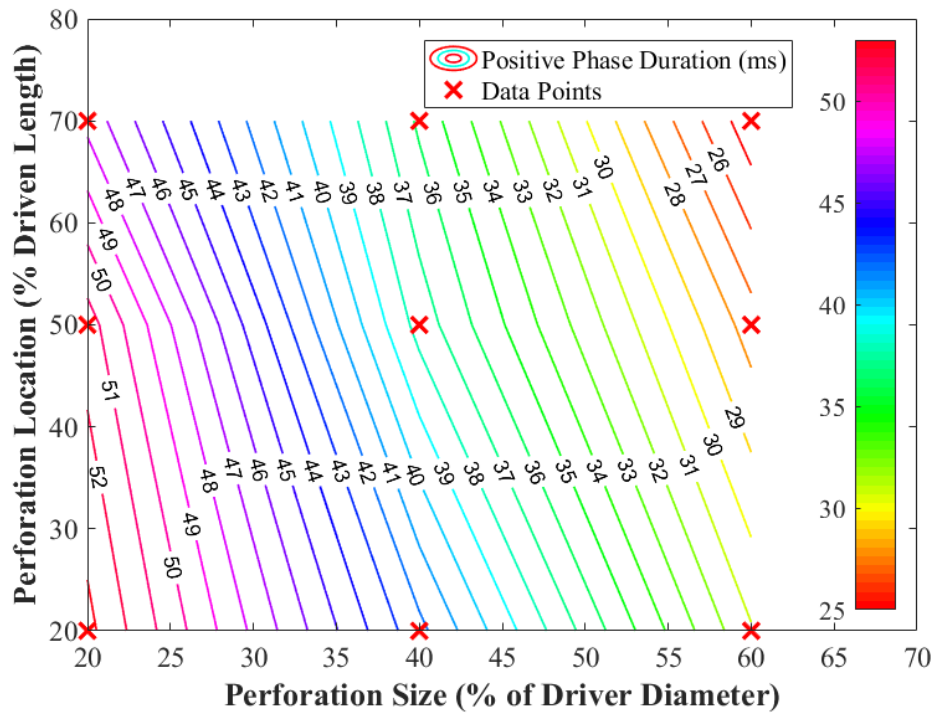


Figure 3.12: Positive phase duration contour as function of perforation size and location when the driver pressure is 4137 kPa, driver length is 3.0 m, driven length is 4.0 m

CHAPTER 4 : PROPOSED CONICAL SHOCK TUBE

4.1. INTRODUCTION

The specifications of the shock tube depend significantly on the particular application or the phenomenon being studied. In this chapter, a large scale, high performance shock tube system with different characteristics is proposed and analyzed to simulate live-explosive generated blast loads on different scaled structural components (1/3 scale, 2/3 scale and full-scale) with different combinations of charge weights and stand-off distances.

4.2. DIMENSIONS

The proposed shock tube consists of a cylindrical driver section, conical expansion section and diaphragm module in between the driver and driven sections. These components are designed according to a parametric study in an effort to generate appropriate blast pressure and impulse combinations similar to those generated by live explosive generated blasts on structural components. The system is being analyzed has a single compressed-air driver with a diameter of 559 mm. Starting with these constraints, a parametric study is performed to reach the optimum pressure profiles over different structural components.

The driver section consists of three different tubes with an inner diameter of 559 mm and 1.0 m, 2.0 m and 4.0 m lengths. The tubes are rated for a maximum pressure of 6895 kPa (10,000 psi). The driver section varies between 1.0 m and 7.0 m, as shown in Figure 4.1. Piezoelectric dynamic pressure sensors will be installed every 1.0 m to measure the incident pressure time history along the driven section. These measurements

are useful in some applications to validate the different parameters controlling the shock wave obtained from the shock tube. In addition, one sensor in each tube will be installed in the driver section in order to record the pressure history. The conical driven section consists of three cones with an angle of 6° . These cones and the driver section are separated by a diaphragm module. As shown in Figure 4.1, the first cone diameter increases from 559 mm to 1,414 mm over a length of 4.0 m that can be used for to 1/3 scale structural component testing. The length of the second cone is 7.0 m and its diameter increases from 1,414 mm to 2,828 mm. The diameter of the third cone increases from 2,828 mm to 4,242 mm over a length 7.0 m similar to the second cone. The entire length of the conical expansion section is 18.0 m while the whole shock tube length is 25.0 m.

4.3. PERFORMANCE

The proposed conical shock tube can simulate the pressure conditions that are typically observed after the detonation of hemispherical and spherical TNT charges, as shown in Figure 4.2. This is only investigated using the driver pressure and length as the two control parameters for simplicity. A number of charge weights and standoff distance combinations are assumed to generate a sufficiently large pressure-impulse database, based on the approximate formulations provided by (Szuladzinski, 2009),

Hemispherical charge:

$$p_r = 13450 Z^{-1.63} \quad \text{for} \quad 0.2 < Z \leq 0.4 \quad (4.1a)$$

$$p_r = 9050 Z^{-2.1} \quad \text{for} \quad 0.4 < Z \leq 1.0 \quad (4.1b)$$

$$p_r = 7625 Z^{-2.4} \quad \text{for} \quad 1.0 < Z \leq 5.0 \quad (4.1c)$$

$$p_r = 880 Z^{-1.3955} \quad \text{for} \quad 5.0 < Z \leq 38.0 \quad (4.1d)$$

$$i_r = 826 \frac{M^{1/3}}{Z^{1.581}} \quad \text{for} \quad 0.2 < Z \leq 0.7 \quad (4.1e)$$

$$i_r = 910 \frac{M^{1/3}}{Z^{1.232}} \quad \text{for} \quad 0.7 < Z \leq 5.0 \quad (4.1f)$$

$$i_r = 681 \frac{M^{1/3}}{Z^{1.0537}} \quad \text{for} \quad 5.0 < Z \leq 39.0 \quad (4.1g)$$

$$\text{where; } Z = \frac{r}{M^{1/3}}$$

The reflected pressure p_r is in kPa, the impulse i_r in kPa-ms, and Z , r and M , are the scaled distance ($\text{m}/\text{kg}^{1/3}$), the distance from the center of the charge to the target (m), and the charge mass (kg), respectively.

Figure 4.2(a) shows of the pressure-impulse of the proposed shock tube over 1.0 m x 1.0 m specimen (driven length is 4.0 m) when the driver pressure and driver length change from 100 to 1,400 kPa (i.e. vertical dotted lines) and 2.0 to 4.0 m (i.e. inclined dotted lines), respectively. While Figure 4.2(b) shows the peak reflected pressures and impulses from hemispherical TNT charges with mass ranging from 50 to 20,000 kg (i.e. thick solid lines) and standoff distances from 30 to 100 m (i.e. thin solid lines) which can be simulated by the proposed design, according to Equations 4.1. The performance of the proposed shock tube (dashed lines) is mapped in terms of equivalent hemispherical blast scenarios (charge weight and standoff distance combinations, solid lines), as can be seen in Figure 4.3. For example, if a 500 kg charge (TNT equivalent) at 40 m standoff distance

(90 kPa reflected pressure, 1000 kPa-ms impulse) scenario is to be simulated, according to Figure 4.3, a 2.0 m long shock tube driver must be pressurized to 300 kPa.

To show the effectiveness of the conical shock tube proposed in this study, Figure 4.4(a) shows the performance of these shock tubes over 2.0 m x 2.0 m specimens. The driver pressure and length change from 689 to 6895 kPa and 2.0 to 7.0 m, respectively, that can produce reflected pressure from 90 to 600 kPa and impulse from 700 to 50,000 kPa-ms. The performance of the University of Ottawa shock tube (Lloyd, 2010) as a function of driver pressure and length is shown in Figure 4.4(b), to facilitate a direct comparison. As can be seen from Figures 4.4(a and b), different stronger blast scenarios can be simulated by using the proposed shock tube in comparison to those using the University of Ottawa shock tube. A blast scenario of 1,000 kg charge mass with a 50 m standoff distance (90 kPa reflected pressure and 1,421 kPa-ms reflected impulse) is the strongest blast scenario that can be achieved using the University of Ottawa shock tube (Figure 4.4(a)). However, the proposed shock tube can generate up to 600 kPa reflected pressure and a 52,000 kPa-ms reflected impulse (Figure 4.4(b)).

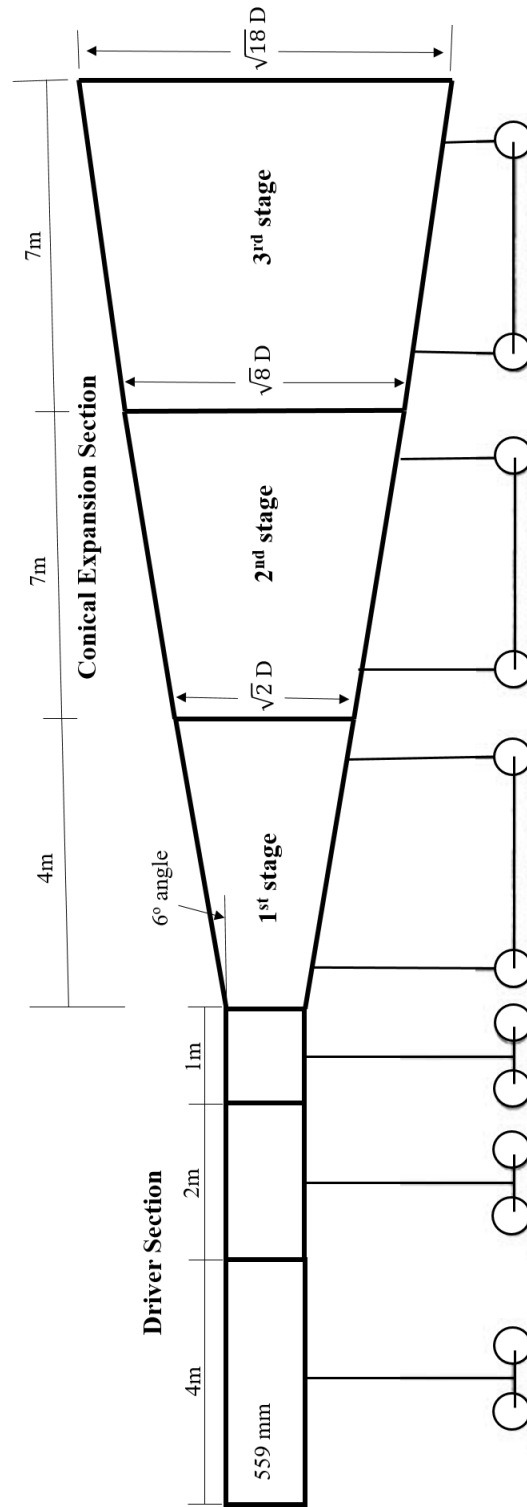
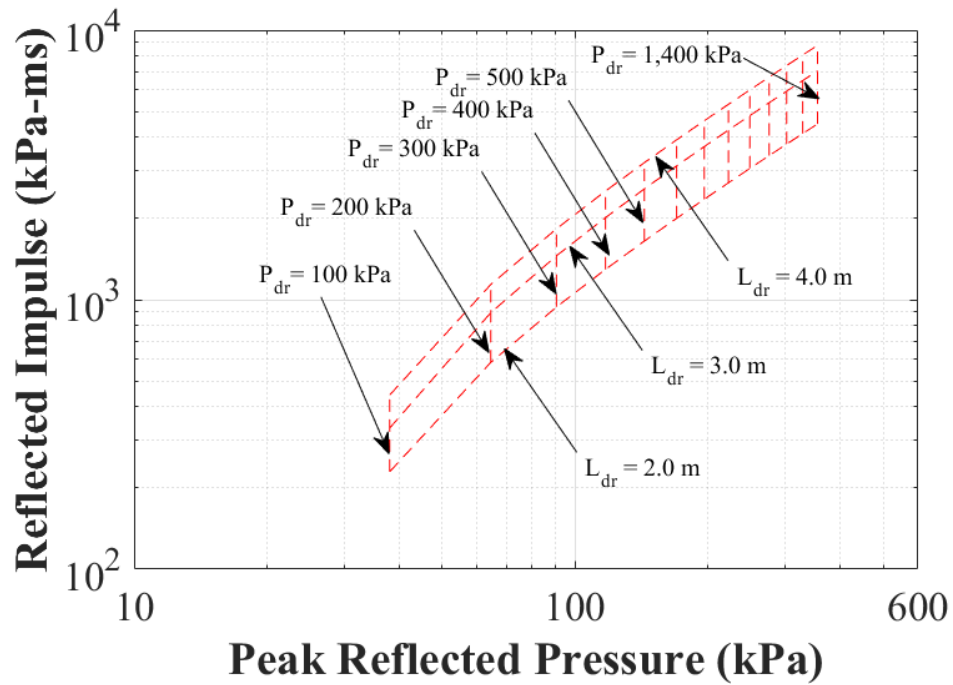


Figure 4.1: The designed shock tube

(a)



(b)

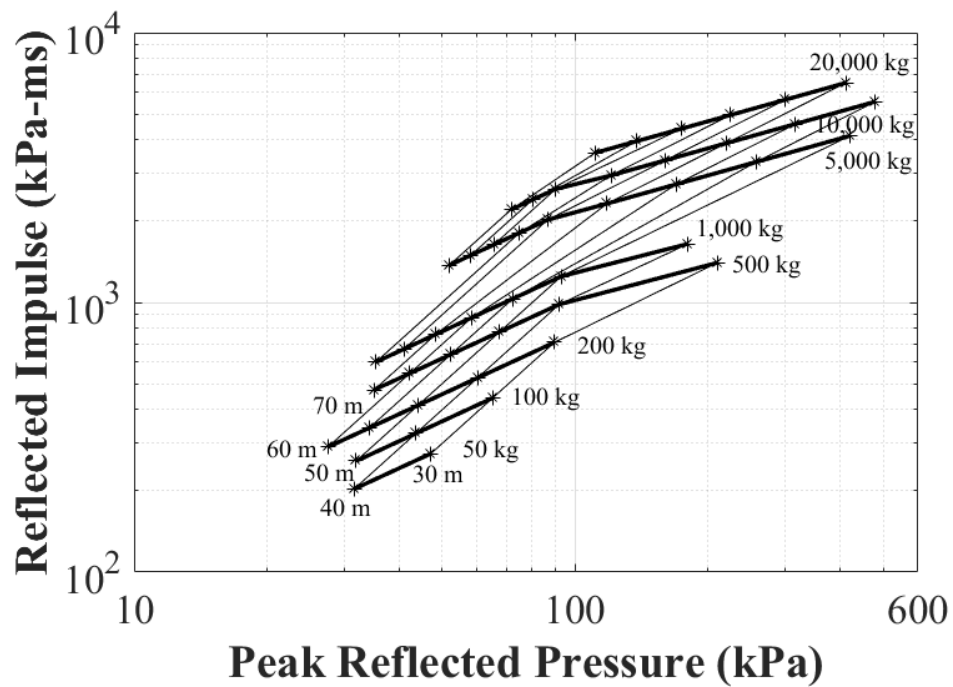


Figure 4.2: The pressure-impulse relation: (a) the performance of the proposed shock tube as function of driver pressure and length (over 1.0 m x 1.0 m specimen), (b) the simulated equivalent hemispherical TNT charges scenarios

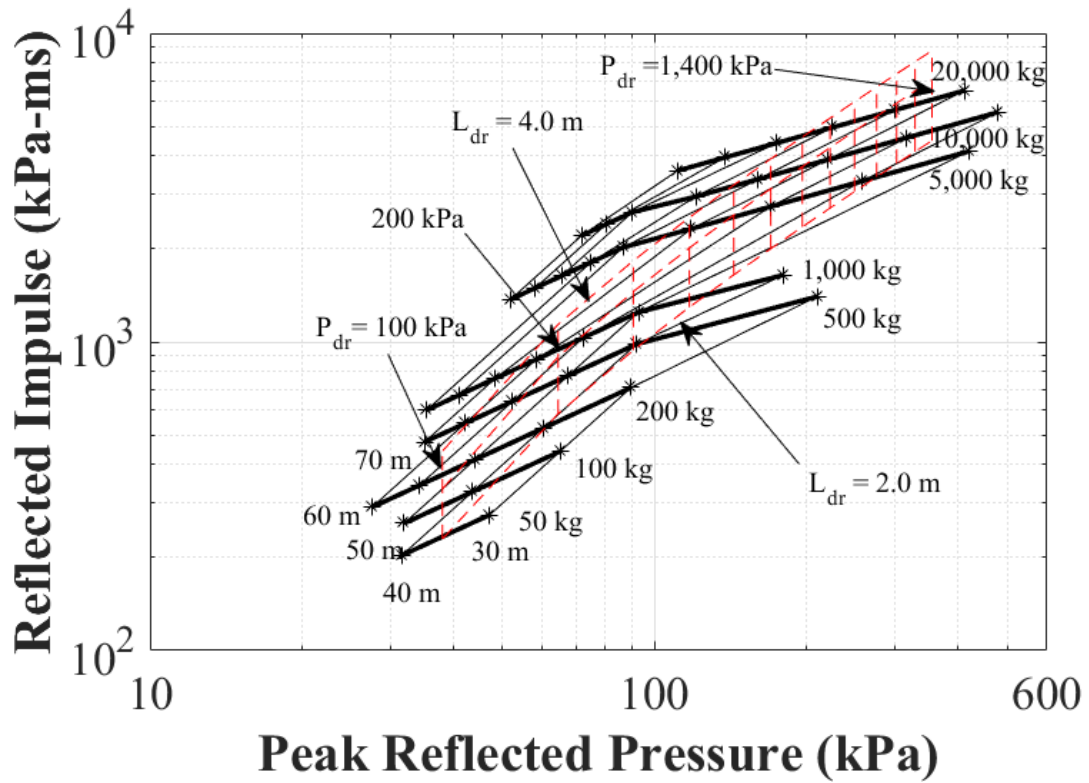
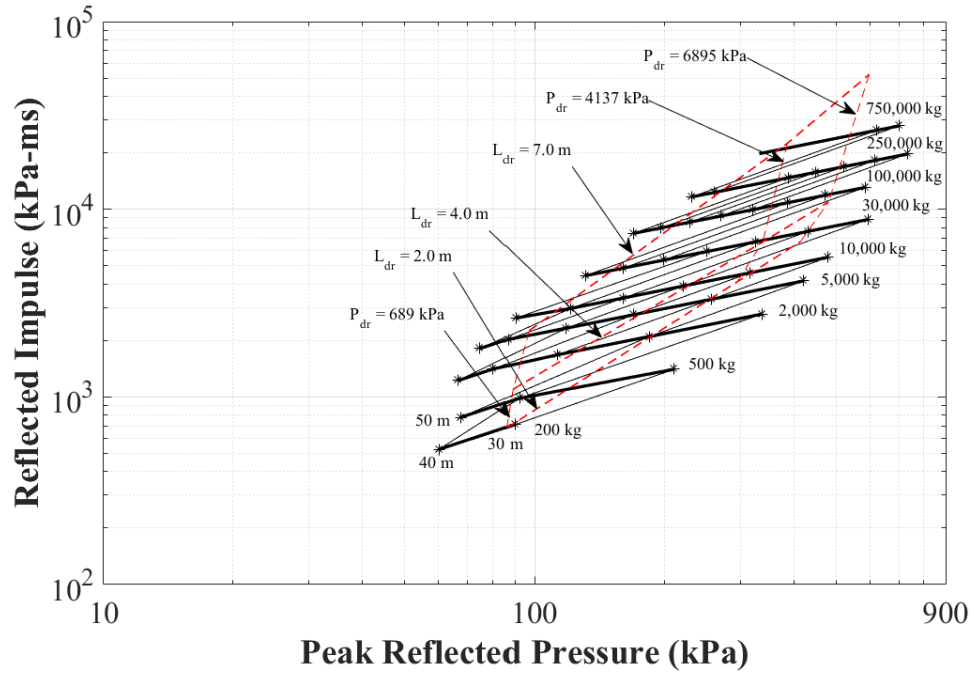


Figure 4.3: Mapping of the pressure-impulse performance of the proposed shock tube (dashed lines) in terms of equivalent hemispherical TNT charges scenarios (charge weight and standoff distance combinations, solid lines)

(a)



(b)

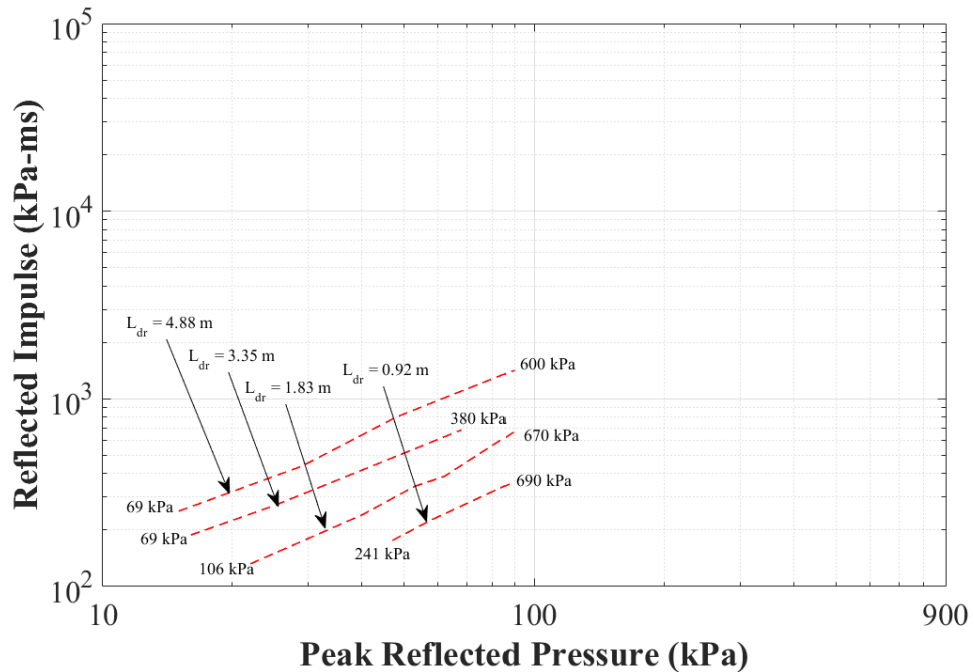


Figure 4.4: Pressure-impulse performance: (a) The proposed shock tube (dashed lines) if the specimen is 2.0 m x 2.0 m in terms of equivalent blast loads scenarios (charge weight and standoff distance combinations, solid lines), (b) the University of Ottawa shock tube performance (Lloyd, 2010)

CHAPTER 5 : CONCLUSIONS AND FUTURE RECOMMENDATIONS

5.1. CONCLUSIONS

An extensive literature review on the available blast shock tubes and their applications, findings, and constraints were presented. In addition, a literature review on shock tube simulation approaches and the influence of perforation on shock tube performance were presented. Subsequently, this study focused on developing numerical models (i.e. 2D & 3D) to evaluate the capabilities of a 559 mm diameter shock tube to simulate several explosion scenarios. Finally, an extensive parametric analysis is used to evaluate the shock tube dimensions in order to simulate a wide range of TNT masses at different stand-off distances (i.e. scaled distances).

Based on the numerical simulations carried out in this study, the results of a 3D unsteady flow simulation were found to be similar to those generated using a relatively simple 2D axisymmetrical flow simulation. However, for shock tubes with square-pyramid expansion sections that cannot be simplified using 2D axisymmetrical models, 3D models would be required to simulate their performance. Nonetheless, both models (i.e. 2D and 3D) show good agreement with relevant experimental results in terms of the pressure, density, and velocity.

In general, the study explored how the shock tube control variables (driver section pressure p_{dr} , driver section length L_{dr} , driven section length L_{dn} , circular perforation diameter D_p and location of perforation L_p) influence the blast wave parameters (peak

reflected pressure, reflected impulse and positive phase duration). Key findings of this analysis for the particular shock tube dimensions are as follows:

- The peak reflected pressure increases as: (1) the driver pressure increases, (2) the driven length decreases, (3) the perforation diameter decreases and (4) the perforations are located further away from the exit (closer to the diaphragm). The influence of the driver length is not discernible. However, for a short driver length, the pressure is changed due to the shock front interaction with the reflected rarefaction waves.
- The positive phase duration increases as: (1) the driver pressure increases, (2) the driven length increases, (3) the driven length increases, (4) the perforation diameter decreases and (5) the perforations are located closer to the exit (furthest away from the diaphragm). Although shock tubes provide several advantages—including safety, cost-effectiveness, and repeatability—they are not suited for short standoff distances because they generate excessively large positive phase durations compared to field test measurements. However, perforations located closer to the diaphragm can be used to address this issue in order to simulate TNT charges at short stand-off distances.

Finally, the proposed shock tube can simulate hemispherical TNT charges—with masses ranging from 50 to 20,000 kg and detonated at standoff distances ranging from 30 to 100 m on a 1.0 m x 1.0 m specimen. When the specimen is increased to 2.0 m x 2.0 m, blast scenarios with large masses with long standoff distances (up to 740,000 kg charge weight at 220 m standoff distance) can be simulated. The performance of

the proposed shock tube shows higher ranges of blast loads that can be simulated using the University of Ottawa shock tube.

5.2. FUTURE RECOMMENDATIONS

There are still several challenges that need to be investigated in future research, including:

- Investigating the 2D axisymmetric model implemented in the FLUENT software using different gases (e.g. Helium or Nitrogen).
- Optimization of the driver section diameter that could lead to shortening the expansion section, with consequent higher overpressure at the exit.
- Investigating the use of perforations with different configurations to reduce the positive phase duration, without causing prematurely decaying in the overpressure.
- Studying the influence of mesh sensitivity on the performance of shock tubes with perforations.
- Studying the influences of shock tube control parameters on the negative phase duration.

APPENDIX A

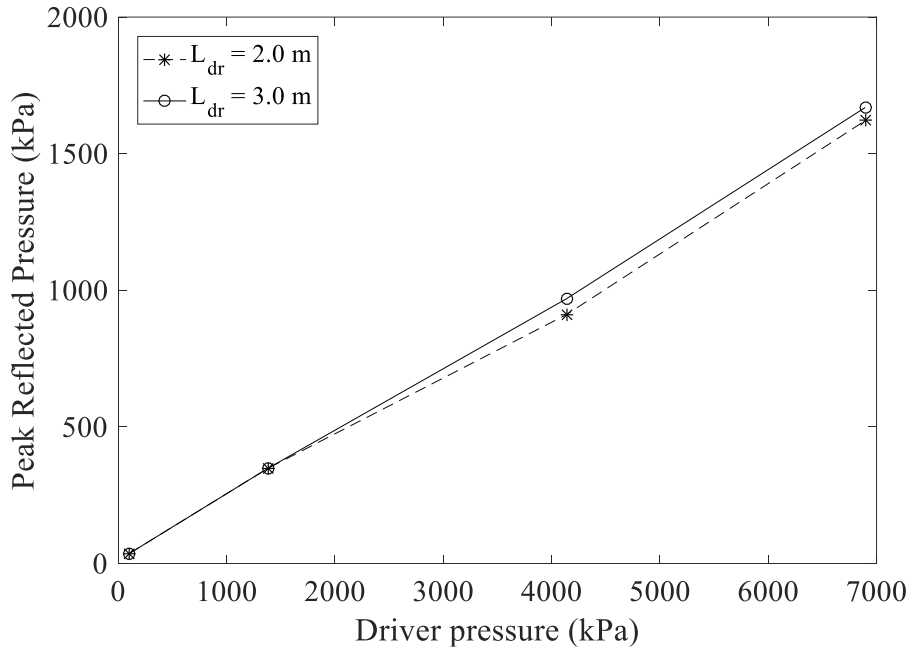


Figure A.1: Peak reflected pressure versus driver pressure when the driven section length is 3.0 m and the driver section length is changed from 2.0 to 3.0 m

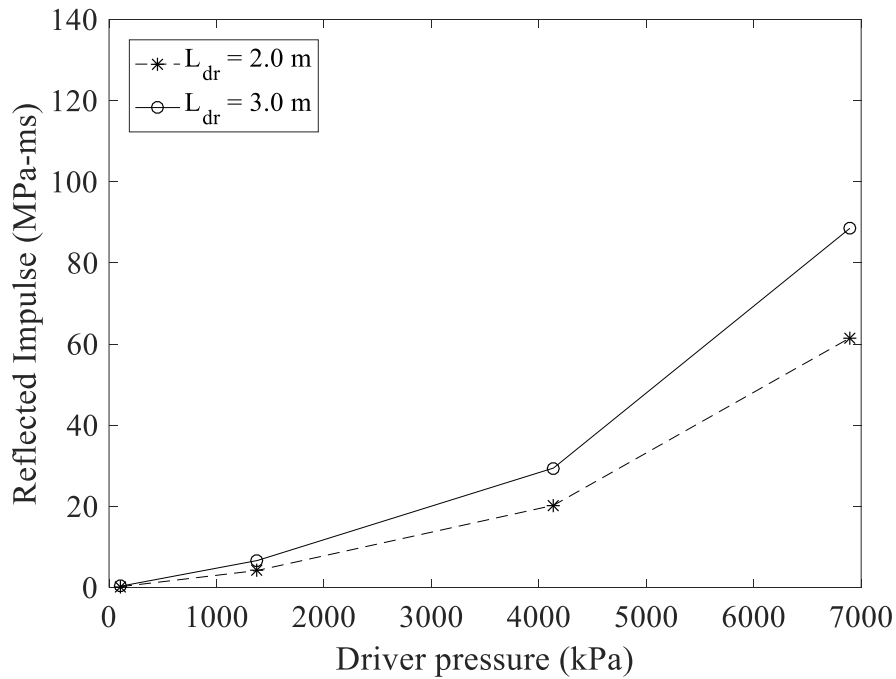


Figure A.2: Reflected impulse versus driver pressure when the driven section length is 3.0 m and the driver section length is changed from 2.0 to 3.0 m

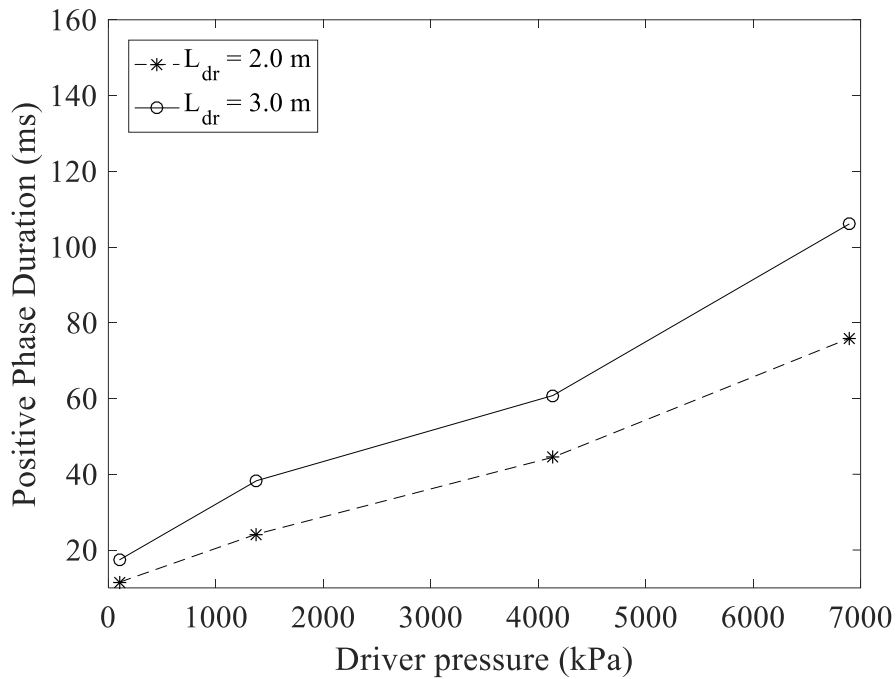


Figure A.3: Positive phase duration versus driver pressure when the driven section length is 3.0 m and the driver section length is changed from 2.0 to 3.0 m

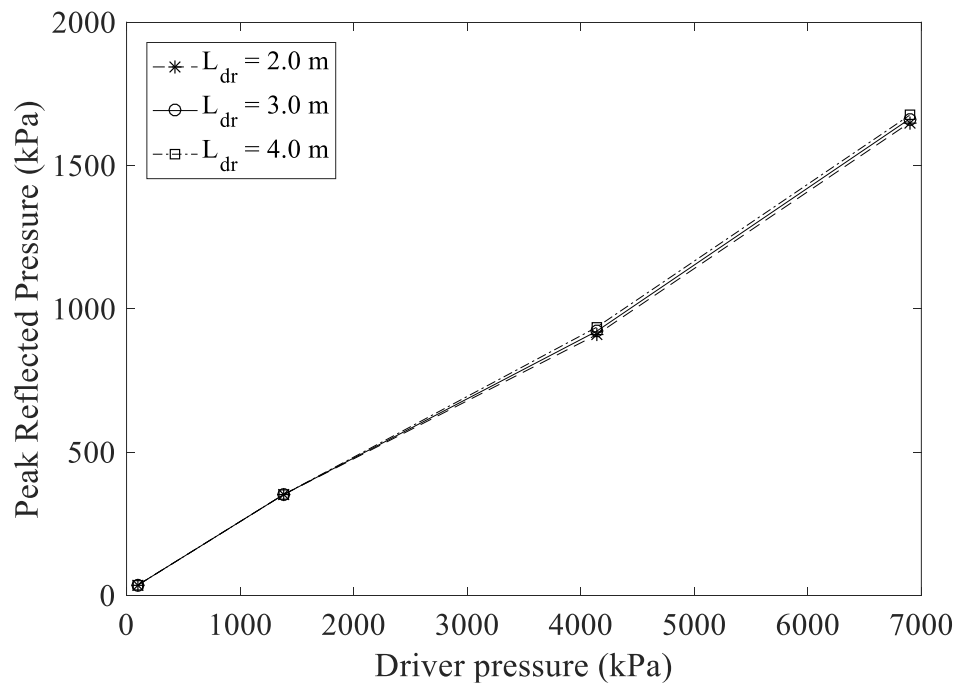


Figure A.4: Peak reflected pressure versus driver pressure when the driven section length is 5.0 m and the driver section length is changed from 2.0 to 4.0 m

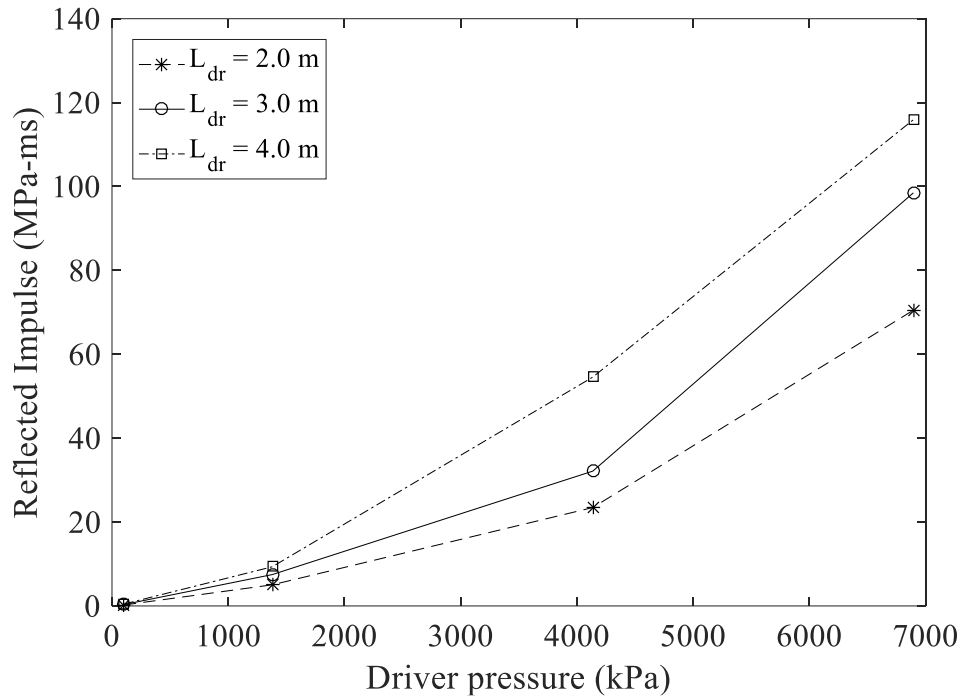


Figure A.5: Reflected impulse versus driver pressure when the driven section length is 5.0 m and the driver section length is changed from 2.0 to 4.0 m

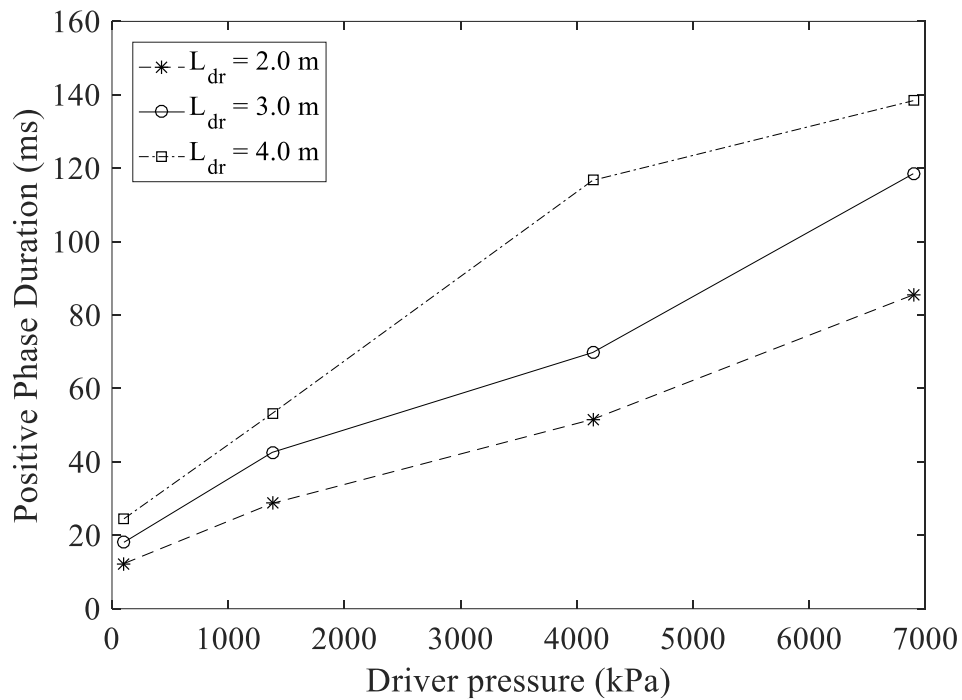


Figure A.6: Positive phase duration versus driver pressure when the driven section length is 5.0 m and the driver section length is changed from 2.0 to 4.0 m

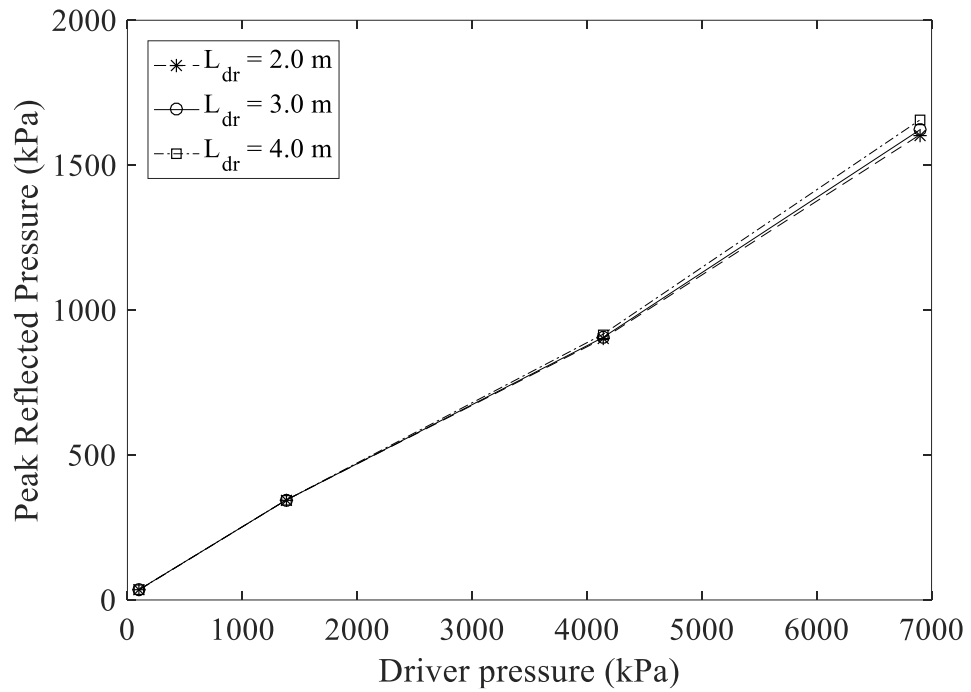


Figure A.7: Peak reflected pressure versus driver pressure when the driven section length is 6.0 m and the driver section length is changed from 2.0 to 4.0 m

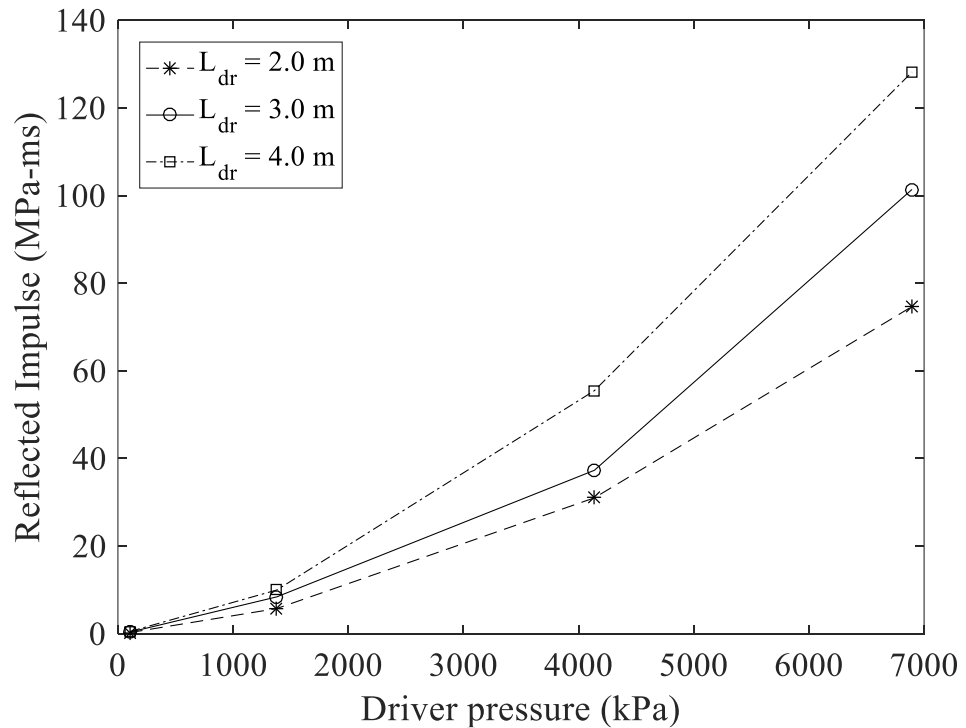


Figure A.8: Reflected impulse versus driver pressure when the driven section length is 6.0 m and the driver section length is changed from 2.0 to 4.0 m

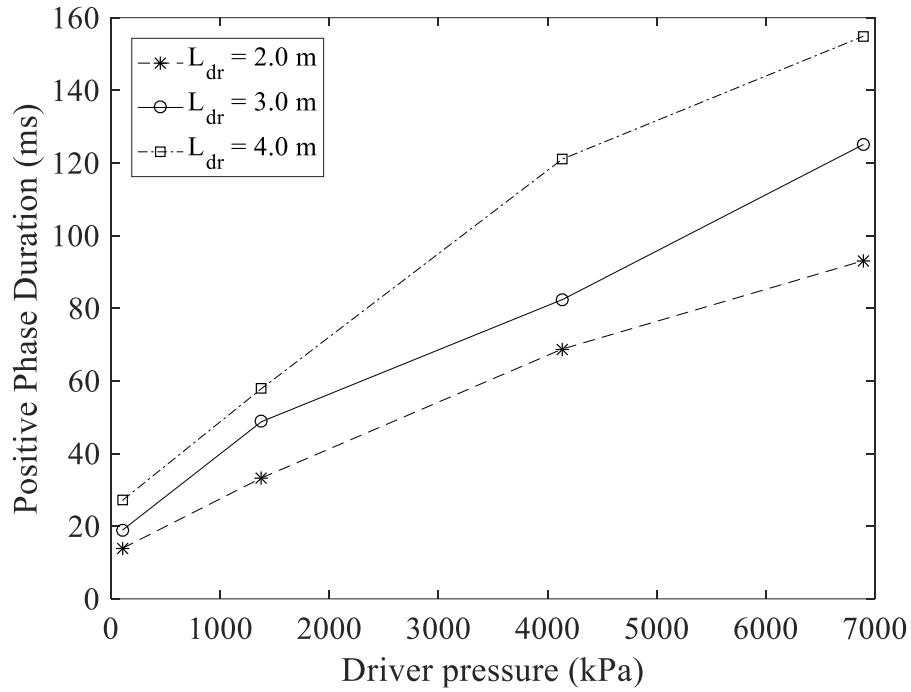


Figure A.9: Positive phase duration versus driver pressure when the driven section length is 6.0 m and the driver section length is changed from 2.0 to 4.0 m

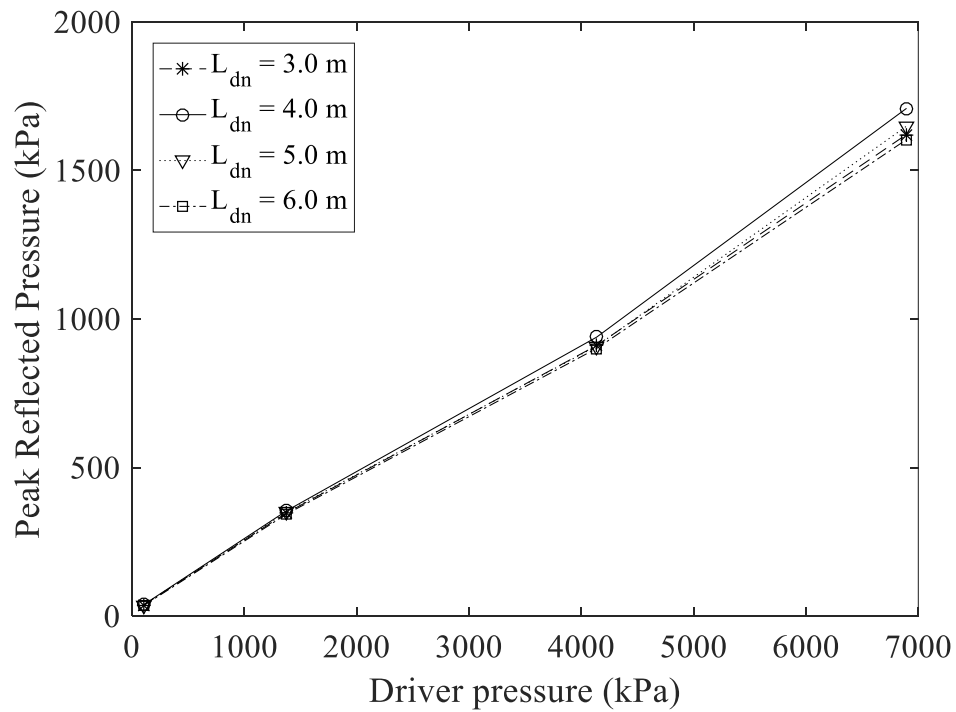


Figure A.10: Peak reflected pressure versus driver pressure when the driver section length is 2.0 m and the driven section length is changed from 3.0 to 6.0 m

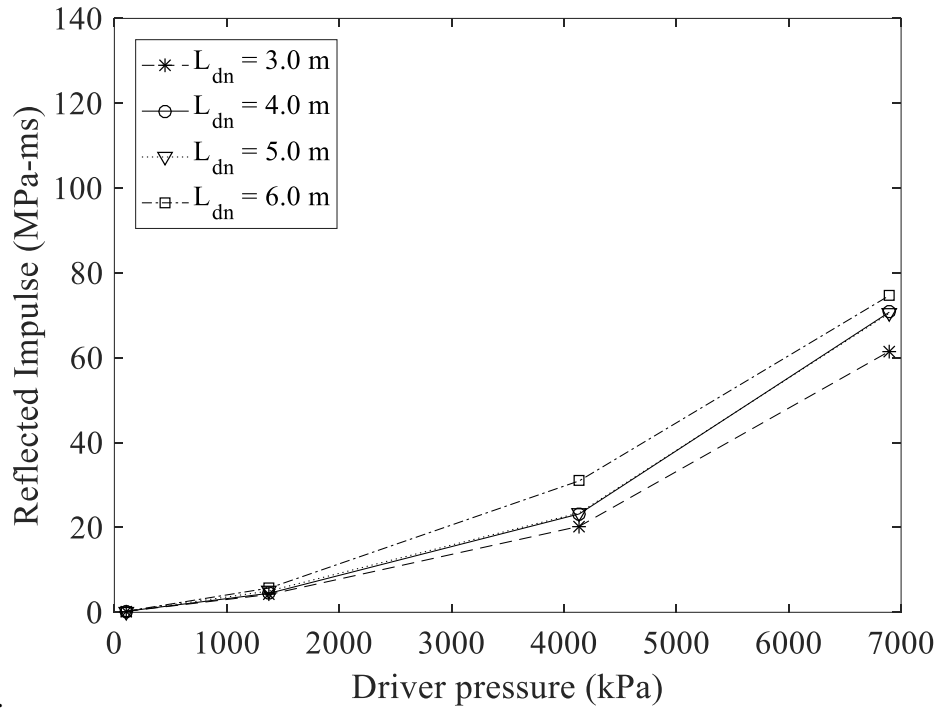


Figure A.11: Reflected impulse versus driver pressure when the driver section length is 2.0 m and the driven section length is changed from 3.0 to 6.0 m

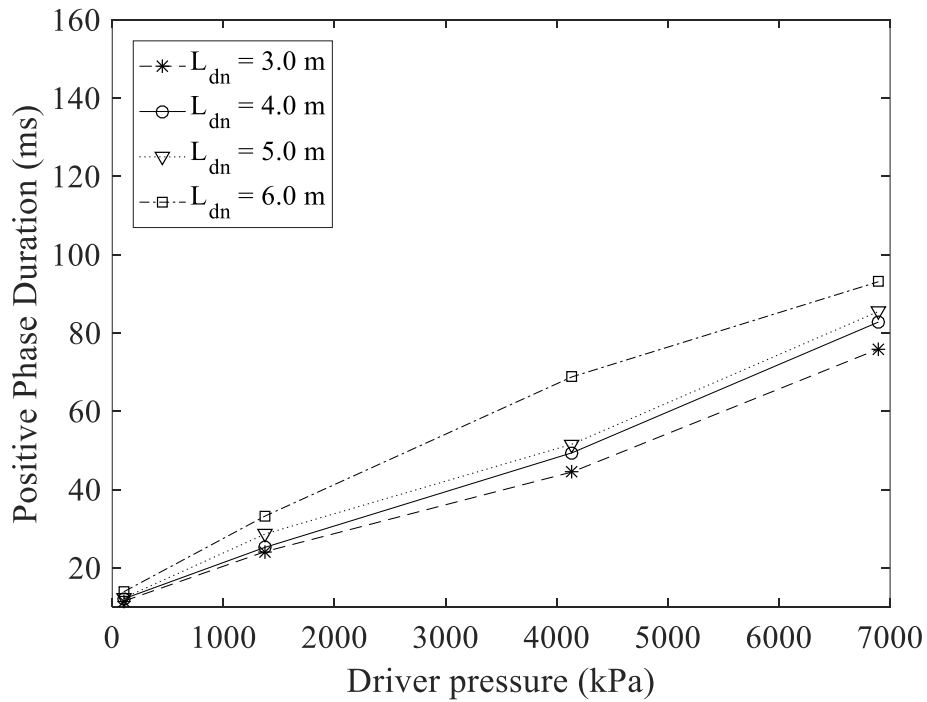


Figure A.12: Positive phase duration versus driver pressure when the driver section length is 2.0 m and the driven section length is changed from 3.0 to 6.0 m

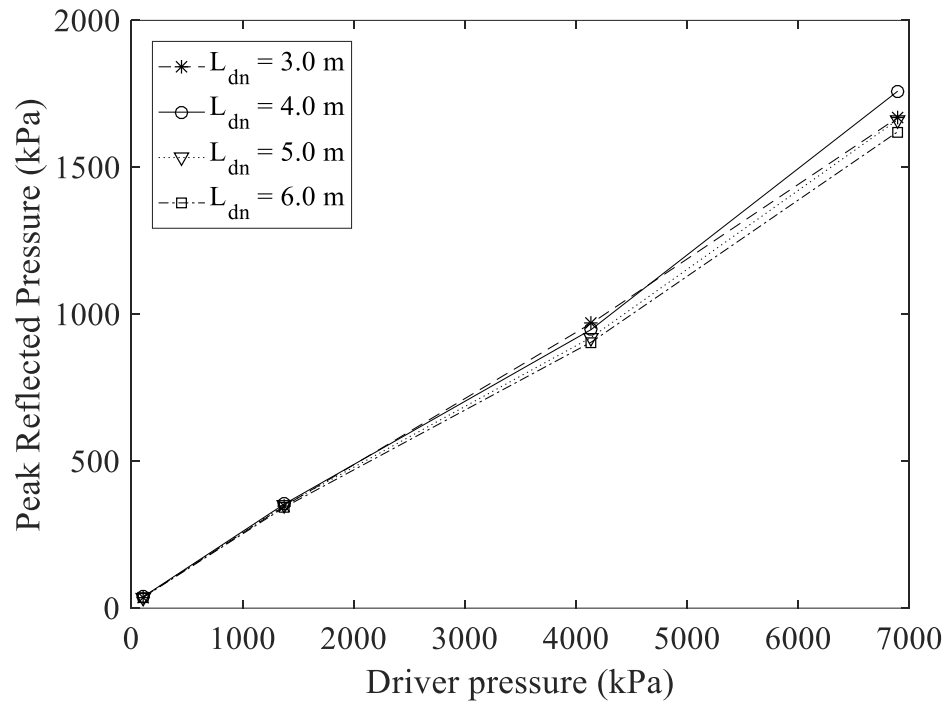


Figure A.13: Peak reflected pressure versus driver pressure when the driver section length is 3.0 m and the driven section length is changed from 3.0 to 6.0 m

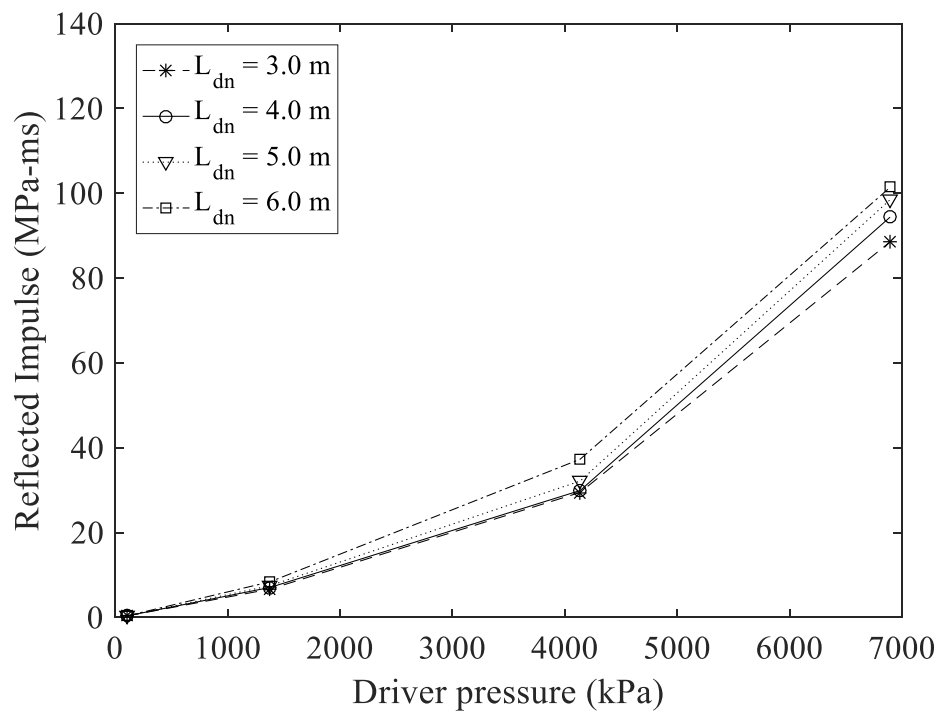


Figure A.14: Reflected impulse versus driver pressure when the driven section length is 3.0 m and the driver section length is changed from 3.0 to 6.0 m

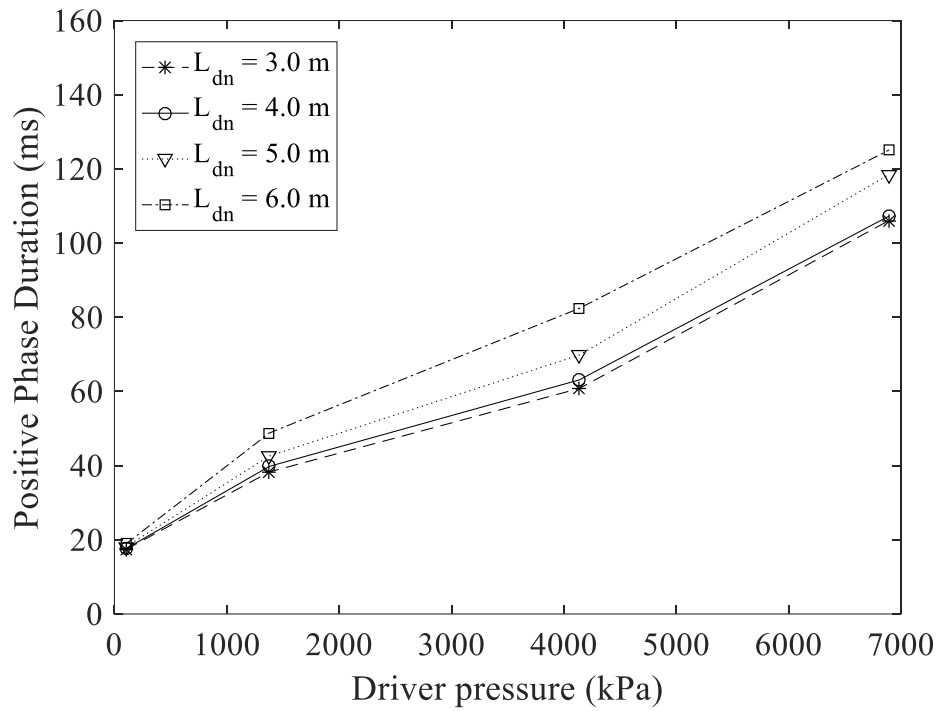


Figure A.15: Positive phase duration versus driver pressure when the driver section length is 3.0 m and the driven section length is changed from 3.0 to 6.0 m

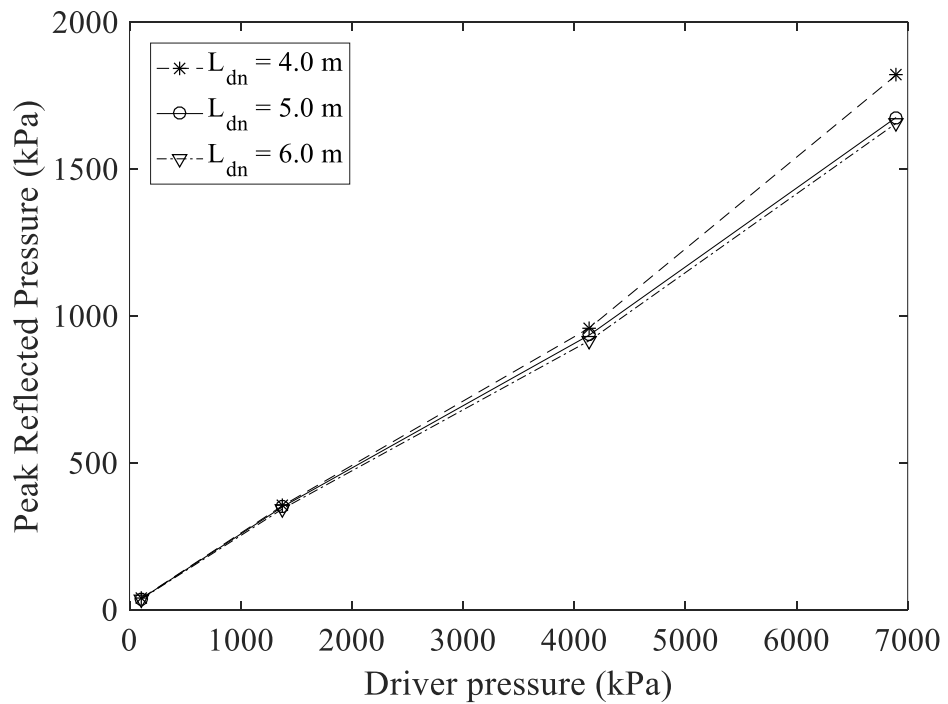


Figure A.16: Peak reflected pressure versus driver pressure when the driver section length is 4.0 m and the driven section length is changed from 4.0 to 6.0 m

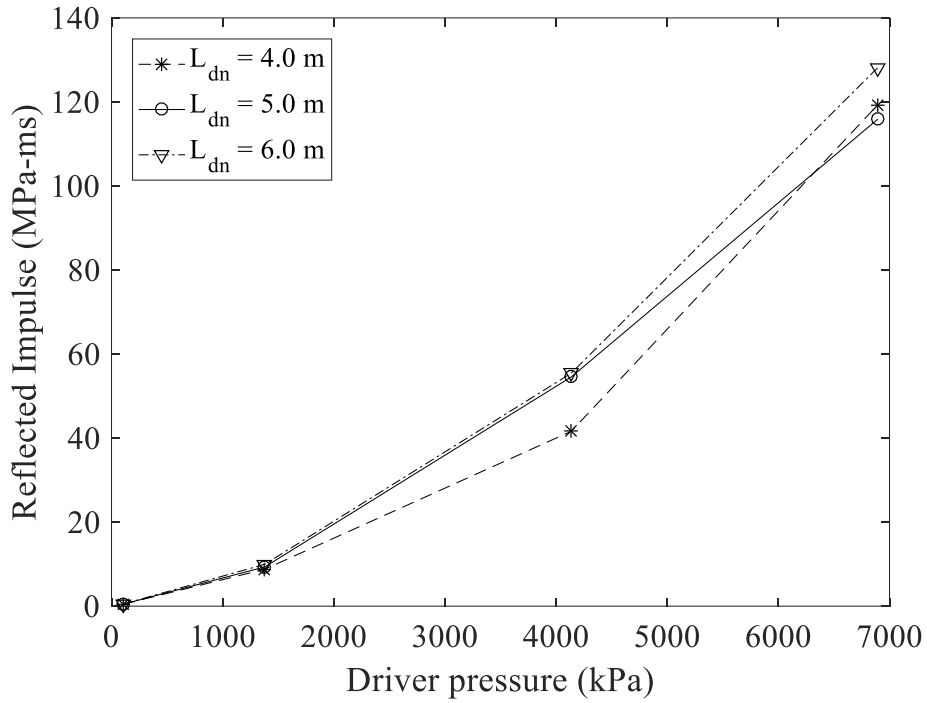


Figure A.17: Reflected impulse versus driver pressure when the driver section length is 4.0 m and the driven section length is changed from 4.0 to 6.0 m

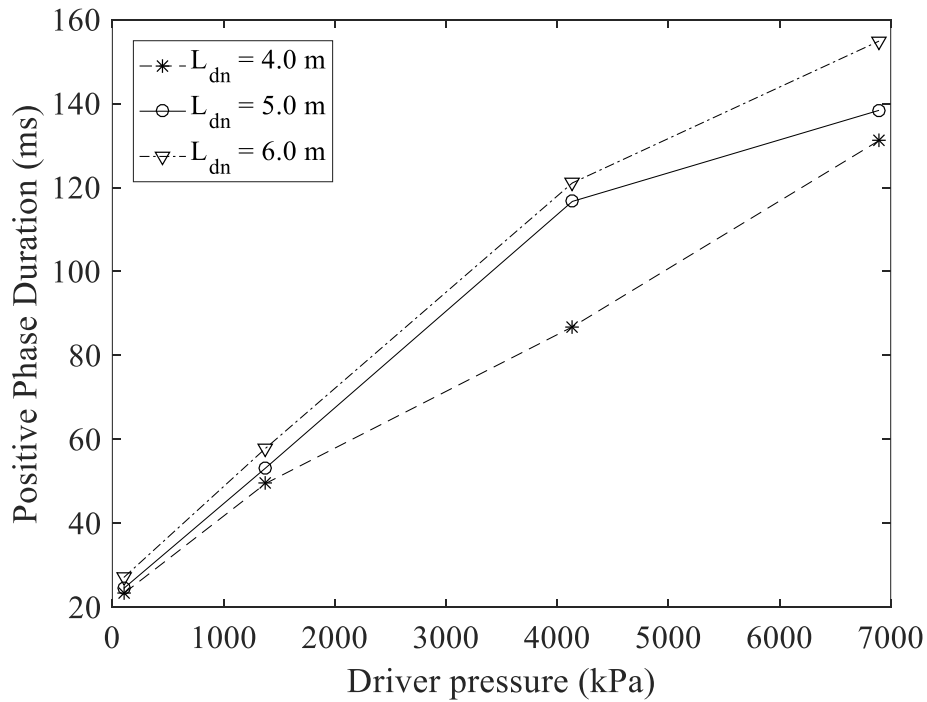


Figure A.18: Positive phase duration versus driver pressure when the driver section length is 4.0 m and the driven section length is changed from 4.0 to 6.0 m

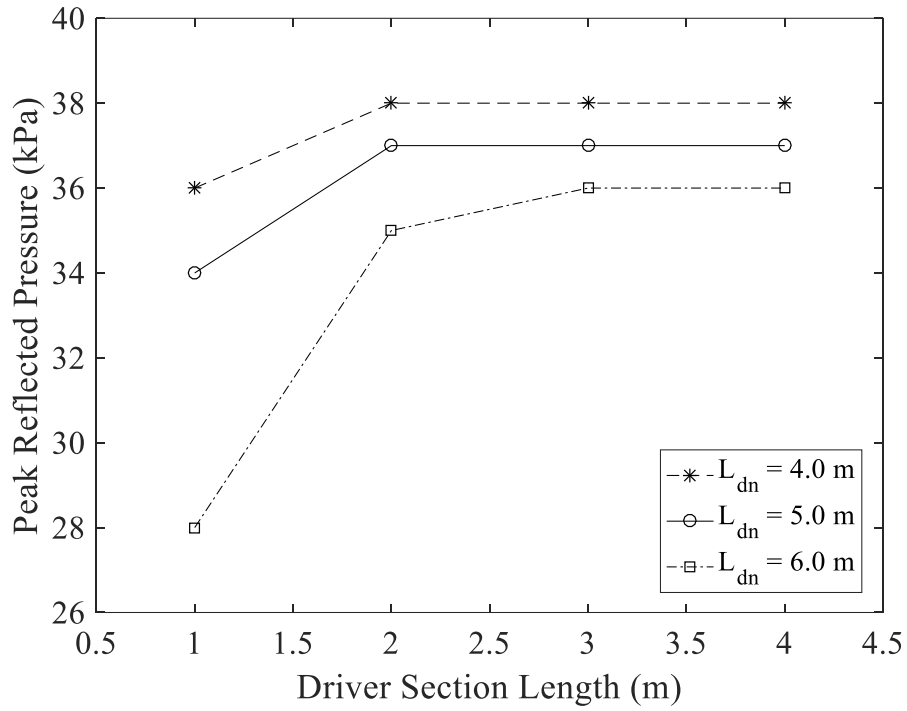


Figure A.19: Peak reflected pressure versus driver section length when the driver pressure is 103 kPa and the driven section length is changed from 4.0 to 6.0 m

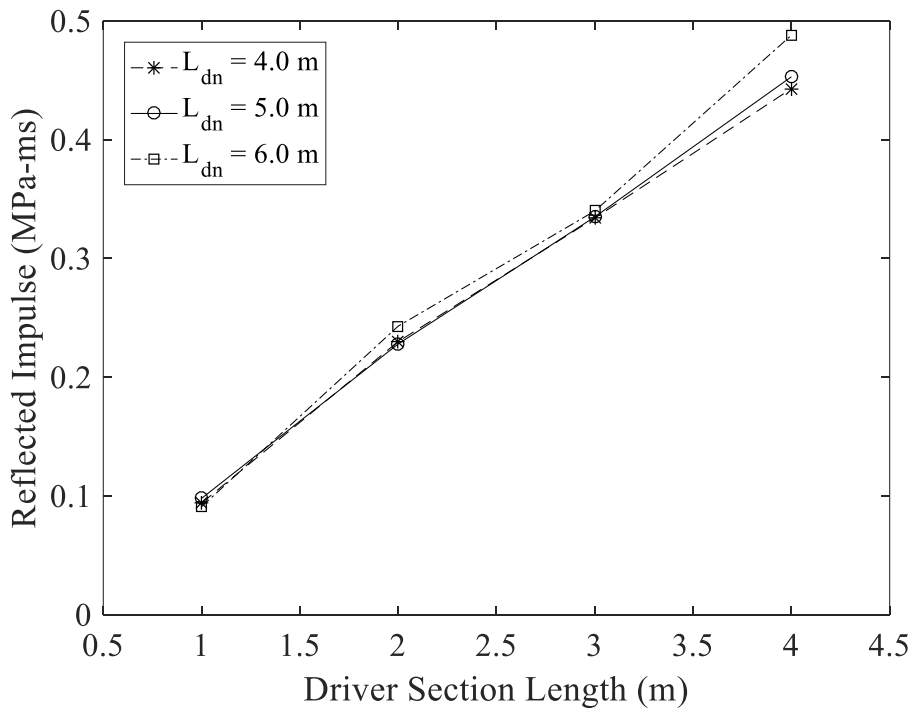


Figure A.20: Reflected impulse versus driver section length when the driver pressure is 103 kPa and the driven section length is changed from 4.0 to 6.0 m

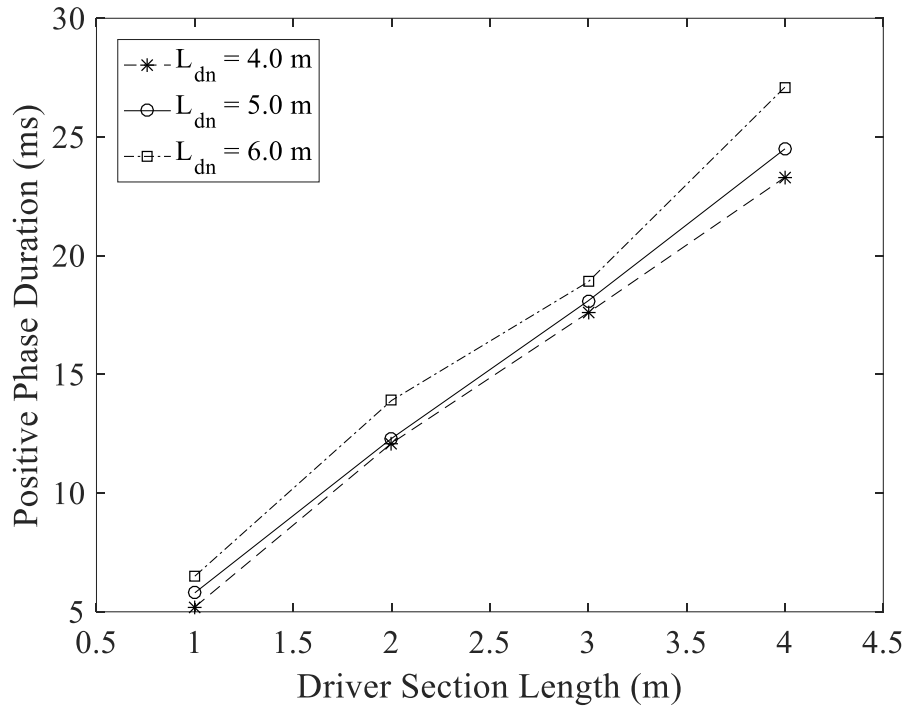


Figure A.21: Positive phase duration versus driver section length when the driver pressure is 103 kPa and the driven section length is changed from 4.0 to 6.0 m

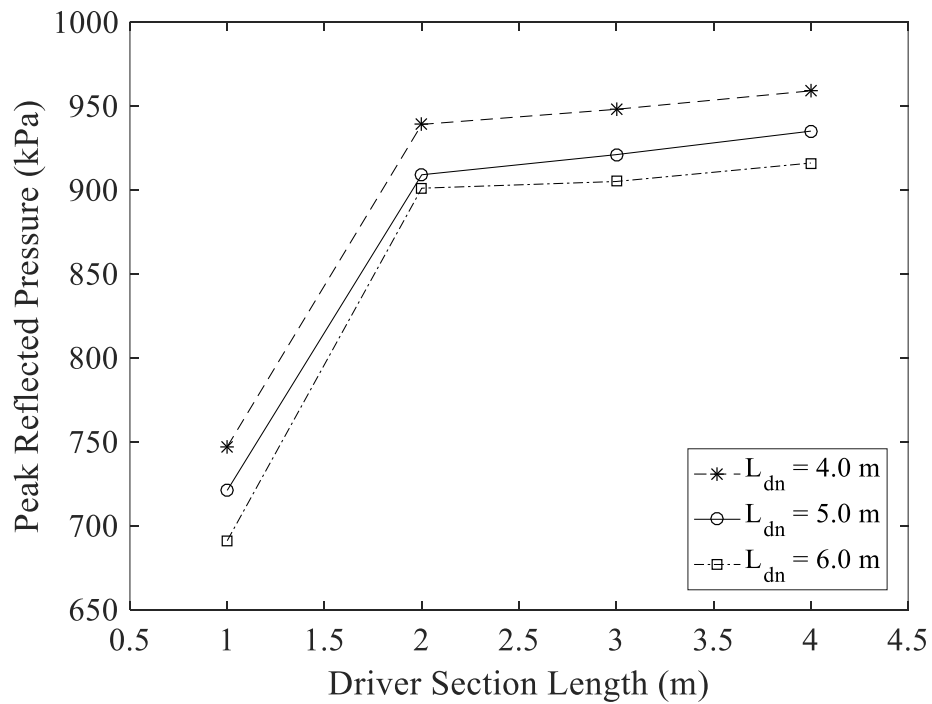


Figure A.22: Peak reflected pressure versus driver section length when the driver pressure is 4137 kPa and the driven section length is changed from 4.0 to 6.0 m

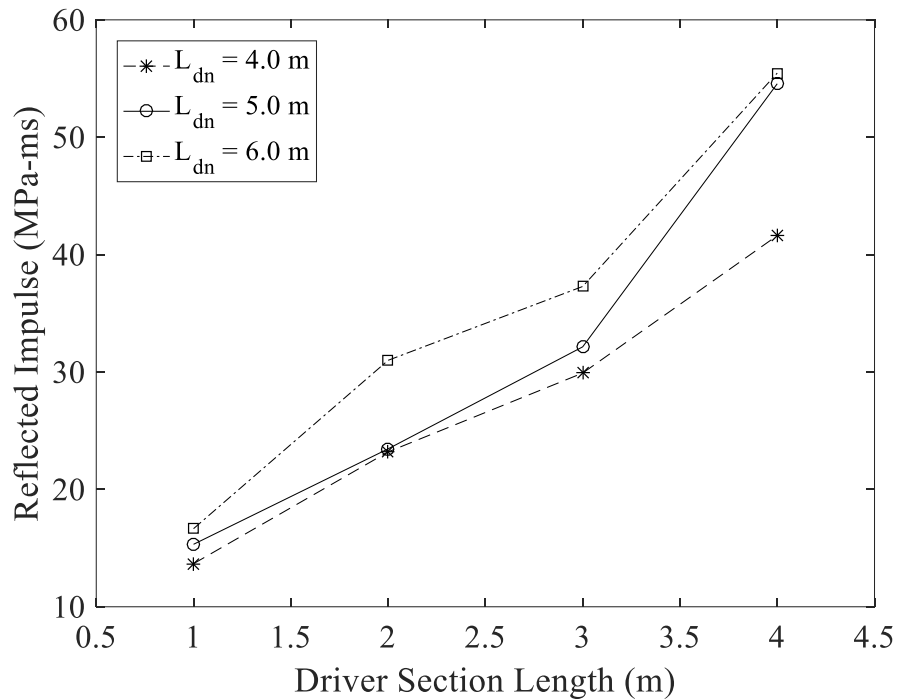


Figure A.23: Reflected impulse versus driver section length when the driver pressure is 4137 kPa and the driven section length is changed from 4.0 to 6.0 m

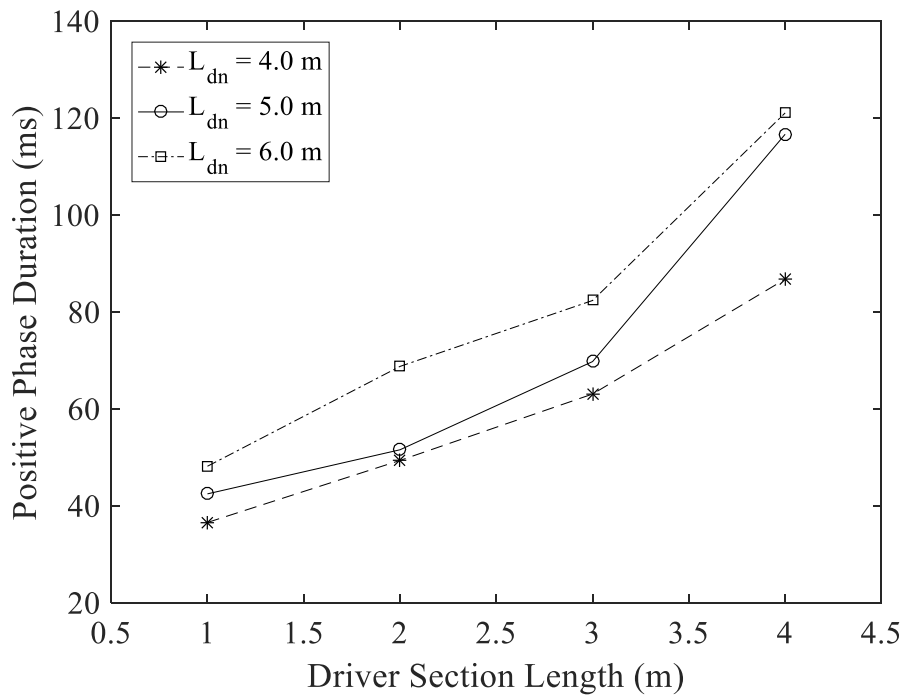


Figure A.24: Positive phase duration versus driver section length when the driver pressure is 4137 kPa and the driven section length is changed from 4.0 to 6.0 m

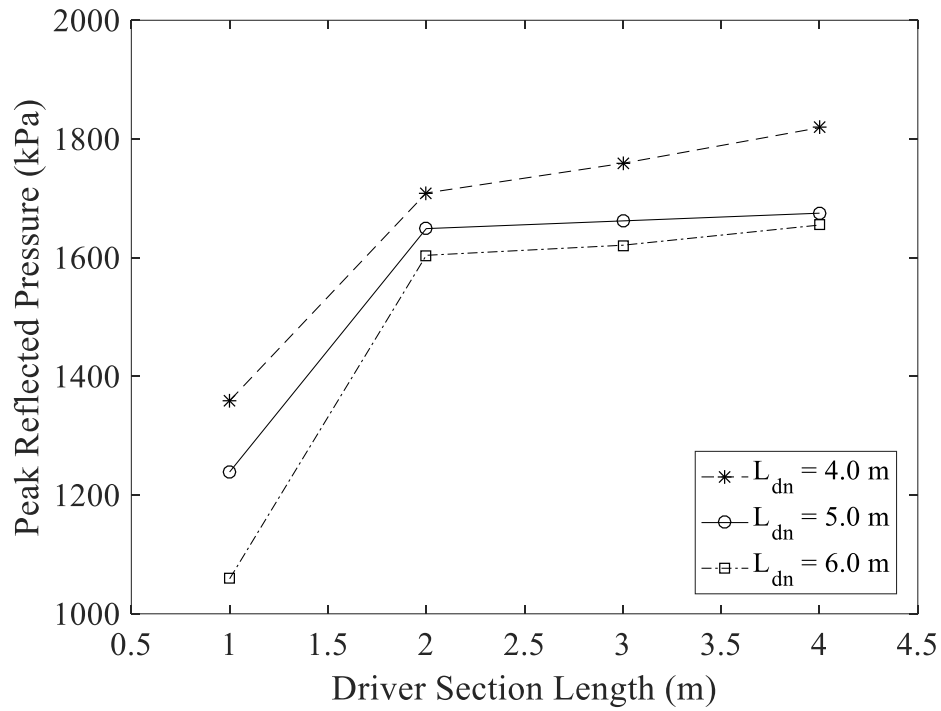


Figure A.25: Peak reflected pressure versus driver section length when the driver pressure is 6895 kPa and the driven section length is changed from 4.0 to 6.0 m

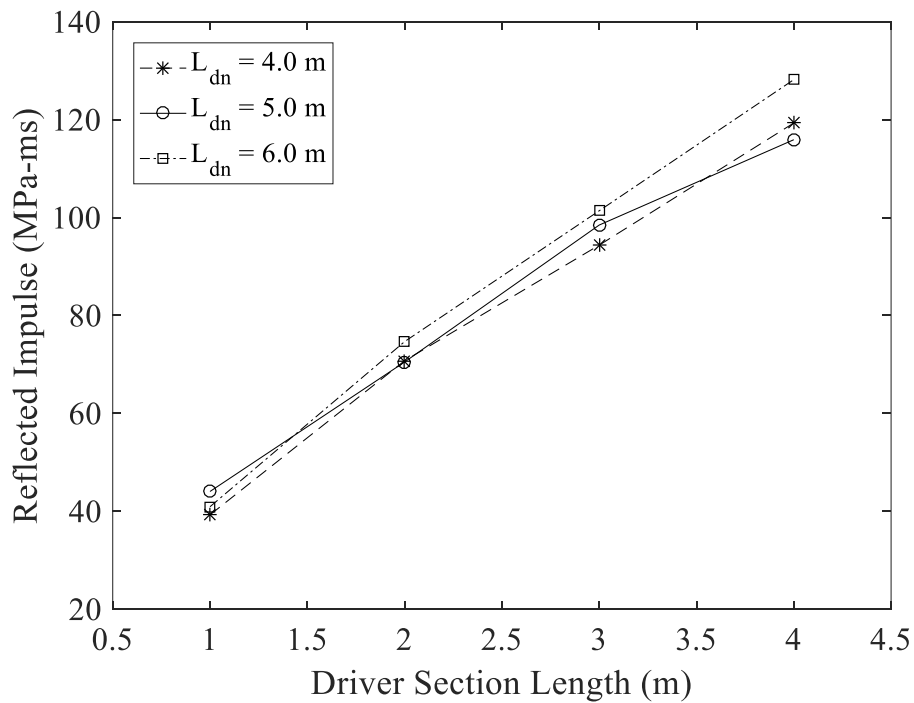


Figure A.26: Reflected impulse versus driver section length when the driver pressure is 6895 kPa and the driven section length is changed from 4.0 to 6.0 m

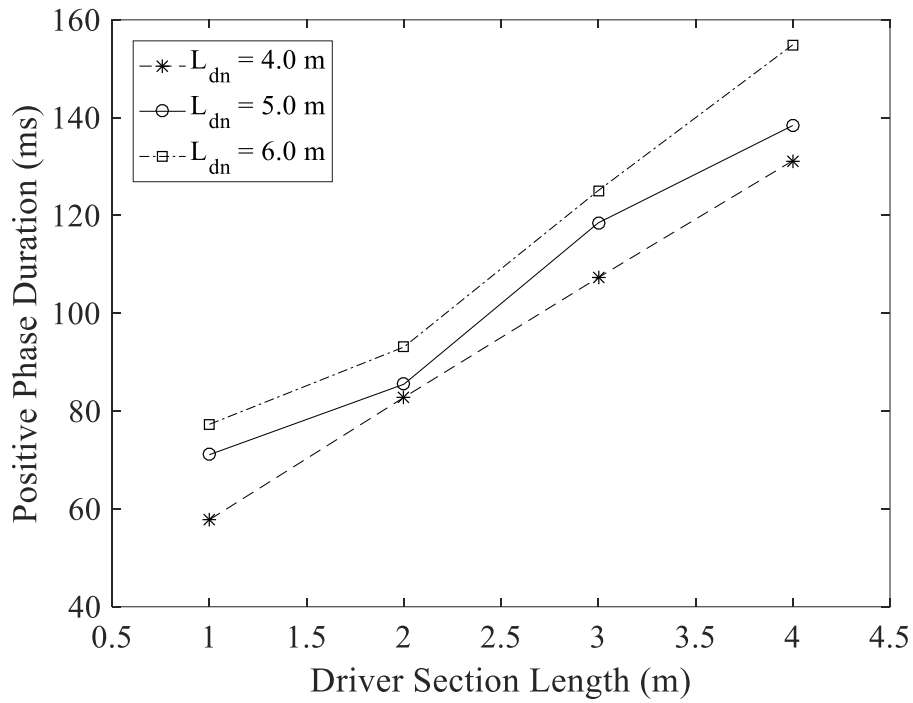


Figure A.27: Positive phase duration versus driver section length when the driver pressure is 6895 kPa and the driven section length is changed from 4.0 to 6.0 m

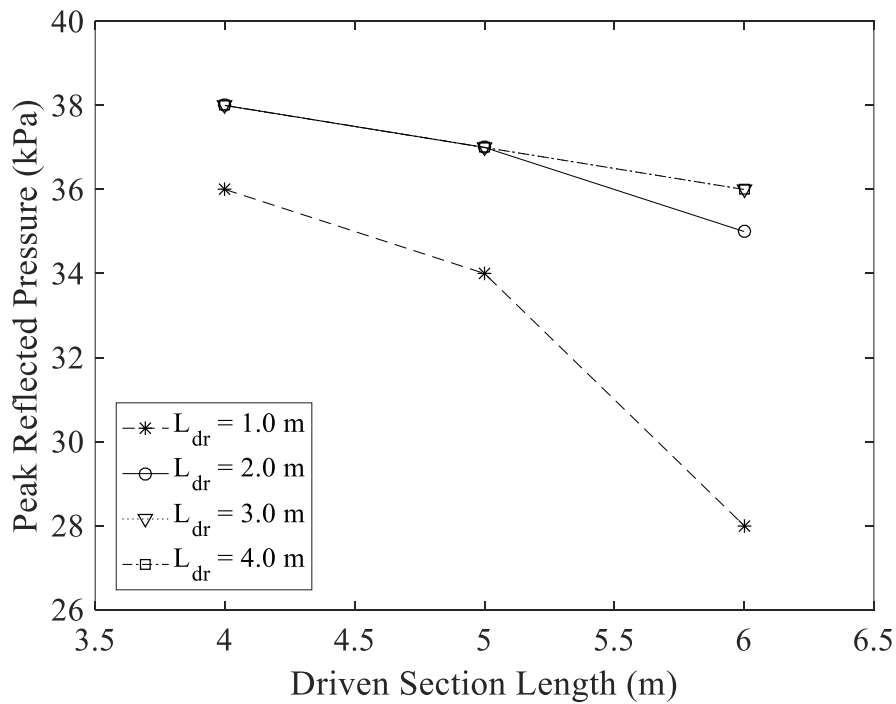


Figure A.28: Peak reflected pressure versus driven section length when the driver pressure is 103 kPa and the driver section length is changed from 1.0 to 4.0 m

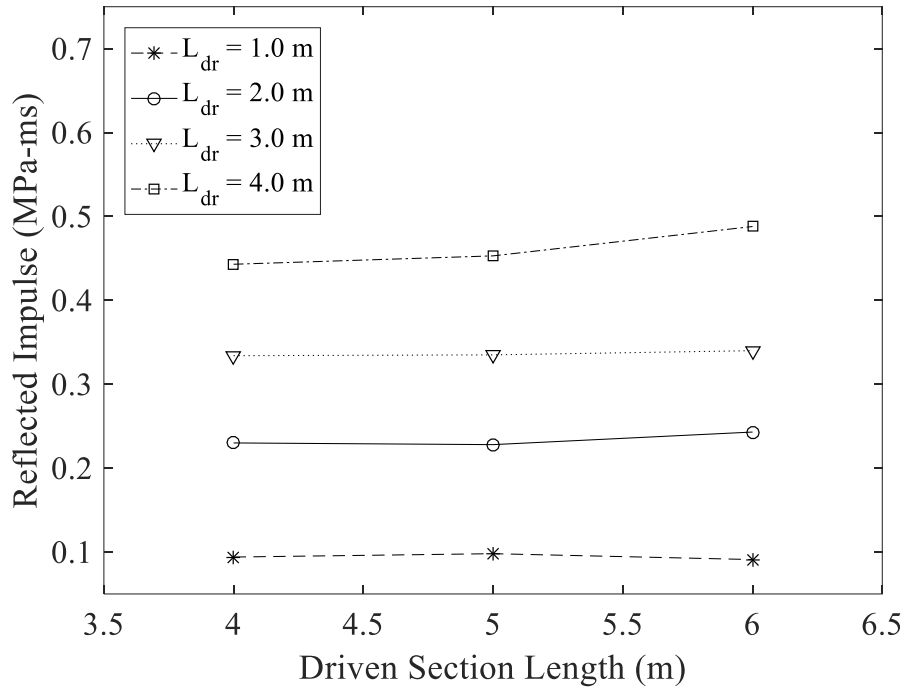


Figure A.29: Reflected impulse versus driven section length when the driver pressure is 103 kPa and the driver section length is changed from 1.0 to 4.0 m

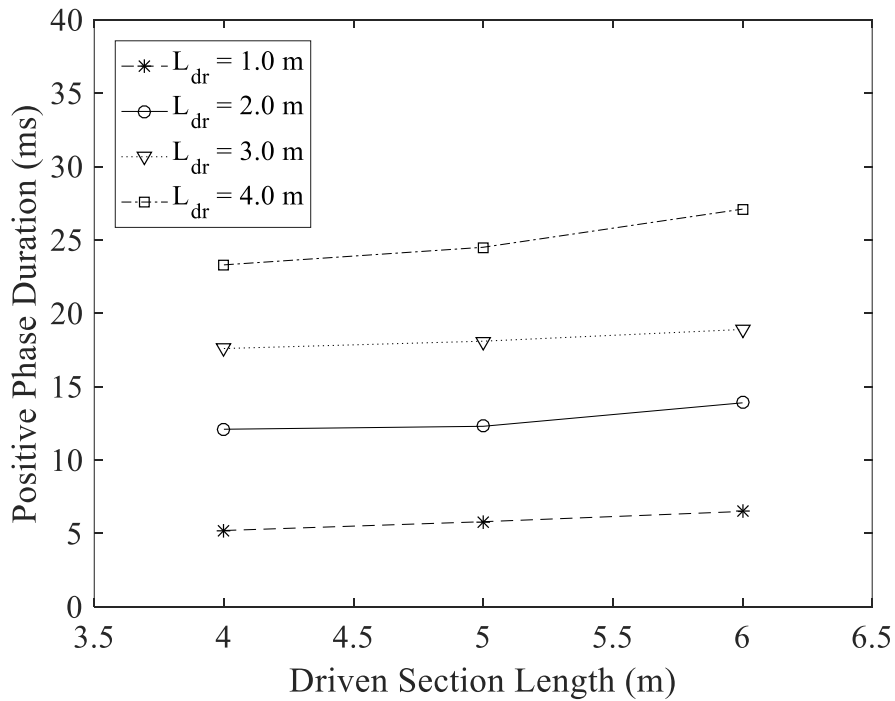


Figure A.30: Positive phase duration versus driven section length when the driver pressure is 103 kPa and the driver section length is changed from 1.0 to 4.0 m

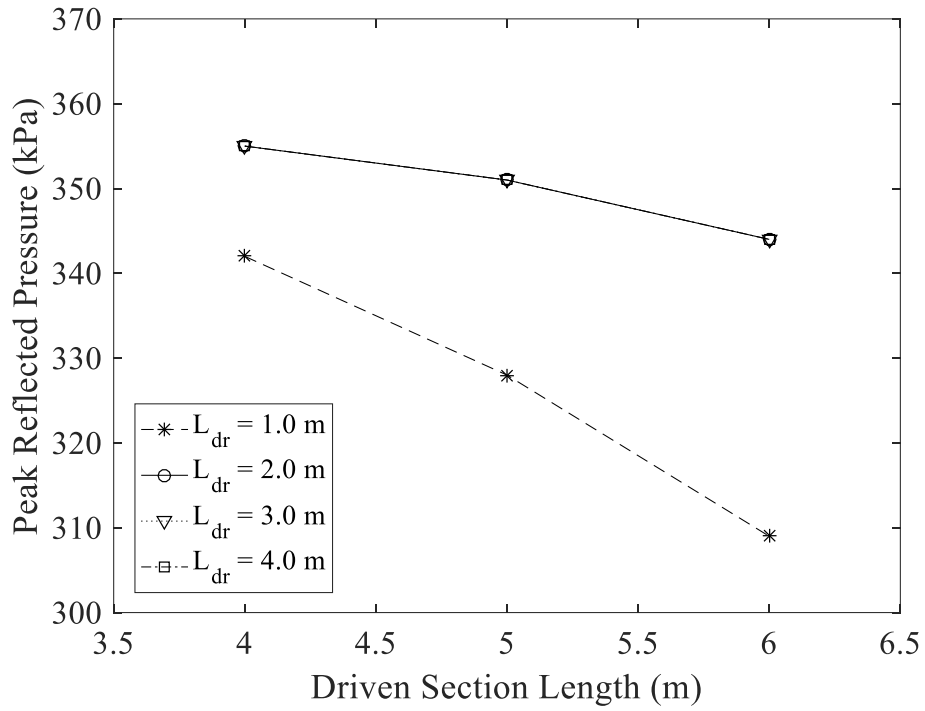


Figure A.31: Peak reflected pressure versus driven section length when the driver pressure is 1379 kPa and the driver section length is changed from 1.0 to 4.0 m

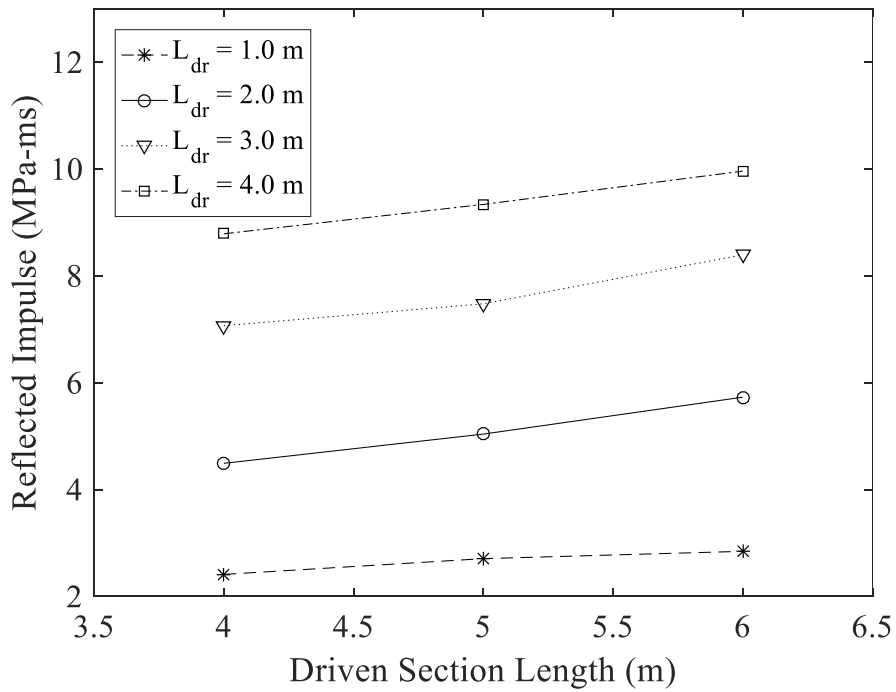


Figure A.32: Reflected impulse versus driven section length when the driver pressure is 1379 kPa and the driver section length is changed from 1.0 to 4.0 m

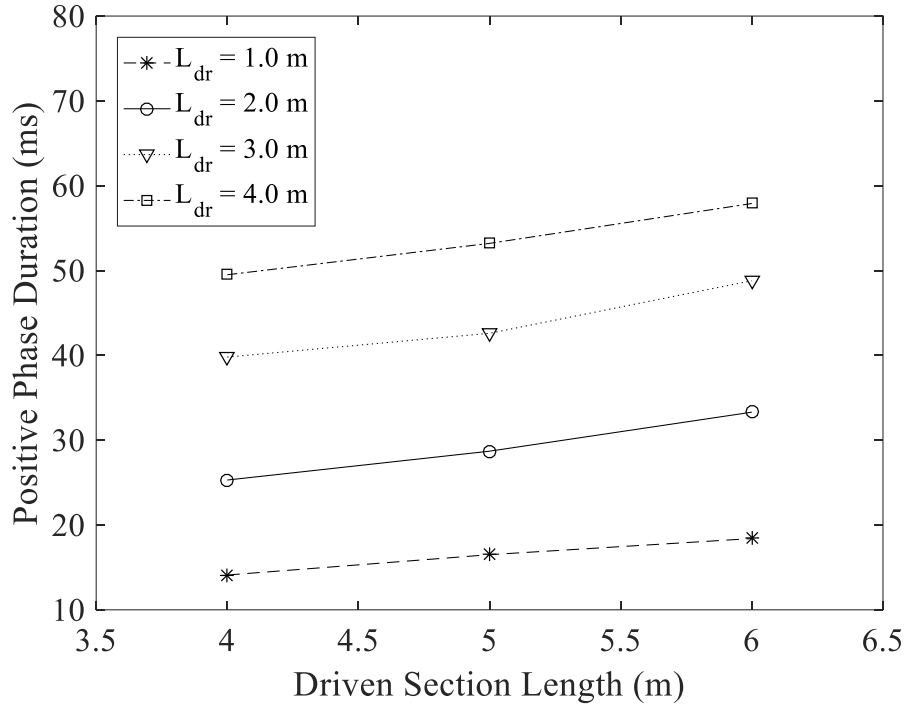


Figure A.33: Positive phase duration versus driven section length when the driver pressure is 1379 kPa and the driver section length is changed from 1.0 to 4.0 m

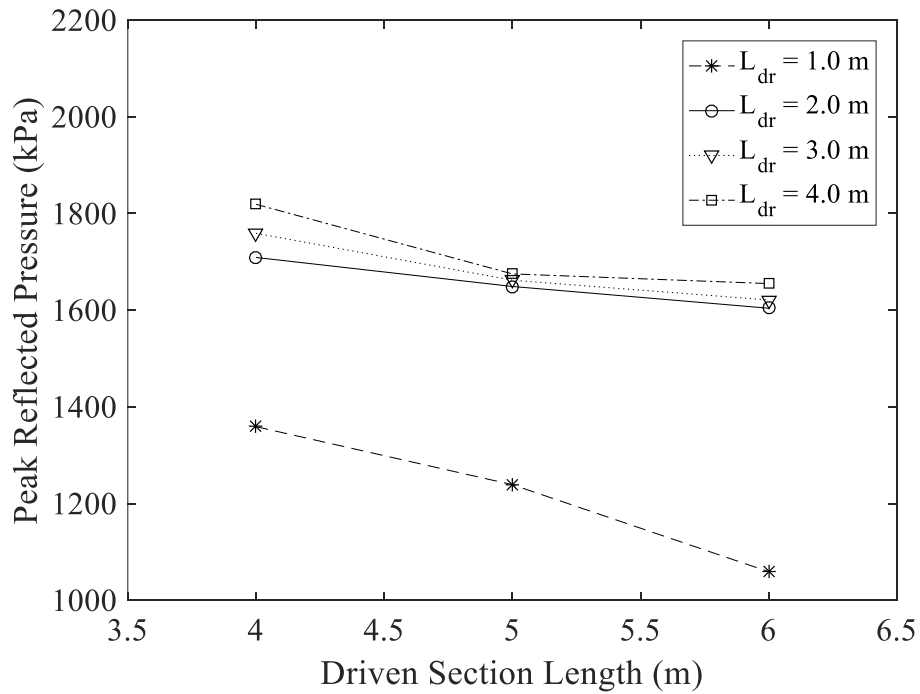


Figure A.34: Peak reflected pressure versus driven section length when the driver pressure is 6895 kPa and the driver section length is changed from 1.0 to 4.0 m

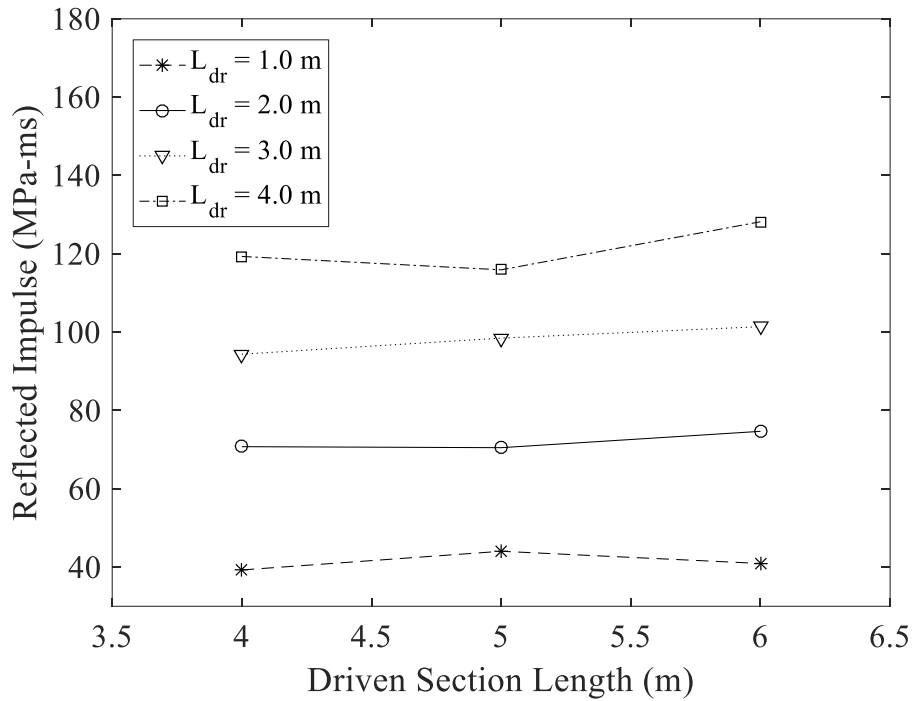


Figure A.35: Reflected impulse versus driven section length when the driver pressure is 6895 kPa and the driver section length is changed from 1.0 to 4.0 m

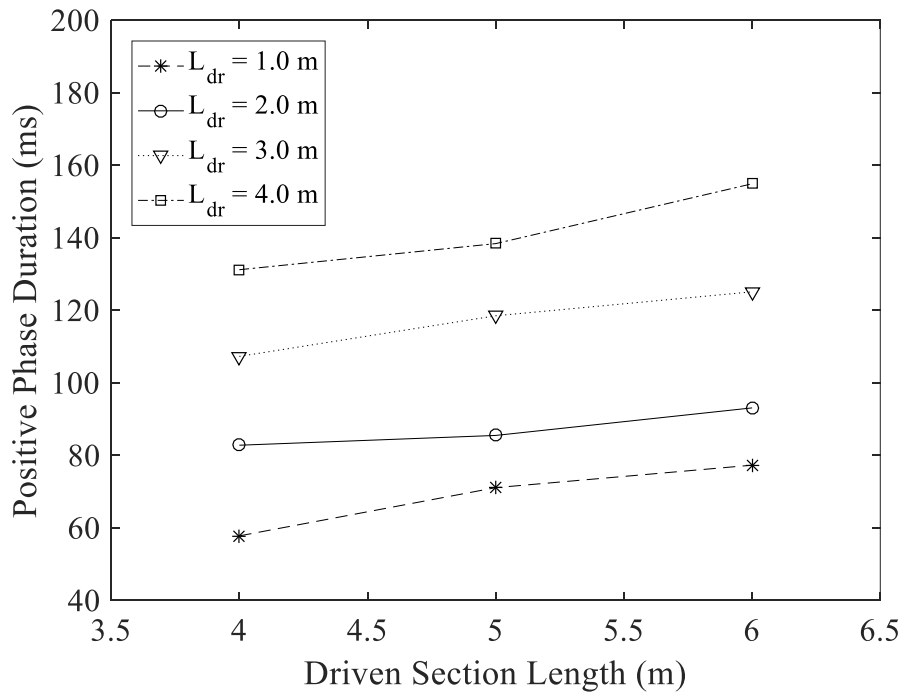


Figure A.36: Positive phase duration versus driven section length when the driver pressure is 6895 kPa and the driver section length is changed from 1.0 to 4.0 m

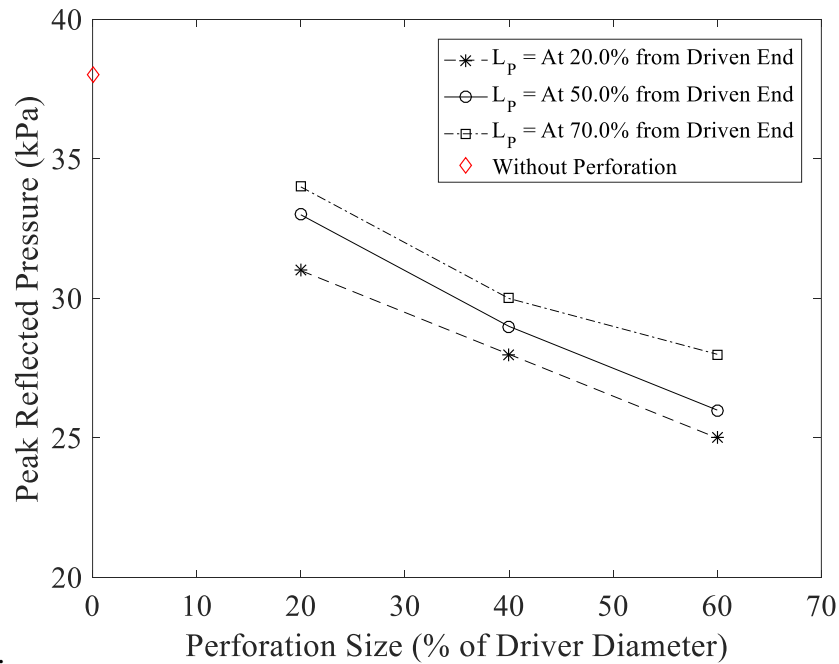


Figure A.37: Peak reflected pressure versus perforation size when the driver pressure is 103 kPa, driver length is 3.0 m, driven length is 4.0 m and the perforation is located at 20.0, 50.0 and 70.0 % of the driven length

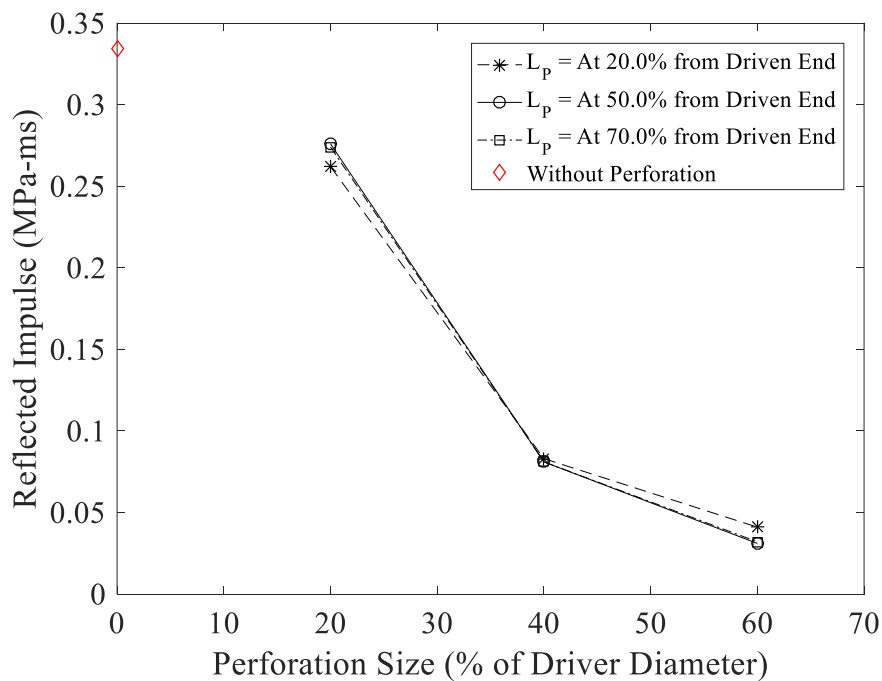


Figure A.38: Reflected impulse versus perforation size when the driver pressure is 103 kPa, driver length is 3.0 m, driven length is 4.0 m and the perforation is located at 20.0, 50.0 and 70.0 % of the driven length

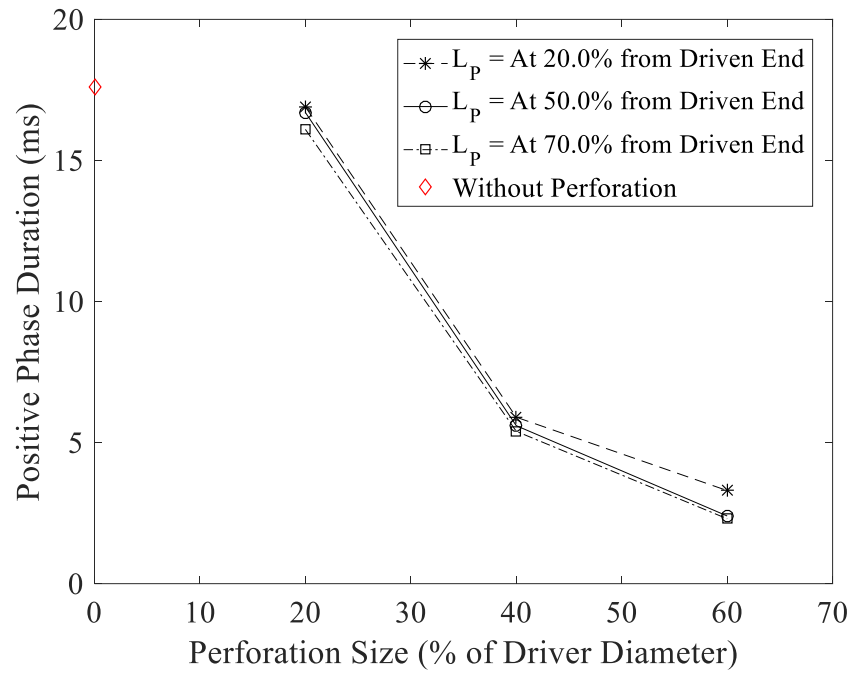


Figure A.39: Positive phase duration versus perforation size when the driver pressure is 103 kPa, driver length is 3.0 m, driven length is 4.0 m and the perforation is located at 20.0, 50.0 and 70.0 % of the driven length

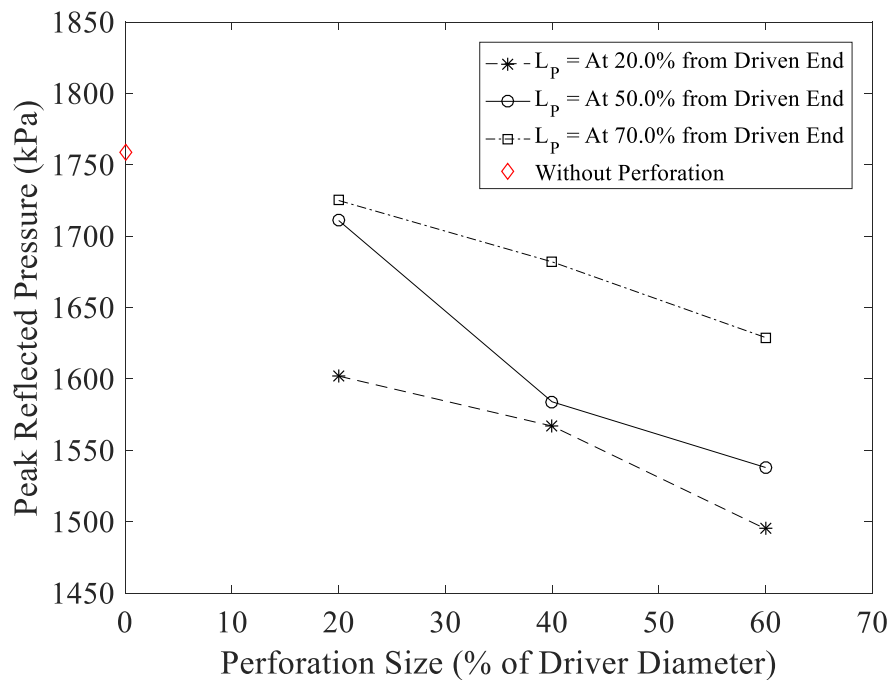


Figure A.40: Peak reflected pressure versus perforation size when the driver pressure is 6895 kPa, driver length is 3.0 m, driven length is 4.0 m and the perforation is located at 20.0, 50.0 and 70.0 % of the driven length

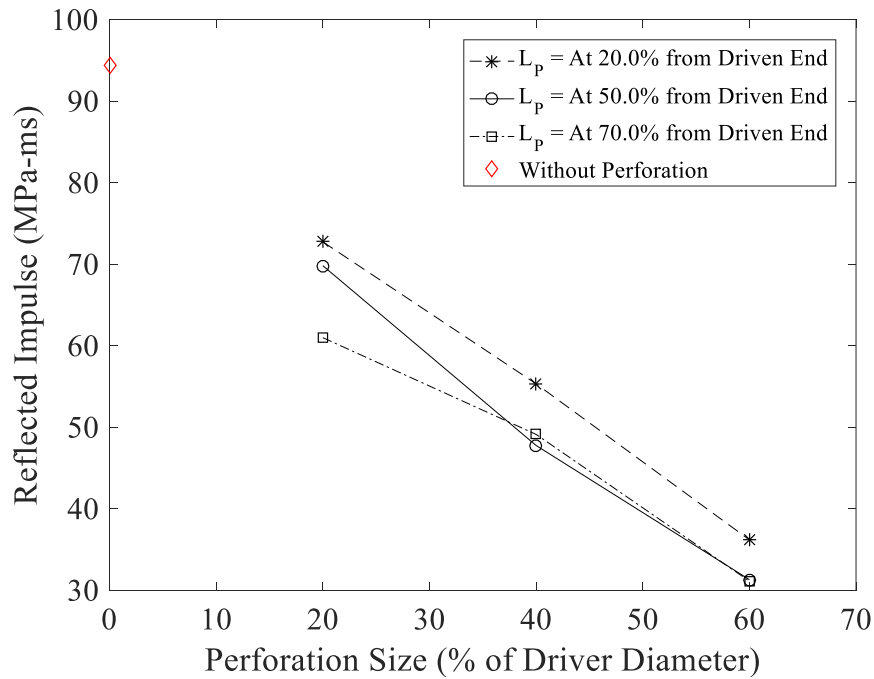


Figure A.41: Reflected impulse versus perforation size when the driver pressure is 6895 kPa, driver length is 3.0 m, driven length is 4.0 m and the perforation is located at 20.0, 50.0 and 70.0 % of the driven length

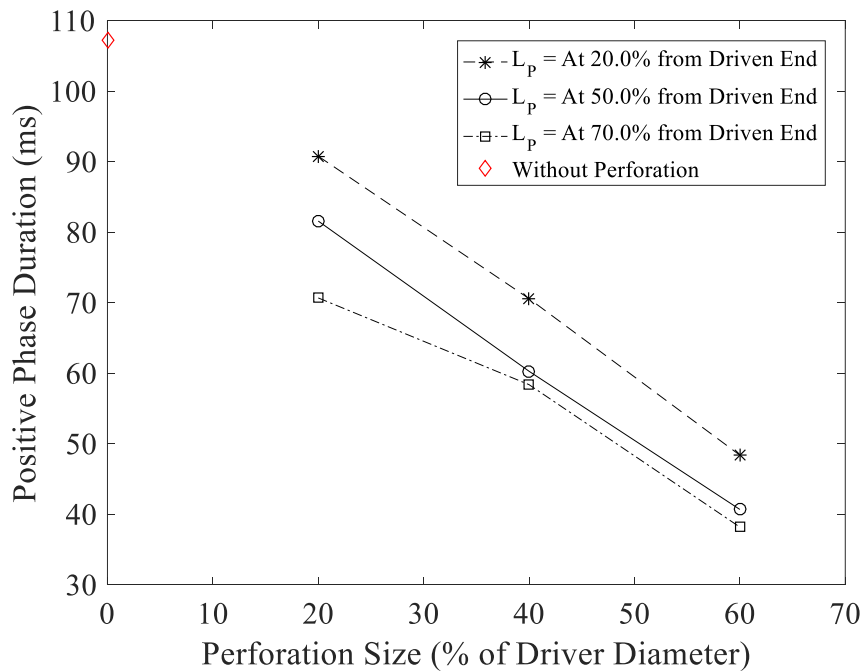


Figure A.42: Positive phase duration versus perforation size when the driver pressure is 6895 kPa, driver length is 3.0 m, driven length is 4.0 m and the perforation is located at 20.0, 50.0 and 70.0 % of the driven length

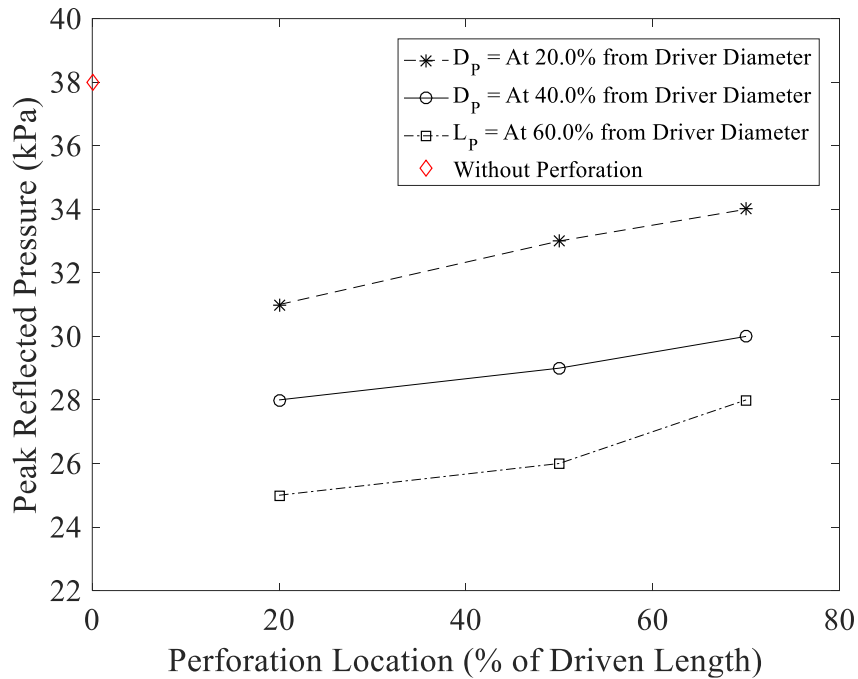


Figure A.43: Peak reflected pressure versus perforation location when the driver pressure is 103 kPa, driver length is 3.0 m, driven length is 4.0 m and the perforation size is increased from 20.0 to 60.0 % of the driver diameter

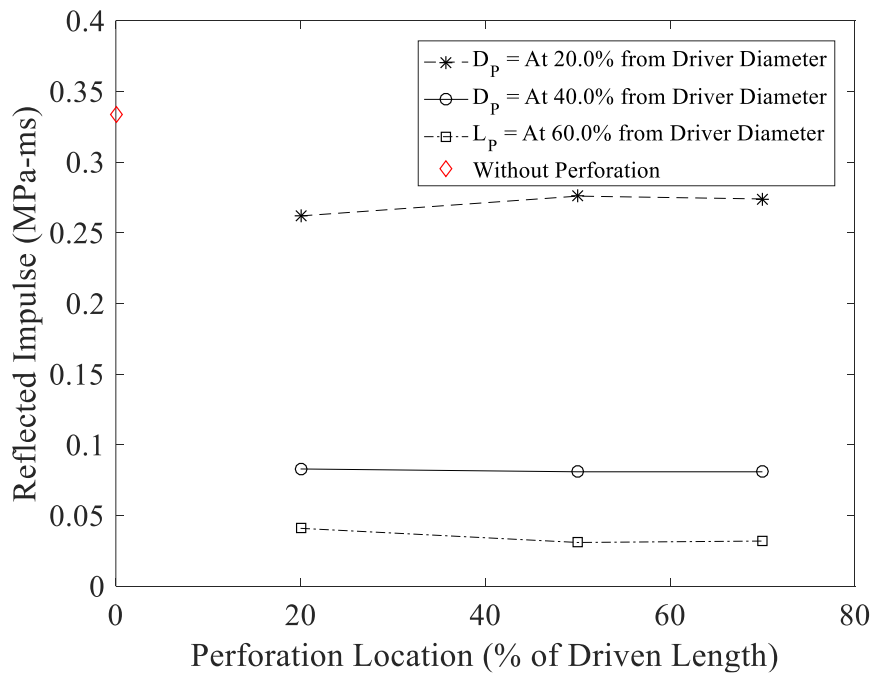


Figure A.44: Reflected impulse versus perforation location when the driver pressure is 103 kPa, driver length is 3.0 m, driven length is 4.0 m and the perforation size is increased from 20.0 to 60.0 % of the driver diameter

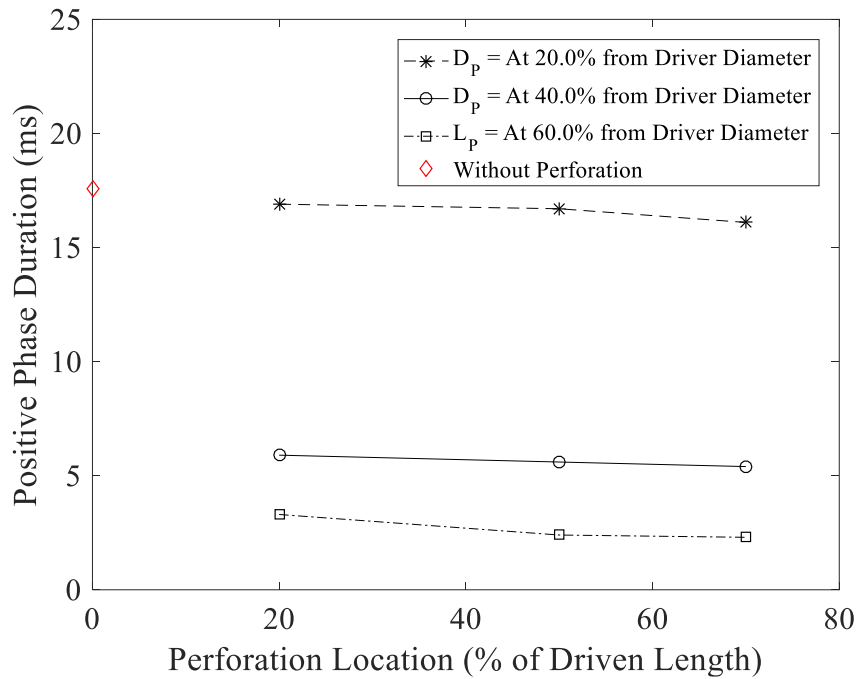


Figure A.45: Positive phase duration versus perforation location when the driver pressure is 103 kPa, driver length is 3.0 m, driven length is 4.0 m and the perforation size is increased from 20.0 to 60.0 % of the driver diameter

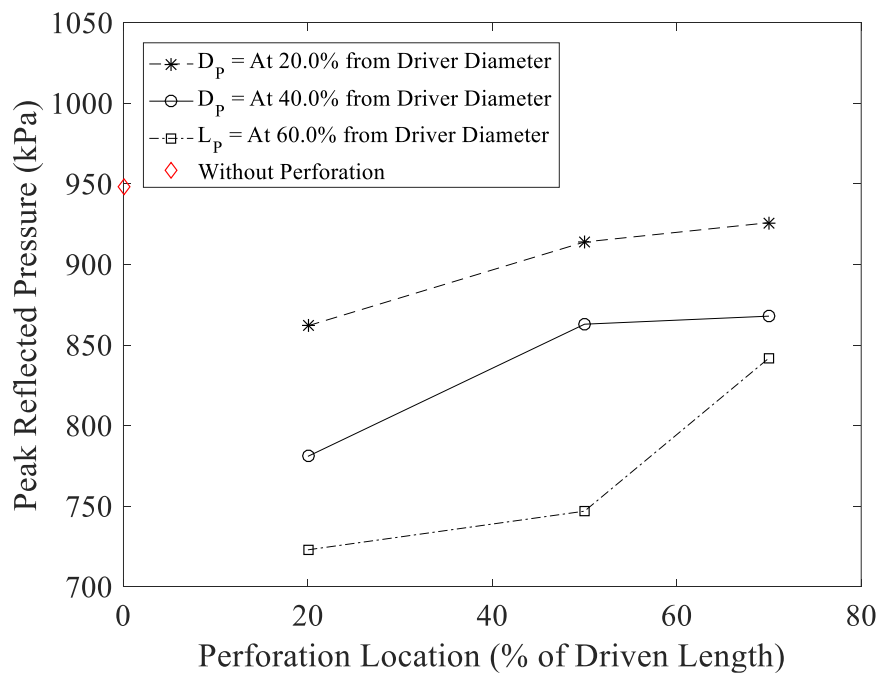


Figure A.46: Peak reflected pressure versus perforation location when the driver pressure is 4137 kPa, driver length is 3.0 m, driven length is 4.0 m and the perforation size is increased from 20.0 to 60.0 % of the driver diameter

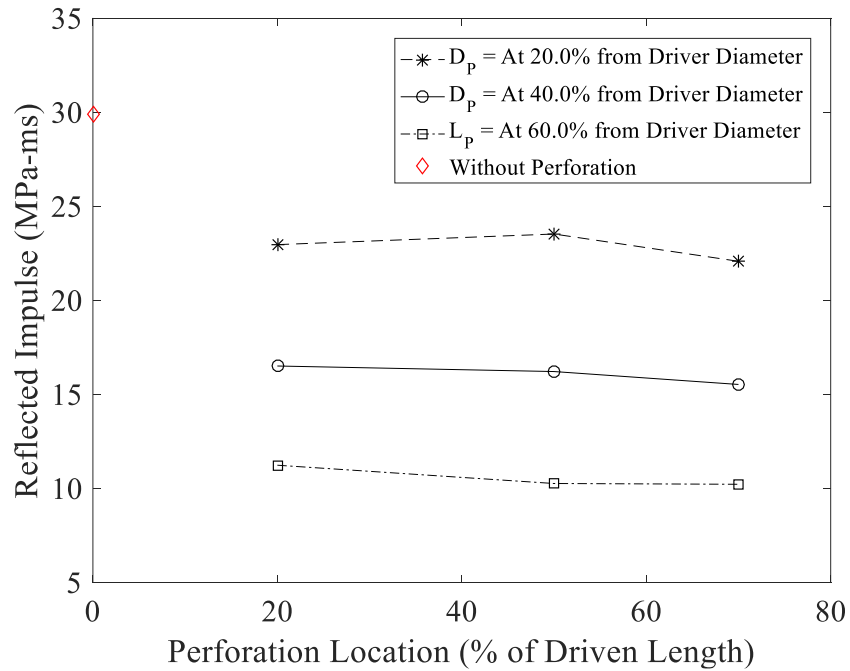


Figure A.47: Reflected impulse versus perforation location when the driver pressure is 4137 kPa, driver length is 3.0 m, driven length is 4.0 m and the perforation size is increased from 20.0 to 60.0 % of the driver diameter

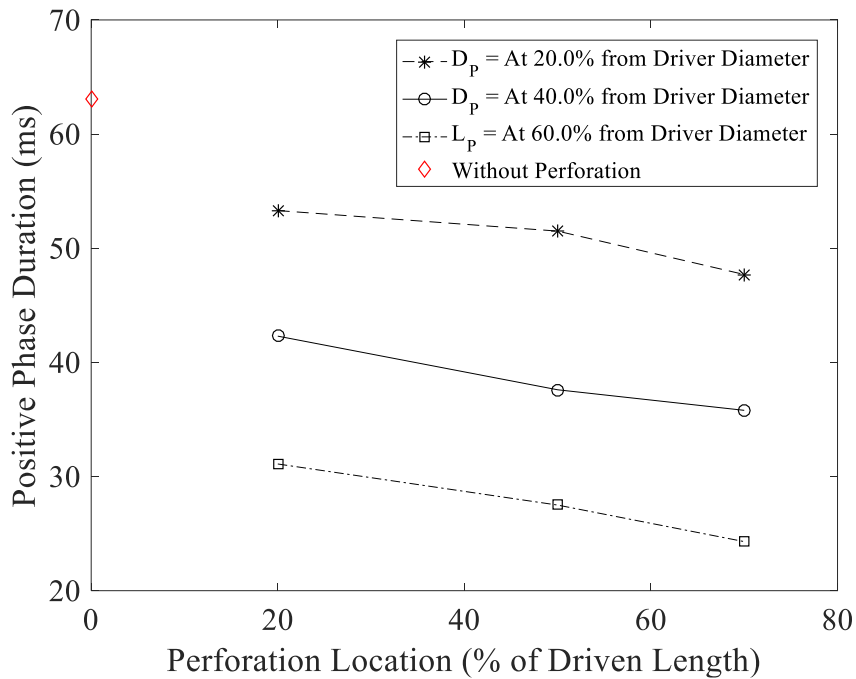


Figure A.48: Positive phase duration versus perforation location when the driver pressure is 4137 kPa, driver length is 3.0 m, driven length is 4.0 m and the perforation size is increased from 20.0 to 60.0 % of the driver diameter

REFERENCES

- Abou-Zeid, B., El-Dakhakhni, W., Razaqpur, A. & Foo, S., 2011. Performance of unreinforced masonry walls retrofitted with externally anchored steel studs under blast loading. *Journal of Performance Constructed Facilities*, Volume 25, p. 441–453.
- Amman, H. O., 1977. *Model tests for a large diameter simulator driven by several generators filled with compressed air*. Stockholm, s.n.
- ANSYS, 2013. *software manual, release 15.0*, Canonsburg, PA 15317, USA: ANSYS INC..
- Argow, B., 1996. Computational analysis of Dense Gas Shock tube Flow. *Shock Waves*, Volume 6, pp. 241-248.
- Arisman, C., Johansen, C., Bathel, B. & Danehy, P., 2015. Investigation of Gas Seeding for Planar Laser-Induced Fluorescence in Hypersonic Boundary Layers. *AIAA JOURNAL*, 53(12).
- Armstrong, J., 2015. *Design of a Free Field Blast Simulating Shock Tube*, Ottawa: M.A.Sc., University of Ottawa.
- Awad, N., 2014. *Study of blast-induced mild traumatic brain injury: laboratory simulation of blast shock wave*. s.l.:Ph.D. Thesis, McMaster University.
- Beam, R. & Warming, R., 1976. An implicit finite-difference algorithm for hyperbolic systems in conservation-law form. *Journal of Computational Physics*, 22(1), pp. 87-110.

- Berger, S., Ben-Dor, G. & Sadot, O., 2015. Experimental and numerical investigations of shock-wave attenuation by geometrical means: A single barrier configuration. *European Journal of Mechanics B/Fluids*, Volume 50, p. 60–70.
- Berger, S., Ben-Dor, G. & Sadot, O., 2016. Experimental and Numerical Investigation of Shock Wave Attenuation by Dynamic Barriers. *Journal of Fluids Engineering*, 138(3).
- Bokil, M., 2010. *Characterization of the pressure wave from a shock tube using numerical simulations*. s.l.:M.Sc. Thesis, The University of Utah.
- Britan, A. et al., 2004. Experimental and Numerical Study of Shock Wave Interaction with Perforated Plates. *Journal of Fluids Engineering*, 126(3), pp. 399-409.
- Carriere, M., Heffernan, P., Wight, R. & Braimah, A., 2009. Behaviour of steel reinforced polymer (SRP) strengthened RC members under blast load. *Canadian Journal of Civil Engineering*, 36(8), pp. 1356-1365.
- Chandra, N. et al., 2012. Evolution of blast wave profiles in simulated air blasts: experiment and computational modeling. *Shock Waves*, Volume 22, p. 403–415.
- Chaudhuri, A., Hadjadj, A., Sadot, O. & Ben-Dor, G., 2013. Numerical study of shock-wave mitigation through matrices of solid obstacles. *Shock Waves*, Volume 23, p. 91–101.
- Cocchi, J., Saurel, R. & Loraud, J., 1996. Treatment of Interface Problems with Godunov-type Schemes. *Shock Waves*, Volume 5, pp. 347-357.
- Cocchi, J., Saurel, R. & Loraud, J., 1998. Some remarks about the resolution of high velocity flows near low densities. *Shock Waves*, Volume 8, p. 119–125.

- Colombo, M., di Prisco, M. & Martinelli, P., 2011. A New Shock Tube Facility for Tunnel Safety. *Experimental Mechanics*, Volume 51, p. 1143–1154.
- Cook, A. W., 2004. A high-wavenumber viscosity for high resolution numerical method. *Journal of Computational Physics*, p. 594–601.
- Fomin, N. A., 2010. 110 years of experiments on shock tubes. *Journal of Engineering Physics and Thermophysics*, 83(6), pp. 1058-1071.
- Godunov, S., 1959. A Difference Scheme for Numerical Solution of Discontinuous Solution of Hydrodynamic Equations. *Matematicheskii Sbornik*, 47(89).
- Gottlieb, J. & Groth, C., 1988. Assessment of riemann solvers for unsteady one-dimensional inviscid flows of perfect gases. *Journal of Computational Physics*, 78(2), pp. 437-458.
- Gottlieb, S., Ketcheson, D. & Shu, C., 2009. High order strong stability preserving time discretizations. *Journal of Scientific Computing*, Volume 38, p. 251–289.
- Hallquist, J. O., 2006. *LS-DYNA theory manual*, s.l.: Livermore Software Technology Corporation, Version 970 edition.
- Harten, A., 1983. High resolution schemes for hyperbolic conservation laws. *Journal of Computational Physics*, 49(3), pp. 357-393.
- Hisley, D. M., Gion, E. J. & Bertrand, B. P., 1985. *Performance and predications for a large blast simulator model*, Maryland: BRL-TR-2647, US Army Ballistic Research Laboratory, Aberdeen Proving Ground.

- Hisley, D. M. & Molvik, G. A., 1988. *Axisymmetric calculation for the large blast/thermal simulator (LB/TS) shock tube configuration*, Maryland: BRL-TR-2935, US Army Ballistic Research Laboratory, Aberdeen Proving Ground.
- Holst, T. L., 1975. *Numerical computation of three-dimensional blunt body flow fields with an impinging shock*, s.l.: Ph.D. thesis, Iowa State University.
- Ikui, T., Matsuo, K. & Negi, M., 1969. Investigations of the Aerodynamic Characteristics of the Shock tubes. *Bulletin of JSME*, 12(52), pp. 774-782.
- KASIMIR, 1996. *Shock tube simulation program, instruction manual* , s.l.: Shock Wave Laboratory, RWTH Aachen University.
- Kawai, S. & Lele, S., 2008. Localized artificial diffusivity scheme for discontinuity capturing on curvilinear meshes. *Journal of Computational Physics*, Volume 227, p. 9498–9526.
- Lamnaouer, M., 2010. *Numerical modeling of the shock tube flow fields before and during ignition delay time experiments at practical conditions*. s.l.:Ph.D. Thesis, the University of Central Florida.
- Lax, P., 1954. Weak solutions of nonlinear hyperbolic equations and their numerical computation. *Communications on Pure and Applied Mathematics* , 7(1), p. 159–193.
- Lax, P. & Wendroff, B., 1960. Systems of conservation laws. *Communications on Pure and Applied Mathematics*, 13(2), p. 217–237.
- Leblanc, J., Shukla, A. & Rousseau, C., 2007. Shock loading of three-dimensional woven composite materials. *Composite Structures*, 79(3), p. 344–355.

- Liou, M.-S. & Steffen, C., 1993. A New Flux Splitting Scheme. *Journal of Computational Physics*, 107(1), pp. 23-39.
- Lloyd, A., 2010. *Performance of reinforced concrete columns under shock tube induced shock wave loading*. s.l.:M.Sc. thesis, University of Ottawa.
- MacCormack, R., 1969. The effect of viscosity in hypervelocity impact cratering. *AIAA*, Volume 7, pp. 69-354.
- Mark, A., 1981. *Computational design of large scale blast simulators*. St. Louis, Missouri, s.n.
- Opalka, K. O., 1987. *Large Blast-wave Simulators (LBS) with Cold-Gas drivers: Computational design studies*, Maryland: BRL-TR-2786, US Army Ballistic Research Laboratory, Aberdeen Proving Ground.
- Opalka, K. O., 1989. *Large blast and thermal simulator advanced concept driver design by computational fluid dynamics*, Maryland: BRL-TR-3026, US Army Ballistic Research Laboratory, Aberdeen Proving Ground.
- Petrie-Repar, P. & Jacobs, P., 1998. A computational study of shock speeds in high-performance shock tubes. *Shock Waves*, Volume 8, p. 79–91.
- Puckett, A. & Stewart, H., 1950. The thickness of a shock wave in air. *Quarterly of Applied Mathematics*, 7(4).
- Reichenbach, H., 1992. In the footsteps of Ernst Mach – A historical review of shock wave research at the Ernst-Mach-Institut. *Shock waves*, Volume 2, pp. 65-79.

- Ritzel, D. V., 2007. *Upgrade of the DRDC Suffield blast tube facility*, s.l.: Defence R&D Canada, Contract Report DRDC Suffield CR 2009-018, .
- Roe, P., 1981. Approximate Riemann solvers, parameter vectors, and difference schemes. *Journal of Computational Physics*, 43(2), pp. 357-372.
- Sha, S., Chen, Z. & Jiang, X., 2014. Influences of obstacle geometries on shock wave attenuation. *Shock Waves*, 24(6), p. 573–582.
- Sheng, Y., Sislian, J. & Liu, L., 1998. A computational technique for high enthalpy shock tube and shock tunnel flow simulation. *Shock Waves*, Volume 8, p. 203{214.
- Sod, G. A., 1978. A survey of several finite difference schemes for hyperbolic conservation laws. *Journal of Computational Physics*, 27(1), pp. 1-31.
- Sundaramurthy, A. & Chandra, N., 2014. A parametric approach to shape field-relevant blast wave profiles in compressed gas driven shock tube. *Frontiers in Neurology*, Volume 5.
- Szuladzinski, G., 2009. *Formulas for Mechanical and Structural Shock and Impact*. s.l.:CRC Press.
- Thomas, J. et al., 2004. *Shock tube*. United States, Patent No. 6763696.
- Toutlemonde, F., Boulay, C. & Gourraud, C., 1993. Shock-tube tests of concrete slabs. *Materials and Structures*, 26(1), p. 38–42.
- UFC 3-340-02, 2008. *Structures to resist the effects of accidental explosions*, Washington DC: Department of Defense.

- UFC 4-010-01, 2013. *DOD Minimum antiterrorism standards for buildings*, Washington DC: Department of Defence.
- United Kingdom Glazing Hazard Guide, 1997. *Glazing hazard guide, cubicle standoffs, tables and charts*, London: Security Facilities Executive Special Service Group - Explosive protection, Cabinet Office.
- Van Leer, B., 1979. Towards the Ultimate Conservative Difference Scheme. V. A Second Order Sequel to Godunov's Sequel.. *Journal of Computational Physics*, 32(1), pp. 101-136.
- Vasil'ev, E. & Danil'chuck, E., 1994. Numerical Solution of the Problem of Shock Tube Flow Development with Transverse Diaphragm Withdrawal. *Fluid Dynamics*, 29(2), pp. 270-276.
- Wan, Q. & Eliasson, V., 2015. Numerical Study of Shock Wave Attenuation in Two-Dimensional Ducts Using Solid Obstacles: How to Utilize Shock Focusing Techniques to Attenuate Shock Waves. *Aerospace*, 2(2), pp. 203-221.
- White, D. R., 1958. Influence of diaphragm opening time on shock-tube flows. *Journal of Fluid Mechanics*, 4(6), pp. 585-599.
- Wu, C., Huang, L. & Oehlers, D., 2011. Blast testing of aluminum foam-protected reinforced concrete slabs. *Journal of Performance Constructed Facilities*, Volume 25, p. 464-474.
- Xu, K., 2001. A Gas-Kinetic BGK Scheme for the Navier-Stokes equations and its connection with artificial dissipation and Godunov. *Journal of Computational Physics*, Volume 171, pp. 289-335.

Xu, K., 2014. *Direct Modeling for Computational Fluid Dynamics: Construction and Application of Unified Gas-Kinetic Schemes*. Volume 4 ed. Singapore: World Scientific Publishing.

Zipf, R. K., Mohamed, K. M. & McMahan, G. W., 2009. *Design and analysis of a new method to test mine seals*. San Diego, California, s.n.